VOLUME 12 (1959) No. 3

NUCLEAR PHYSICS

JOURNAL DEVOTED TO THE EXPERIMENTAL AND THEORETICAL STUDY OF THE FUNDAMENTAL CONSTITUENTS OF MATTER AND THEIR INTERACTIONS

EDITOR: L. ROSENFELD - COPENHAGEN

R. J. GRIFFITHS and R. M. EISBERG, The mechanism of the direct interaction process at intermediate energies 225

N. H. MARCH and W. H. YOUNG, Approximate solutions of the density matrix equation for a local average field. 237

T. J. GOODING, Proton total reaction cross sections at 34 MeV 241

T. J. KENNETT and L. M. BOLLINGER, The multiple scattering of neutrons at resonances 249

M. L. SEHGAL, H. S. HANS and P. S. GILL, Thermal neutron cross-sections for producing some isomers 261

HARTMUT PILKUHN, Quadrupole interaction in SU_3-coupling and cranking model 269

I. E. McCARTHY, E. V. JEZAK and A. J. KROMMINGA, Momentum distribution of nucleons in the nuclear surface. 274

LOS ALAMOS PHYSICS AND CRYOGENICS GROUPS, Total neutron cross sections of the hydrogen and helium isotopes 291

B. ZEIDMAN and J. L. YNTEMA, (α, d) reactions on N^{11} and Li^6 298

NORTH-HOLLAND PUBLISHING COMPANY - AMSTERDAM

July (2) 1959

EDITORIAL BOARD

AUSTRALIA & NEW ZEALAND:	H. Messel (Sydney), M. L. Oliphant (Canberra)
AUSTRIA:	B. Karlik, (Vienna), H. Thirring (Vienna)
BELGIUM:	M. de Hemptinne (Louvain), J. Verhaeghe (Ghent)
CANADA:	G. Volkoff (Vancouver)
DENMARK:	C. Møller (Copenhagen), S. Rozental (Copenhagen)
FINLAND:	L. Simons (Helsinki)
FRANCE:	A. Berthelot (Paris), S. Gorodetzky (Strasbourg)
GERMANY (DEM. REP.):	G. Hertz (Leipzig)
GERMANY (FED. REP.):	W. Gentner (Freiburg i. B.), J. H. D. Jensen (Heidelberg)
GREAT BRITAIN:	S. Devons (Manchester), T. H. R. Skyrme (Harwell)
HUNGARY:	L. Janossy (Budapest)
INDIA:	H. Bhabha (Bombay), R. Ramanna (Trombay)
IRISH REPUBLIC:	J. McConnell (Maynooth)
ISRAEL:	G. Racah (Jerusalem)
ITALY:	E. Amaldi (Rome)
JAPAN:	S. Kikuchi (Tokyo), S. Tomonaga (Tokyo)
MEXICO:	M. Moshinsky (Mexico)
NETHERLANDS:	H. Brinkman (Groningen), S. R. de Groot (Leiden)
NORWAY:	E. Hylleraas (Oslo), A. Lundby (Oslo), H. Wergeland (Trondheim)
POLAND:	L. Infeld (Warsaw)
PORTUGAL:	J. M. Araújo (Porto), J. R. de Almeida Santos (Coimbra)
SOUTH AMERICA:	G. Beck (Saõ Paulo), J. Leite Lopes (Rio de Janeiro)
SPAIN:	J. M. Otero (Madrid), C. Sanchez del Rio (Madrid)
SWEDEN:	O. Klein (Stockholm), K. Siegbahn (Uppsala), I. Waller (Uppsala)
SWITZERLAND:	P. Huber (Basel), P. Scherrer (Zürich)
U.A.R. & ARAB COUNTRIES:	F. El Bedewi (Alexandria), M. G. Nooh (Cairo)
U.S.A.	H. H. Barschall (Madison, Wisconsin), V. Weisskopf (Cambridge, Mass.)
U.S.S.R.:	M. A. Markov (Moscow), I. S. Shapiro (Moscow), D. V. Skobeltzyn (Moscow)
YUGOSLAVIA:	I. Supek (Zagreb)

CONTRIBUTIONS may be sent to the Editor, Professor L. Rosenfeld, NORDITA, Blegdamsvej 17, Copenhagen Ø, either directly, or preferably through the intermediary of one of the members of the Editorial Board of the country or region in which the author is working. They may be written in English, French or German.

NUCLEAR PHYSICS is published in monthly issues. The subscription price a volume of 700 pages is fl 57.00; 114s; a 15.00. Postfree.

SUBSCRIPTIONS should be sent to the publishers, NORTH-HOLLAND PUBLISHING COMPANY, P.O.Box 103, Amsterdam or to any subscription-agent.

BOOKS FOR REVIEW should be sent to Professor Rosenfeld.

No part of this issue may be reproduced in any form, by print, photoprint, microfilm or any other means without written permission from the publisher. Reprints, photoprints or microfilms are obtainable at cost from the publisher.

Printed in the Netherlands

2.F *Nuclear Physics* **12** (1959) 225—236; © *North-Holland Publishing Co., Amsterdam*

Not to be reproduced by photoprint or microfilm without written permission from the publisher

THE MECHANISM OF THE DIRECT INTERACTION PROCESS AT INTERMEDIATE ENERGIES

R. J. GRIFFITHS † and R. M. EISBERG

School of Physics, University of Minnesota, Minneapolis, Minnesota ††

Received 6 April 1959

Abstract: At intermediate energies, most inelastic proton scattering reactions are due to non-compound nucleus processes which are called direct interactions. Several mechanisms for direct interactions have been suggested: (a) nucleon-nucleon collisions in the diffuse surface of the nucleus, (b) nucleon-nucleon collisions occurring throughout the nucleus, (c) direct excitation of low-lying rotational states. Each of these appears to be capable of explaining the experimental data currently available (the energy and angular distribution of single inelastically scattered protons). To obtain additional data for the purpose of distinguishing between these mechanisms, we have made measurements of the angular correlation of pairs of protons emitted in direct interactions.

Using large solid angle plastic scintillation counters, and coincidence resolving times of ten millimicroseconds, measurements were made on the angular correlation in the range of separation angles 40° to 105°. The energy of the bombarding protons was 40 MeV and Cu, Ni and Pb were used as targets.

The results of the experiment indicate that mechanism (a) is predominant at these energies, and that the momentum of the struck nucleon is significantly lower than has been observed in experiments which measure the momentum distribution of nucleons which may be located anywhere within the nucleus.

1. Introduction

The characteristic features of inelastic proton scattering reactions at intermediate energies are: the energy distributions contain a large number of high energy inelastically scattered protons; the angular distributions of these protons are peaked forward, the total cross section for these processes is a fairly large fraction of the total reaction cross section [1]). Since each of these characteristics is in contradiction to the predictions of the compound nucleus model [2]), it is concluded that these reactions involve non-compound nucleus processes, which are called direct interactions. A number of different direct interaction mechanisms have been proposed, and three have been considered seriously.

1.1. NUCLEON-NUCLEON COLLISIONS IN THE DIFFUSE SURFACE OF THE NUCLEUS

This mechanism, suggested by Austern, Butler and McManus [3]) and also by Eisberg and Igo [1]), can give a very adequate explanation of the character-

† Present address: A.E.R.E., Harwell, England.

†† Supported in part by the U.S. Atomic Energy Commission.

istics of the direct interaction. A collision between the incident nucleon and a nucleon in the diffuse surface of the target nucleus would be approximately like a collision between a particle and a second stationary free particle of equal mass. For such a collision, the energy and angular distributions of the scattered particle are qualititatively similar to those observed in the direct interaction processes. Furthermore, the cross section for this mechanism would be comparable to the cross section for striking the diffuse surface, which is a large fraction of the total cross section for striking the nucleus. Quantitative calculations based on this mechanism [3]), particularly calculations which take into account the optical characteristics of the nucleus [4]), are in good agreement with the experimental data.

1.2. NUCLEON-NUCLEON COLLISIONS OCCURRING THROUGHOUT THE NUCLEUS

This mechanism was considered by Hayakawa, Kawai and Kikuchi [5]), who found that it, too, was capable of providing a successful fit to the experimental data. On the other hand, Elton and Gomes [6]) have raised objections to this mechanism by showing that there is a high probability that nucleons resulting from collisions in the interior of the nucleus will be trapped by internal reflection in the optical potential.

1.2. DIRECT EXCITATION OF LOW-LYING ROTATIONAL STATES

It should be possible for a proton to strike the edge of the nucleus and scatter off, leaving the nucleus in a rotational state. Since there are many low-lying rotational states, there should be many high energy inelastically scattered protons. Furthermore, a simple classical calculation balancing angular momentum shows that these protons will characteristically be scattered at forward angles. Quantitative calculations for such a mechanism have been performed by Yoshida [7]), and by Hayakawa and Yoshida [8]), who show that it can provide good agreement with the experimental data.

Which is the predominant mechanism for the direct interaction process? Since all three are capable of fitting (to one extent or another) the experimental data, it is apparent that data of a new variety are needed. It was suggested some time ago by Eisberg [9]) that a measurement of the angular correlation between two high energy nucleons emitted in time coincidence in a direct interaction might provide a sensitive test of the validity of the surface nucleon-nucleon collision mechanism. If direct interactions do involve nucleon-nucleon collisions in the surface of the nucleus, then occasionally both the incident and the struck nucleon should escape. Furthermore, one might expect to see in the angular correlation of these two nucleons some vestige of the sharp 90° angular correlation which characterizes the collision of two equal mass particles.

Such an experiment was attempted in 1956 by Eisberg and Hintz [10]) at the Minnesota proton linear accelerator, who looked for two coincident

protons from (p, 2p) processes on Cu and Pb at 40 MeV. The attempt was unsuccessful because, since the cross section is small, the 0.5 % duty cycle of the machine resulted in an accidental coincidence counting rate which was much larger than the real coincidence counting rate, for the one microsecond resolving time which was used. In the following year some results on a similar experiment were obtained by Cohen [11]). He investigated the (p, 2p) reaction on Ni^{58} initiated by 23 MeV protons from the 100 % duty cycle Oak Ridge Cyclotron, and used 0.1 microsecond resolving time. However, the major effort was expended on measuring the energy distributions of the protons emitted in coincidence and not enough data was obtained on the angular correlation to determine its characteristics. Measurements of the energy distributions (but not the angular correlations) of coincident protons emitted in (p, 2p) reactions in light elements at 185 MeV have been performed recently at the Uppsala cyclotron by Maris and Hillman [12]). The motivation of their experiments was quite different from that outlined above, since it has been known for some time that reactions at high energies on light elements proceed primarily through the volume nucleon-nucleon collision mechanism.

By using very large solid angle detectors and very short resolving times, it was finally possible to make the desired measurements at Minnesota. However, it was only barely possible. Despite the fact that hundreds of hours of machine time were used, the statistical accuracy of the data leaves much to be desired. Nevertheless, we report the results of these measurements which we feel to be quite interesting.

2. Experimental Apparatus

The experiment was performed on the University of Minnesota linear accelerator which produces a 39.8 ± 0.2 MeV proton beam with a duty cycle of 0.5 %. The proton beam was deflected by a magnet, focused by magnetic quadrupole lenses, and collimated to produce a non-diverging, mono-energetic low-intensity beam.

The experimental apparatus is shown in fig. 1. The scattering chamber was a $5\frac{1}{2}$ inch diameter chamber with a large wrap-around 0.002 inch mylar window which allows full view of the target by large solid angle detectors. It was mounted at the centre of an 8 foot scattering stand with two remotely controlled rotating arms, which held two detectors on either side of the incident beam. The two detectors and the incident beam were co-planar, the angular orientation of one detector was fixed, and the second detector was free to move from 20° to 80° measured from the direction of the incident beam.

The detectors were $2 \times 1 \times \frac{1}{2}$ inch plastic scintillators coupled by lucite light pipes to 14 stage RCA 6810A photomultipliers. The scintillators were

placed with their faces 3 inches from the centre of the target and subtended 0.226 steradians at the target. Lead shields were placed on the small angle side of the detectors to prevent detection of protons scattered from the window.

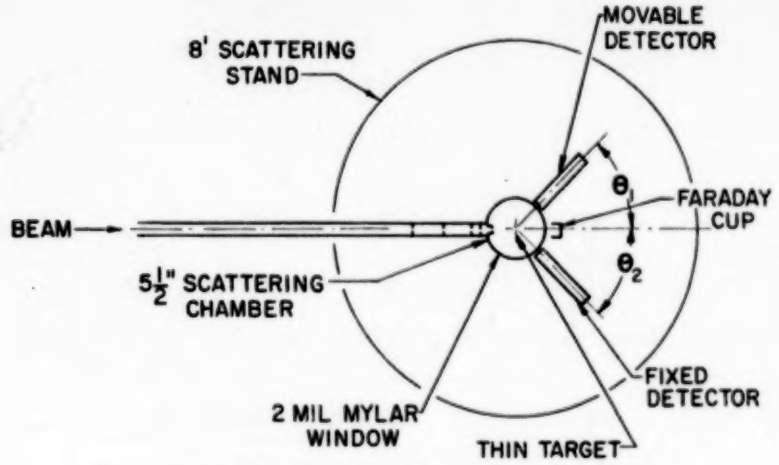

Fig. 1. Experimental apparatus.

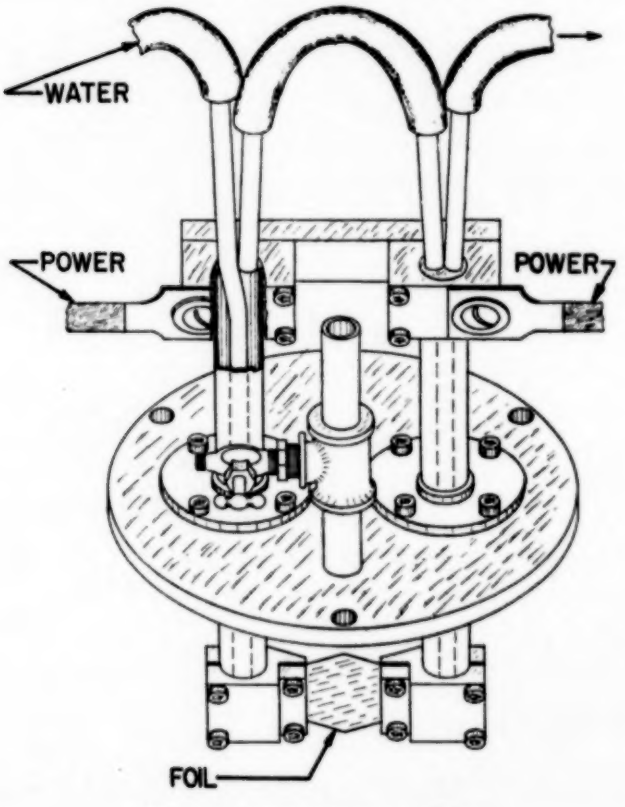

Fig. 2. Foil heater assembly.

The experiment was extremely sensitive to hydrogen contamination in the targets since this produces coincident protons from p—p scattering. To avoid the accumulation of pump oil, etc., it was necessary to continuously heat the 0.001 inch foil targets. Fig. 2 shows the apparatus used. The target

frame was arranged so that heating current of 200 A would be passed through the foil when in the evacuated scattering chamber. Teflon insulation around the copper stems acted both as insulators and as vacuum seals. The stems contain two concentric pipes which pass cooling water through the system and prevent anything except the foil from being heated. The assembly of the stems and the target could be raised out of the line of the beam when it was desired to make "target out" measurements.

The incident beam was monitored by collecting it in a small Faraday cup and measuring the charge with a 100 % feedback electrometer circuit. An auxiliary monitoring device, which will be described later, was also used.

A block diagram of the electronic apparatus is shown in fig. 3. Each phototube produces both negative and positive pulses. The negative pulses were clipped and amplified in cascaded Hewlett Packard distributed ampli-

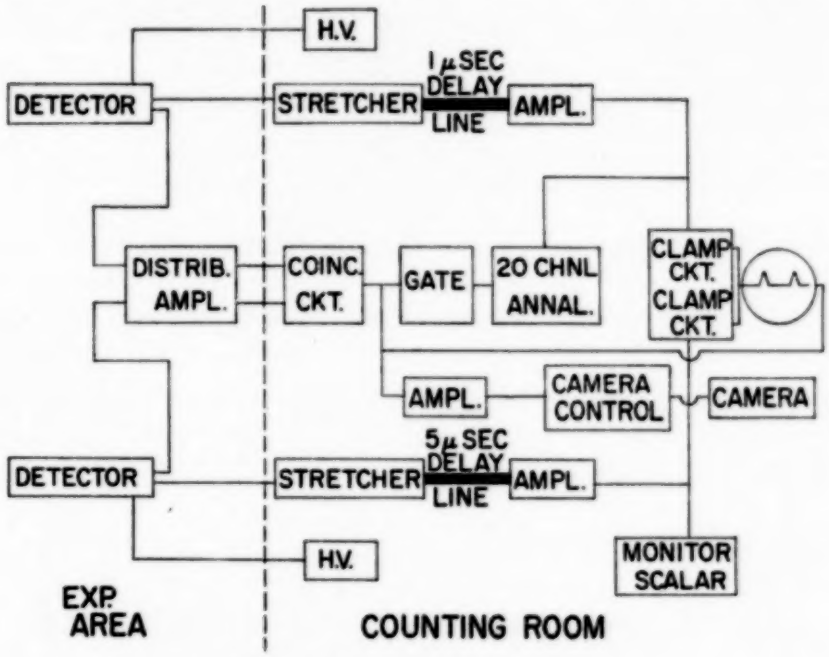

Fig. 3. Electronic block diagram.

fiers before being sent through long cables to the coincidence circuit in the counting room. The coincidence circuit was a modified Garwin type with biased diode threshold inputs. Its resolving time was 3 millimicroseconds and it had a single to double ratio of 30 to 1 (a very necessary feature since the circuit was required to accept pulses from a pair of 5 MeV protons and reject a single 40 MeV proton). The output of the coincidence circuit was used to trigger the gating circuit, the oscilloscope and the camera advance control.

The positive pulses from each of the detectors were amplified, fed into stretcher circuits, delayed by different times, and then displayed on a single oscilloscope trace which was photographed to record the energy of each of the

protons of a coincident pair. In addition, the positive pulse from the stationary detector was sent to a beam monitoring scalar and the positive pulse from the movable detector was sent to a twenty-channel pulse height analyzer. For each coincident pulse, the oscilloscope was triggered and the film advanced one frame after the photograph had been taken.

3. Experimental Procedure

The resolution of the coincidence circuit was measured under the actual conditions of the experiment by plotting, as a function of the length of cable added to one leg, the number of p—p scattering coincidences per unit beam obtained by scattering from a hydrogenous target at $\theta_1 = \theta_2 = 45°$. The resolution was shown to be limited by the width of the pulses, which was 10 millimicroseconds full width at half maximum. This measurement was also used to match the lengths of the long cables leading to the counting room.

The phototube voltages were adjusted so that pulses from two 5 MeV protons would just trigger the coincidence circuit, the 20 channel analyzer was calibrated, and the energy scale of the oscilloscope was calibrated.

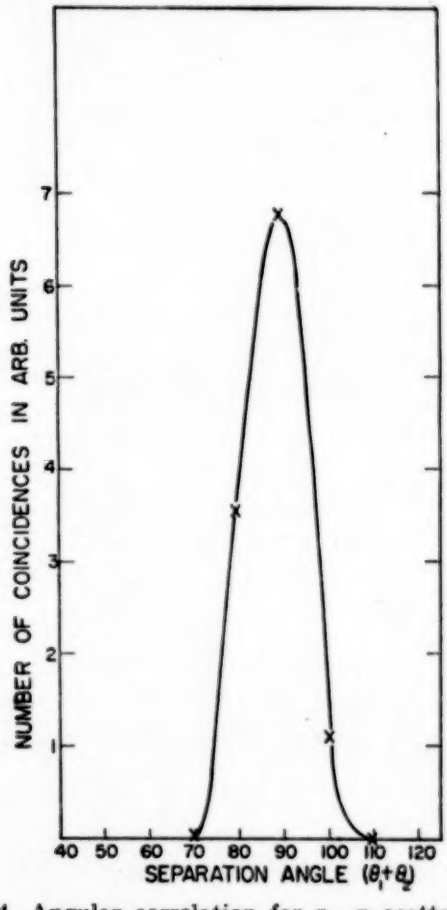

Fig. 4. Angular correlation for p—p scattering.

Protons of variable energy for making these calibrations were obtained by looking at p—p scattering from a hydrogenous target at various angles (using a small diaphragm in front of one detector to obtain good angular resolution).

To test the entire system, measurements were made of the angular correlation and energy distributions of proton pairs from p—p scattering in a hydrogenous target. Fig. 4 shows the angular correlation. The full width at half maximum is about 18°, which agrees with what would be expected from the angular width of the counters.

A clean metallic target was then inserted in the target holder and heated in vacuum. At each set of angles a photographic record was obtained of the amplitude of both pulses of each coincident pair, and also 20 channel analyzer pulse height distributions were obtained for the pulses from the movable detector. Measurements were made with targets of Ni, Cu, and Pb. In consideration of the angular resolution, it was not appropriate to make measurements of the angular correlation at points closer than 10°. With the fixed counter at $\theta_2 = 45°$, and the target perpendicular to the beam, measurements were made with the movable counter covering the angular range $\theta_1 = 25°-65°$. Next, setting the fixed counter at $\theta_2 = 25°$, and with the target rotated by 20°, measurements were made with the movable counter covering the range $\theta_1 = 25°-80°$. Additional data were obtained at $\theta_1 = \theta_2 = 20°$ for Ni and at $\theta_2 = 35°$, $\theta_1 = 65°$ and 80° for Cu.

At each angular setting, data was obtained both with the 20 channel analyzer gated to respond only when there was a coincidence, and also with the analyzer ungated so that it would respond to all the pulses in the movable detector. In a typical gated spectrum, a few pulses would be observed at an energy greater than 40 MeV—5 MeV—Q. (40 MeV is the energy of the incident protons, 5 MeV is the lower limit of a pulse in the fixed detector which can trigger the coincidence circuit, and Q is the Q-value for a (p, 2p) reaction.) Pulses in the gated spectrum above this energy correspond to events which are energetically impossible. These pulses must be due to accidental coincidences. They can be used to good advantage since they provide a convenient measure of the number of accidental coincidences in the lower energy part of the pulse height spectrum. The energy spectrum of accidental coincidences must have the same shape as the ungated spectrum. Therefore, by measuring the ungated spectrum and the number of energetically impossible accidental coincidences in the gated spectrum, it is easy to find the number of accidental coincidences in the part of the spectrum in which the true coincidences appear. The validity of this procedure was verified by making measurements of the gated spectra with an extra 20 feet of cable in one leg of the coincidence circuit, which is the standard technique for measuring accidental coincidences. Throughout the experiment the

accidental coincidence counting rate was kept below 25 % of the real coincidence counting rate.

Finally we mention that a number of checks were made to insure that the experiment was free from various kinds of background, neutron sensitivity of the scintillators, counting rate effects, etc.

4. Experimental Results

The angular correlation curves are shown in fig. 5. The data are presented in terms of the ratio of the number of coincident pairs to the number of single inelastic protons detected in the fixed detector, as a function of the separation angle $\theta_1+\theta_2$. All three curves are drawn to the same scale, but

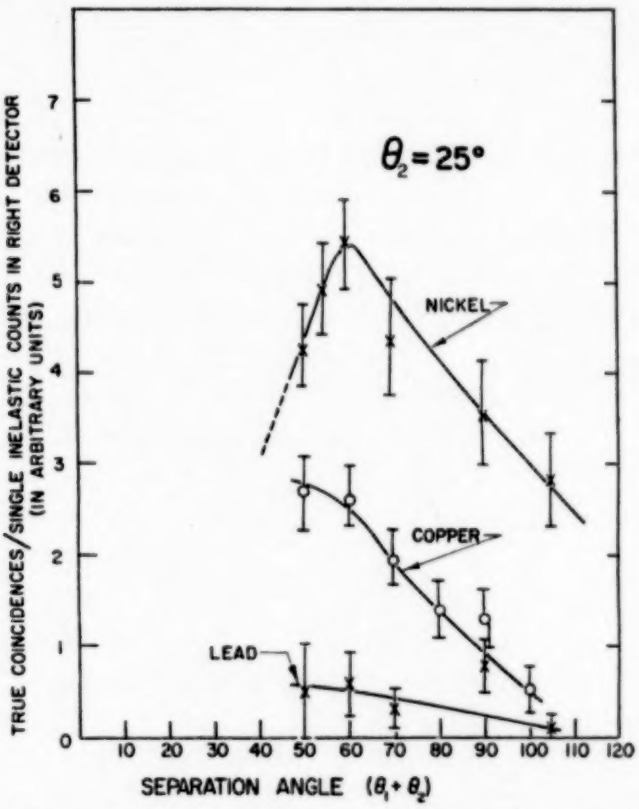

Fig. 5. Angular correlation for (p, 2p) reaction. The dotted portion of the Ni curve passes through the $\theta_1 = \theta_2 = 20°$ point.

that scale is arbitrary. The angular correlations have not been corrected for experimental angular resolution since the correction would be small. The data presented in this figure were all obtained with $\theta_2 = 25°$, except that the dotted portion of the Ni curve is drawn so as to pass through the point measured for $\theta_1 = \theta_2 = 20°$. Each data point represents the average of at least three or four separate measurements. In each of these measurements the general trends of the curves — particularly the fact that the Ni angular correlation has a maximum at about 60° — were consistently

reproduced. The flags on each point represent counting statistics which were, by far, the predominant source of error.

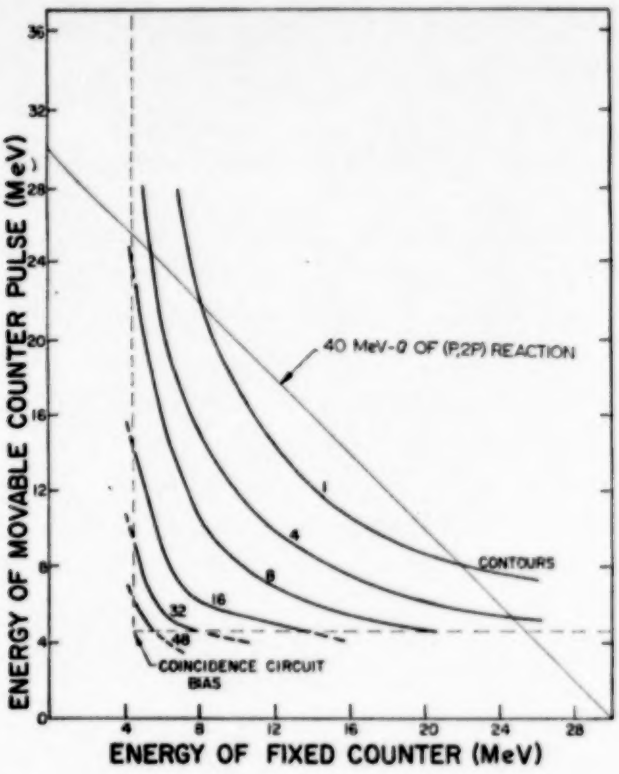

Fig. 6. Typical two-dimensional energy spectrum.

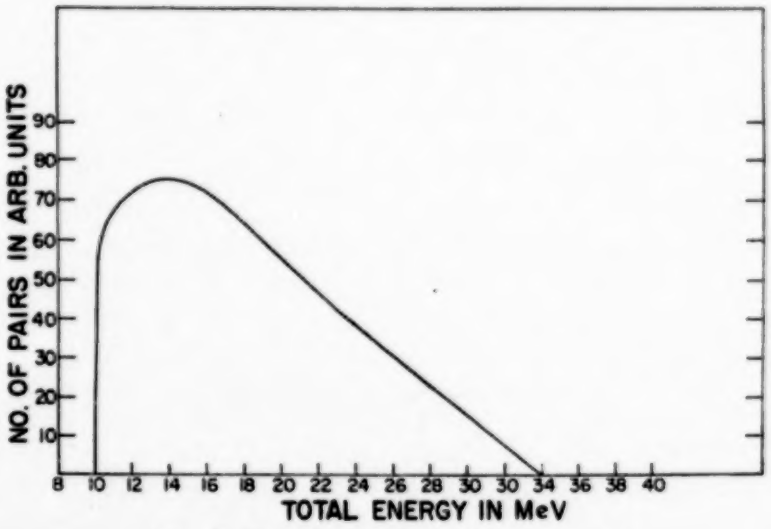

Fig. 7. Typical total energy spectrum.

Fig. 6 shows a contour plot of a typical two-dimensional energy spectrum. In such a spectrum, a point is plotted for each coincident pair with an abssisca and ordinate equal to the energies of the protons detected in the fixed and movable counters respectively. The distribution of these points is indicated by

a set of contour lines. These data show that it is most probable for the two protons to be emitted with an asymmetric sharing of the total energy, and that in most of the cases the total energy carried away by the two protons is relatively low. It was found that the features of the two-dimensional energy spectra were the same, within the statistical accuracy of the data, for all sets of angles and all elements.

Fig. 7 shows a typical spectrum of the total energy of the two protons. Again it was observed that the features of these spectra were very similar for all elements and all angles. Of course, the integrals of the total energy spectra, as well as the integrals of the two-dimensional energy spectra, varied as a function of element and angle in the manner indicated in fig. 5. The total energy spectra rise with decreasing energy from a threshold at 40 MeV minus the Q of the (p, 2p) reaction, until reaching a cut-off due to the bias of the coincidence circuit at 5 MeV per proton (and probably due also to the Coulomb barrier). The resolution of the apparatus for measuring the total energy of both protons was about 15 % full width at half maximum. Within this resolution, no evidence was seen for any structure in the total energy spectra.

By integrating the area under the angular correlation curves of Fig. 5, and evaluating the scale of the ordinate of those curves, it is possible to estimate a lower limit to the total number of (p, 2p) processes for each single inelastically scattered proton detected in the fixed detector. Only a lower limit can be obtained since the angular and energy range of the measurements was not complete; e.g., no measurements were made with the movable detector out of the plane defined by the incident beam and the fixed detector. In the case of Ni, such an estimate shows that for each inelastically scattered proton detected in the fixed detector, the probability that there will be another proton emitted in coincidence at any angle and at any energy is *at least* 0.1. It is apparent from fig. 5 that the lower limit of this probability is smaller for Cu and even smaller for Pb; but it is also apparent from the figure that the lower limit has less significance in these cases, and so it will not be quoted.

5. Conclusions

In a collision between an incident proton and a stationary free proton in a zero-potential nucleus, the two protons would be emitted with a sharp angular correlation peaked at 90°. In actuality the struck proton is bound and has an initial momentum distribution, and there is also a nuclear potential in which the emitted protons are refracted, so one would expect that the peak of the angular correlation curve would be shifted from 90° and that the peak would be broadened. Thus the peaked angular correlation measured for Ni qualitatively agrees with the behaviour expected in either

of the nucleon-nucleon collision direct interaction mechanisms, but it is hard to see how this angular correlation could arise if the direct interaction mechanism involved the direct excitation of low-lying rotational states. Although no peak was observed in the Cu angular correlation, the data can be interpreted as indicating only that the peak is shifted to the limit of the angular range accessible to the measurement. For Pb the probability for the coincident emission of two protons is so small (presumably because of the Coulomb barrier) that the angular correlation measurements are not accurate enough to warrant discussing.

Nuclei are relatively opaque to nucleons of the energies involved in this experiment and, furthermore, the potential seriously inhibits the emission of protons from the interior of the nucleus [6]). Thus, unless the collisions occur near the surface, and unless the plane containing the trajectories of the two protons after the collision is approximately tangent to that surface, so that the protons are not required to traverse the opaque core, the probability that both protons are actually emitted would be small. Since the collision plane can have any orientation, the total probability for the emission of a pair of protons would be less than the probability for the emission of a single proton even for the surface nucleon-nucleon collision mechanism — and would be very much less for the volume nucleon-nucleon collision mechanism. For Ni the *lower limit* to the probability of emitting a pair is about 10 % of the probability of emitting a single proton. This argues, perhaps, for the surface collision mechanism. Under any circumstances, this argument shows it is possible that the initial process in a direct interaction is always a nucleon-nucleon collision, even though the experiment indicates that a (p, 2p) reaction probably does not occur each time a single inelastically scattered proton is emitted.

If the direct interaction process occurs in a time short compared to the nuclear re-arrangement time, the total energy carried away by the two protons is a measure of the binding energy of the struck proton. Thus one might expect the spectra of total energy to exhibit peaks corresponding to the independent particle model energy states of protons in the target nucleus. According to the numerical values computed by Green [13]) for the case of Ni, several of these states should be seen even with the 15 % energy resolution of this experiment. Independent particle model energy states have been observed in the (p, 2p) experiments at 185 MeV on very light nuclei [12]), but they are not seen in the present experiment at 40 MeV on intermediate nuclei. However, there is an important difference between the two experiments; in the former experiment the struck proton can be anywhere in the nucleus, but in the latter experiment, the struck proton is probably constrained to be near the surface. It is possible that the contrasting results of these experiments can be explained by this difference.

In an accompanying paper [14]), McCarthy, Jezak and Kromminga analyze the results of this experiment. Their analysis confirms the qualitative conclusions which we have stated above. From the position of the peak of the Ni angular correlation curve and the form of the two-dimensional energy spectrum, they estimate the average refraction of the emitted protons in the nuclear potential. From this they conclude that the average distance from the point of collision to the centre of the nucleus is about 7 or 8×10^{-13} cm. The width of the angular correlation curve is primarily determined by the momentum distribution of the struck nucleon. The analysis indicates that this momentum is quite low (0.5 MeV $< p^2/2m <$ 1.5 MeV), compared to what has been observed in experiments which measure the momentum distribution of nucleons which may be located anywhere within the nucleus. However, since the collisions are confined to the surface in the present experiment, the angular correlation is essentially a measurement of the momentum distribution of nucleons in the nuclear surface. An interpretation of these contrasting measurements in terms of the Wigner phase space distribution function indicates that they are not necessarily in disagreement.

It is a pleasure to thank Drs. N. M. Hintz and I. E. McCarthy for informative discussions, and Messrs. R. P. Featherstone and E. H. Brekhus for technical assistance.

References

1) R. M. Eisberg and G. Igo, Phys. Rev. **93** (1954) 1039
2) Blatt and Weisskopf, Theoretical Nuclear Physics (Wiley and Co., 1952)
3) N. Austern, S. T. Butler and H. McManus, Phys. Rev. **92** (1953) 350
4) C. A. Levinson and M. K. Banerjee, Annals of Phys. **2** (1957) 471
5) S. Hayakawa, M. Kawai and K. Kikuchi, Prog. Theor. Phys. **13** (1955) 415
6) L. R. B. Elton and L. C. Gomes, Phys. Rev. **105** (1957) 1027
7) S. Yoshida, Proc. Phys. Soc. A **69** (1956) 668
8) S. Hayakawa and S. Yoshida, Prog. Theor. Phys. **14** (1955) 1
9) R. M. Eisberg, Univ. of Cal. Rad. Lab. Report UCRL 2240 (1953)
10) R. M. Eisberg and N. M. Hintz, Minnesota Linear Accelerator Progress Report (1957)
11) B. L. Cohen, Phys. Rev. **108** (1957) 768
12) A. J. Maris and P. Hillman, Nuclear Physics **7** (1958) 1
13) A. E. S. Green, Phys. Rev. **104** (1956) 1617
14) I. E. McCarthy, E. V. Jezak and A. J. Kromminga, Nuclear Physics **12** (1959) 274

1.C *Nuclear Physics* **12** (1959) 237—240; © *North-Holland Publishing Co., Amsterdam*
Not to be reproduced by photoprint or microfilm without written permission from the publisher

APPROXIMATE SOLUTIONS OF THE DENSITY MATRIX EQUATION FOR A LOCAL AVERAGE FIELD

N. H. MARCH and W. H. YOUNG
Department of Physics, The University, Sheffield

Received 13 April 1959

Abstract: It is shown that a condition derived by Naqvi [1]) from the density matrix equation, and used by him to generalize the statistical theory, can be regarded as constituting a differential form of the virial theorem. This suggests that Naqvi's condition is satisfied by the customary treatments, and this is demonstrated directly.

A recent paper by Naqvi [1]) in which surface corrections to the statistical theory are examined by means of the density matrix method prompts us to record briefly some results of earlier unpublished work which have a bearing on Naqvi's investigation. We also comment on the relation between our earlier variational approach [2]) and Naqvi's procedure.

For brevity, we restrict our considerations to a one-dimensional case with a local average field, although various generalizations can be made to three dimensions, as described by Naqvi. Then, for particles moving in a common local potential $V(x)$, we wish to solve the equation

$$\frac{\partial^2\rho}{\partial x'^2}-\frac{\partial^2\rho}{\partial x^2}=\frac{2m}{\hbar^2}[V(x')-V(x)]\rho \tag{1}$$

with normalization, Hermiticity and idempotency conditions on the density matrix $\rho(x', x)$, such that the eigenvalue sum E given by

$$E=-\frac{\hbar^2}{2m}\int\left[\frac{\partial^2\rho(x', x)}{\partial x^2}\right]_{x'=x}\mathrm{d}x+\int\rho(x, x)V\mathrm{d}x \tag{2}$$

is an absolute minimum. Following exactly Naqvi's procedure we use new coordinates

$$\xi=\tfrac{1}{2}(x'+x), \qquad \eta=\tfrac{1}{2}(x'-x)$$

and seek a solution of the resulting equation

$$\frac{\partial^2\rho}{\partial\xi\partial\eta}=\frac{2m}{\hbar^2}[V(\xi+\eta)-V(\xi-\eta)]\rho$$

by expanding about the point $\eta=0$. Thus we write

$$\rho(\xi, \eta)=n(\xi)+\sum_{j=1}^{\infty}\eta^{2j}a_{2j}(\xi), \tag{4}$$

where we have written $n(\xi)$ for the particle density $\rho(\xi, 0)$. By substitution in (3) it is easy to verify that

$$a'_2 = \frac{2m}{\hbar^2} nV', \tag{5}$$

$$a'_4 = \frac{m}{\hbar^2} [a_2 V' + \tfrac{1}{6} nV'''], \tag{6}$$

and higher terms may easily be obtained if required. We note that if the diagonal element were known, the entire matrix could be built up by this method. We should emphasize here that (5) is the essential result in Naqvi's attempt to generalize the statistical theory. Earlier unpublished work by us led to (5) being viewed as constituting a considerable generalization of the virial theorem, a kind of differential form of the customary expression; and the justification for this is outlined below.

Using (2) and (4) the kinetic energy T may immediately be written as

$$T = -\frac{\hbar^2}{4m} \int [\tfrac{1}{2} n''(x) + a_2(x)] \mathrm{d}x \tag{7}$$

and for most cases of interest we can drop the term in n'', although for boundary conditions other than the usual ones its retention may prove necessary. Assuming however that n'' integrates to zero, eq. (7) is easily rewritten as

$$T = \frac{\hbar^2}{4m} \int x a'_2 \mathrm{d}x - \frac{\hbar^2}{4m} (x a_2)_{\text{limits}}. \tag{8}$$

With the reservation again that no contribution arises from the boundaries, the use of (5) in (8) leads to the usual form of the virial theorem

$$2T = \int nxV' \mathrm{d}x. \tag{9}$$

Incidentally, this proof appears to be much more direct than the customary method based on wave functions.

Since the usual statistical theories are known to satisfy the virial theorem, it appeared likely to us that they would also satisfy (5) and this can be verified, as discussed below. This point does not appear to be made clear in Naqvi's work.

In the process of outlining the proof of (5) first for the original Thomas-Fermi theory, it seems worthwhile to note the way in which this approximation fits into the present framework, as we are not aware that this has been pointed out previously. If we go back to (3), and replace $V(\xi+\eta)-V(\xi-\eta)$ by $2\eta V'(\xi)$, corresponding to the neglect of the third and higher derivatives of the potential, the Thomas-Fermi density matrix [3])

$$\rho(\xi, \eta) = \frac{\sin\{2\pi\eta n(\xi)\}}{2\pi\eta} \tag{10}$$

is an exact solution of the resulting differential equation, provided

$$-nn' = \frac{4m}{\hbar^2} V' \tag{11}$$

or, by integration,

$$n^2 = \frac{8m}{\hbar^2} (E'-V), \tag{12}$$

giving the usual Thomas-Fermi density. Unfortunately, of course, this matrix usually corresponds to a cut-off in the particle density and does not satisfy the idempotency condition exactly. Nevertheless, comparing (4) and (10) we find

$$a_2(\xi) = -\tfrac{2}{3}\pi^3 n^3(\xi) \tag{13}$$

and from (11) and (13), eq. (5) is immediately verified.

Naqvi's basic aim in his proposed generalization may now be said to consist in modifying the Thomas-Fermi density matrix in such a way that (5) is preserved while the idempotency condition is satisfied with improved accuracy. It is therefore of interest to demonstrate that the variational density matrix for N particles which we proposed earlier [2]) entirely fulfils Naqvi's requirements. This matrix, which leads to a method intimately connected with von Weizsäcker's scheme, is defined as follows:

$$\rho(\xi, \eta) = \{y_1(\xi+\eta)y_1(\xi-\eta)\}^{\frac{1}{2}} \rho_0(\tfrac{1}{2}(y'+y), \tfrac{1}{2}(y'-y)). \tag{14}$$

Here we have used the notation $y' = y(\xi+\eta)$, $y = y(\xi-\eta)$,

$$\rho_0(\xi, \eta) = \frac{\sin 2\pi N\eta}{\sin 2\pi\eta}$$

and y is the variational function satisfying the Euler equation

$$\frac{\hbar^2}{8m} (N^2-1)y_1^2 + V - \frac{\hbar^2}{4m} \frac{y_3}{y_1} + \frac{\hbar^2}{8m} \frac{y_2^2}{y_1^2} = E', \tag{15}$$

where y_n denotes the nth derivative of y. We then find the following results for the matrix (14), by comparison with (4):

$$n = Ny_1 \tag{16}$$

$$a_2 = -\tfrac{2}{3}\pi^2 N(N^2-1)y_1^3 + \tfrac{1}{2}N\left(y_3 - \frac{y_2^2}{y_1}\right). \tag{17}$$

Again, using (15) and (17), it is a straightforward matter to verify (5). The exact idempotency of this matrix follows immediately as a consequence of its construction from N orthonormal transformed plane waves [2]).

We conclude that the 'differential form of the virial theorem' embodied in (5) is satisfied by existing statistical density matrices, and that it would appear necessary to go to (6) in order that the knowledge obtained by

solution of the differential equation (3) may be used to improve the customary treatments. In this connection, a'_4 may be derived from the matrix (14) above and then compared with the right hand side of (6). While (6) is not exactly satisfied, remarkable similarity between a'_4 and the right hand side is evident, and in particular the terms of highest order in N are identical. Thus, in any given application, this would provide one possible method of testing the accuracy of the matrix (14). In this connection, we note finally that while (14) is satisfactory from a fundamental theoretical point of view, the possibility of obtaining higher numerical accuracy for a given potential by alternative approaches such as that suggested by Naqvi is certainly not excluded.

References

) M. A. Naqvi, Nuclear Physics **10** (1959) 256
2) N. H. March and W. H. Young, Proc. Phys. Soc. **72** (1958) 182
3) N. H. March, Proc. Phys. Soc. A **70** (1957) 839

2.E *Nuclear Physics* **12** (1959) 241—248; © *North-Holland Publishing Co., Amsterdam*

Not to be reproduced by photoprint or microfilm without written permission from the publisher

PROTON TOTAL REACTION CROSS SECTIONS AT 34 MeV

T. J. GOODING †

University of Minnesota, Minneapolis, Minnesota ††

Received 9 March 1959

Abstract: Proton total reaction cross-sections have been measured for five elements at 34 ± 2.5 MeV. Attenuation measurements were made with a dE/dx telescope and a biased E counter, in poor geometry. Corrections for elastic and inelastic scattering were determined experimentally. The results have been compared with optical model analysis to select sets of parameters fitting the elastic scattering angular distributions equally well. For carbon the measurements favour the solution with the smaller radius constant. For the other elements the optical model predictions are in good overall agreement but further analysis is required.

1. Introduction

During the last few years the optical model of the nucleus has been applied extensively to the results of nucleon-nucleus scattering experiments. In the energy range from 10 to 90 MeV the optical model analysis have been mainly restricted to neutron total cross-sections and proton elastic scattering. The need for proton total reaction cross-sections has recently been demonstrated in the analysis by Saxon *et al.*[1]) and Glassgold *et al.*[2]). They have shown that proton elastic scattering angular distributions can be fitted equally well with different sets of optical model parameters. In particular the imaginary part of the potential is not well determined from the elastic scattering alone. Since the total reaction cross-section is fairly sensitive to this parameter measurements of reaction cross-sections would help to resolve these ambiguities.

The measurement of proton total reaction cross-sections in an attenuation experiment is complicated by the energy loss by ionization in the attenuators. The permissable attenuation is thus restricted by the energy resolution desired in the experiment. In neutron attenuation experiments the quantity $nx\sigma$ (the transmission being $\exp(-nx\sigma)$) may be of the order of unity, whereas in a similar proton experiment $nx\sigma$ may be as small as 10^{-3}. Consequently it is extremely difficult to obtain statistical accuracy in proton attenuation experiments, particularly at low energy since $nx\sigma$ for a given percentage energy loss decreases with energy.

† Now at the A.E.R.E., Harwell, England.

†† This work was supported in part by the U.S. Atomic Energy Commission.

Proton total reaction cross-sections have been measured at 134 MeV [3]) and at several energies above 200 MeV. No experimental information below 134 MeV has been reported prior to this experiment. In this experiment proton total reaction cross-sections have been measured for the elements C, Al, Fe, Sn and Pb at 34 ± 2.5 MeV.

2. Experimental Procedure

The attenuation of the proton beam was determined by an anti-coincidence measurement of the number of protons removed from the beam. A counter telescope (henceforth the dE/dx counters) introducing a small energy loss to the beam was placed in front of an attenuator. The protons were stopped in a counter (henceforth the E counter) put into anti-coincidence with the dE/dx counters and placed after the attenuator. The attenuation was measured in poor geometry with the E counter subtending a cone with a half angle of 45° at the attenuator.

To discriminate between elastically and inelastically scattered protons, the E counter was biased just below the full energy. Owing to the energy spread of the elastically scattered protons, and instabilities in the electronics, it was necessary to set the bias 6.0 MeV below the full energy. The proton energy at the E counter after passing through the dE/dx counters and the attenuator was 31.5 MeV. The E counter was therefore biased to accept only protons with energy $\geqq 25.5$ MeV.

In an experiment of this type the total reaction cross-section is determined from the anti-coincidence rate between the dE/dx and E counters from the relation

$$\frac{\text{Number of anti-coincidences}}{\text{Number of incident protons}} = 1 - \exp(-nx\sigma)$$

where the number of anti-coincidences represents the difference between the attenuator-in and attenuator-out counts. Two corrections must be made to this cross-section to allow for elastic scattering outside the solid angle subtended by the E counter and for inelastic scattering into this solid angle with energy above the bias. In this experiment both corrections were small and were determined experimentally.

The major limitation on the accuracy attainable in the experiment was introduced by nuclear interactions in the E counter. Even though a full energy proton had entered the detector it was possible to receive a pulse lower than the bias since the proton could make a nuclear interaction in the scintillator (for example a (p, n) reaction) and transfer only part of its energy to it. It has been shown [4]) that of the order of 2—3 percent of a 40 MeV proton beam stopping in a NaI scintillator suffer nuclear interactions in the

scintillator resulting in an output pulse lower than the pulse received from a full energy proton. For a plastic scintillator this effect is of the order of 4 percent and introduced an attenuator-out counting rate approximately five times the difference between attenuator-in and attenuator-out counts. This severely restricted the statistical accuracy of the measurements. This situation could be improved by increasing the attenuation at the sacrifice of energy resolution. A compromise was made with the attenuators introducing a 5.0 MeV energy loss. The mean proton energy in the attenuators was then 34 MeV. The energy spread of the incident proton beam ($\approx \pm 100$ keV) was negligible.

A further complication was introduced by the energy dependence of the nuclear reactions in the counter. When the attenuator was inserted the energy of the protons incident on the counter changed by 5.0 MeV. Consequently the number of nuclear reactions in the counter for a given amount of proton beam would also change and a simple attenuator-out measurement would not give the true background. To eliminate this effect an absorber was placed in front of the dE/dx counters when the attenuator-out measurements were made. The thickness of this absorber was adjusted so that in the attenuator-out measurements the energy of the protons at the E counter was the same as for the attenuator-in measurements. Now, for protons of the same energy incident on the counter, the percentage of the nuclear reactions would be the same and the attenuator-out measurements would give the true background. Since the absorber was in front of the dE/dx counters it would not affect the anti-coincidence rate between the counters. The second order effect due to the change in energy of the protons incident on the dE/dx counters was negligible.

The absorber thickness was determined by replacing the plastic E counter with NaI and then comparing pulse height spectra first with the absorber and then with the attenuators. In this way it was possible to adjust the attenuators and the absorber so that the proton energy at the E counter was constant to within ± 100 keV. A small error was assigned to allow for this uncertainty.

3. Experimental Apparatus

The experimental arrangement is shown in fig. 1. The 40 MeV beam of the Minnesota Linear Accelerator, drawn from the second tank of the accelerator was coasted through the third tank, collimated, and magnetically deflected 10° into the experimental area. After deflection the beam was further collimated and passed through a 0.001″ dural foil into the dE/dx telescope. The absorber discussed in the previous section was placed between the second and third tanks of the accelerator. In this type of experiment it is

essential to have a monoenergetic beam with a small cross sectional area to define the solid angle subtended by the E counter at the attenuator. $\frac{1}{8}''$ collimators were placed before and after the magnet, and a $\frac{1}{4}''$ anti-scattering baffle was located 8′ from the last collimator.

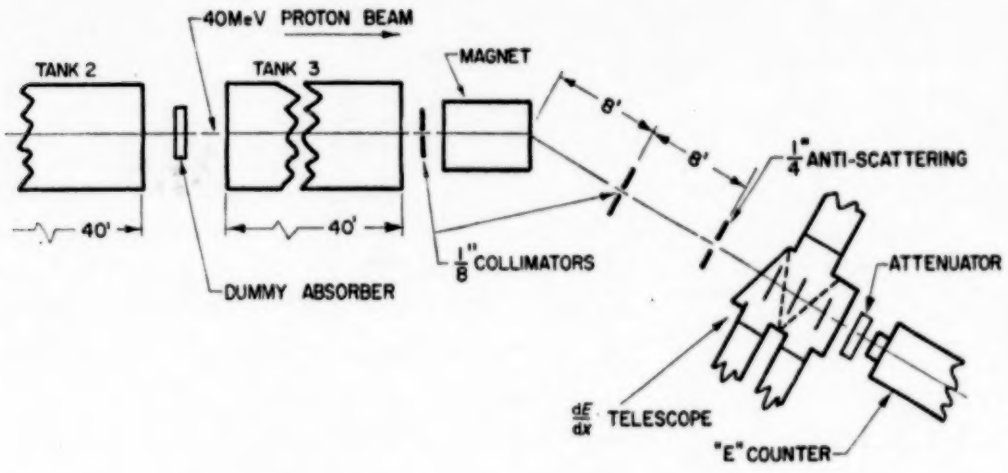

Fig. 1. Schema of the experimental apparatus.

The $\mathrm{d}E/\mathrm{d}x$ telescope consisted of three identical plastic scintillators ($\frac{1}{2}'' \times \frac{1}{2}'' \times 0.025''$) introducing approximately 3.0 MeV energy loss to the beam. It was not sufficient to have a single $\mathrm{d}E/\mathrm{d}x$ counter since a low energy proton entering the detector could produce a large pulse in $\mathrm{d}E/\mathrm{d}x$ and a small pulse in E resulting in a false anti-coincidence. Furthermore a broad statistical distribution of pulses would be obtained from a single thin $\mathrm{d}E/\mathrm{d}x$ counter due to the Landau effect. It has been shown by Igo and Eisberg [5]) that if several $\mathrm{d}E/\mathrm{d}x$ counters are used in coincidence always selecting the smallest of the pulses from the counters then the width of the resulting statistical distribution will be reduced.

The E counter was a $2\frac{1}{4}''$ diameter $\times \frac{1}{2}''$ thick plastic scintillator connected via a lucite light pipe to a Dumont 6292 photomultiplier. A brass cap was placed over the scintillator blocking off the outside rim to eliminate edge effects.

The electronic arrangement is shown in fig. 2. The average counting rate in the $\mathrm{d}E/\mathrm{d}x$ telescope was of the order of 3 000 counts/minute. Since the accelerator is a pulsed machine the corresponding instantaneous rate was approximately 10^4 counts/second. Particular care was necessary to avoid counting rate effects. To obtain statistical accuracy $\approx$ 7 to 10 percent it was necessary to count at this rate for approximately 20 hours per element. Consequently stringent stability requirements had to be placed on the equipment in

particular that associated with the E counter, up to and including the discriminator.

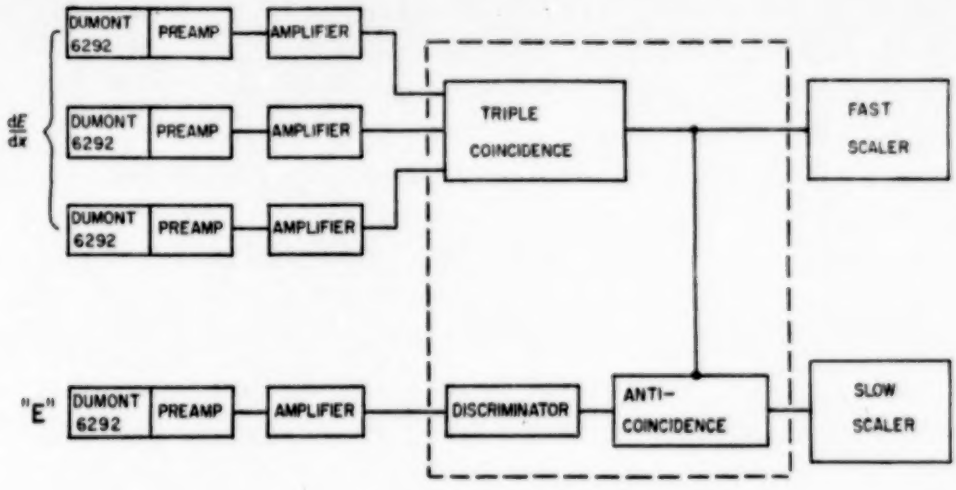

Fig. 2. Block diagram of the electronics.

4. Corrections

The correction for elastic scattering outside the solid angle subtended by the E counter was determined by integrating graphically the elastic scattering angular distributions of Hintz [6]) and Brussel [7]) at 40 MeV and Leahy [8]) and Wright [9]) at 31 MeV in the angular range from 45° to 180°. The errors introduced by the integration and the interpolation to 34 MeV were small compared with the statistical errors. For aluminium the integrated cross-sections were 63 mb at 30.6 MeV and 102 mb at 40 MeV. The interpolated value was 82 ± 10 mb and should be compared with the uncorrected result of 662 ± 40 mb. A summary of the corrections and the uncorrected results is shown in table 1.

TABLE 1

Summary of the elastic and inelastic corrections and the uncorrected results. The final results are obtained by adding the inelastic correction and subtracting the elastic correction.

Element	Elastic Scattering (mb)	Inelastic Scattering (mb)	Uncorrected Results (mb)
Carbon	57 ± 10	33 ± 8	469 ± 16
Aluminium	82 ± 10	20 ± 10	662 ± 40
Iron	80 ± 20	20 ± 12	962 ± 70
Tin	90 ± 20	25 ± 15	1995 ± 95
Lead	98 ± 15	65 ± 30	1810 ± 110

The inelastic correction was measured at 40 MeV. The total inelastic cross-section is of the order of 15 percent of the total reaction cross-section. The correction required included only the angular range from 0° to 45° and the energy interval from $Q = 0$ to -6.0 MeV. Consequently the correction was expected to contribute only a few percent of the total cross-section, and the error introduced by making the measurement at 40 MeV instead of 34 MeV would be negligible.

The angular distribution of the inelastic scattering to all levels with $|Q| \leqq 6.0$ MeV was measured for the five elements using the small angle scattering chamber discussed in ref. [4]). The chamber was modified for use with solid targets. For carbon only the 4.4 MeV level was excited and could be resolved without difficulty. For the other elements individual levels were not resolved. The procedure was to integrate the energy interval at each angle and plot the integrated cross-section as a function of the scattering angle.

5. Errors

Statistical fluctuations in the number of counts recorded contributed the major source of experimental error. To avoid errors due to instabilities in the electronics alternate attenuator-in and attenuator-out measurements were made at approximately 15 minute intervals. The errors quoted in the uncorrected results in table 1 represent standard deviations on the total number of counts recorded. The errors introduced by the corrections and several second order effects have been folded into the statistical errors in the final analysis.

A small error was introduced by the adjustment of the absorber required to give a constant proton energy at the E counter. To estimate this error the integral pulse height distribution in the E counter was plotted by varying the bias and recording the number of anti-coincidences. From the slope of the curve at the normal bias setting (6.0 MeV below full energy) the uncertainty in energy was translated into an error in the attenuator-out anti-coincidence rate.

The finite size of the proton beam introduced an uncertainty in the solid angle subtended by the E counter. This was allowed for in the integration of the elastic and inelastic scattering angular distributions.

Elastic scattering from the last $\mathrm{d}E/\mathrm{d}x$ scintillator outside of the solid angle subtended by the E counter was minimized by having a thin scintillator and mounting it close to the attenuators. An error was introduced by the change in this scattering due to the 5.0 MeV energy difference when the absorber was inserted in front of the $\mathrm{d}E/\mathrm{d}x$ scintillators.

6. Results and Conclusions

The experimental results † and the predictions of the optical model are shown in table 2. At 40 MeV the elastic scattering angular distributions were fitted equally well with two sets of parameters with the radius constant R_0, and the imaginary part of the potential W shown in table 2. In the

TABLE 2

Comparison of the experimental and theoretical proton total reaction cross-sections. In the optical model analysis at 40 MeV the elastic scattering angular distributions were fitted equally well for two sets of parameters with the radius constant R_0 and the imaginary part of the potential W as shown. At 31.5 MeV R_0 was fixed at 1.33, and W at −15.5 MeV.

Element	Experiment	Optical Model Analysis			
	34 ± 2.5 MeV	Glassgold *et al.* 40 MeV			Saxon *et al.* 31.5 MeV
	σ_R (mb)	R_0 (10^{-13} cm)	W (MeV)	σ_R (mb)	σ_R (mb)
C	445 ± 20	1.20 1.31	− 9.6 − 5.9	381 314	390
Al	600 ± 42	1.20 1.31	−11.1 −10.0	680 705	685
Fe	902 ± 72				1130
Sn	1930 ± 100				
Pb	1775 ± 120	1.31 1.39	−20.0 −14.4	2002 2104	1870

analysis at 31.5 MeV only one set of parameters was considered with the radius constant $R_0 = 1.33$ and $W = -15.5$ MeV. Since the reaction cross-sections calculated with the optical model do not vary rapidly with energy both analyses can be compared with the experiments.

The optical model calculations are in good overall agreement with the experimental results. The measurements do not, however, resolve the ambiguities in the analysis †† except for carbon. For this element at 40 MeV, the solution with $R_0 = 1.31$ gave slightly better agreement with the elastic scattering but since this improvement was at the expense of a very small reaction cross-section it should not be considered seriously. The large cross-section predicted for lead suggests that a smaller radius constant should be tried.

† Eisberg *et al.* at Minnesota using an improved experimental arrangement have recently checked some of these measurements. Good agreement is found except for Sn which falls on a smooth curve joining Fe and Pb.

†† *Editor's Note:* It would seem that such ambiguities ought to be resolved if further calculations were done with the optical model at 31.5 MeV energy.

At the present time optical model calculations are being carried out including a spin-orbit interaction in the potential. Although no quantitative results are available it has been shown qualitatively that the introduction of the spin-orbit term to a given set of parameters does not change the reaction cross-section appreciably. However, when the analysis including the spin-orbit interaction is completed, it may be necessary to change the parameters to give best fits to the elastic scattering and change the reaction cross-section accordingly. It now remains to improve the optical model analysis.

I would like to thank Professor R. M. Eisberg for suggesting this experiment and for his guidance and close cooperation throughout. It is a pleasure to thank Professor J. H. Williams and Professor N. M. Hintz for many helpful suggestions. I am indebted to Mr. E. Brekhus for providing and maintaining the electronic equipment and Mr. R. Featherstone and the crew of the Linac for the operation of the accelerator.

References

1) Meklanaoff, Nodvik, Saxon and Wood, Phys. Rev. **106** (1957) 793
2) Glassgold and Kellogg, Phys. Rev. **109** (1958) 1291
3) Cassels and Lawson, Proc. Phys. Soc. A **67** (1954) 125
4) Johnston and Swenson, Phys. Rev. **111** (1958) 212
5) Igo and Eisberg, Rev. Scient. Instr. **25** (1954) 450
6) N. M. Hintz, Bull. Am. Phys. Soc. **2** (1957) 14
7) M. Brussell, Ann. Prog. Rep., Minnesota Linear Accelerator (1957)
8) J. Leahy, U.C.R.L. Report 3273 (Febr. 1956)
9) B. T. Wright, U.C.R.L. Report 2422 (Nov. 1953)

2.A.1:
6.A.

Nuclear Physics **12** (1959) 249—260; © *North-Holland Publishing Co., Amsterdam*
Not to be reproduced by photoprint or microfilm without written permission from the publisher

THE MULTIPLE SCATTERING OF NEUTRONS AT RESONANCES

T. J. KENNETT and L. M. BOLLINGER
Argonne National Laboratory, Lemont, Illinois †

Received 10 March 1959

Abstract: The effects of multiple scattering of neutrons at resonances have been investigated experimentally and by means of a Monte Carlo calculation. Multiple scattering in thick samples has been shown to produce a peculiar distribution in the time-of-flight spectrum, the characteristics of which have been reproduced by computation. The results of this investigation show that quantitative information about partial cross sections is of questionable value when multiple scattering is an important factor.

1. Introduction

The growing interest in the measurement of partial neutron cross sections has led to an increasing need for a quantitative method of considering the problem of multiple scattering of the neutrons in the sample being studied. In the past, estimates have been made for this effect when it is small [1]). However, when conditions are such that multiple scattering becomes probable, meaningful corrections cannot generally be derived by analytic methods, even though the physical processes involved are thoroughly understood. Therefore, to obtain an accurate solution to the problem we must turn to the Monte Carlo method.

The problem of special interest to us concerned the study of γ-ray transitions resulting from the capture of neutrons in specific resonances of Mn^{55}. For these resonances the radiative capture cross section σ_γ is less than 5 % of the total cross section σ_t, so that multiple scattering of neutrons is the major process for samples thick enough to insure a usably high rate of capture. Since we observe low-energy γ-ray transitions, it is necessary to know the spatial distribution of the captured neutrons in order to correct for γ-ray absorption within the sample. Also, the multiple scattering results in a loss of energy by the incident neutron, so that it is of some importance to know the energy at which the neutron is finally captured. In special cases this moderation of the neutron can produce a most unexpected dependence of the capture probability on the incident energy, with the result that experimental data may be seriously misinterpreted. It is the purpose of this paper to present both calculated and experimental data for neutron capture

† Work performed under the auspices of the U.S. Atomic Energy Commission.

in a resonance where peculiar effects are observed. Our hope is that these results will serve as a warning of the difficulty of deriving even qualitative information about partial cross sections from measurements on samples for which multiple scattering of the neutron is an important effect.

2. Experimental Results

The geometric arrangement of the sample and detector used in the study of γ-rays resulting from capture in neutron resonances is shown in fig. 1.

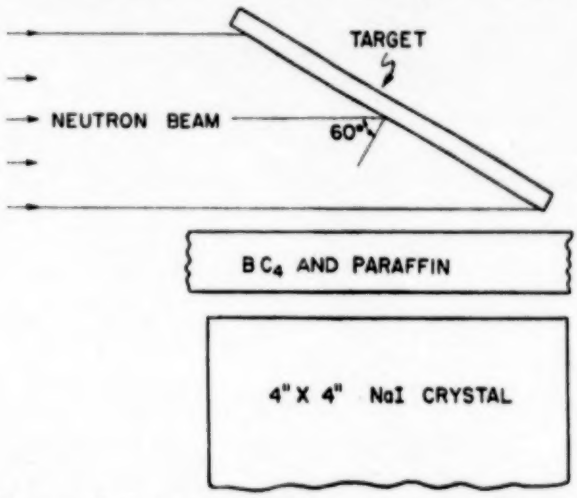

Fig. 1. Schematic diagram of the experimental arrangement. The target consisted of Mn powder in a thin-walled aluminium container having dimensions of $13 \times 17 \times 0.5$ cm. The dimensions of the neutron beam were 5×10 cm.

The Argonne fast chopper [2]) was used to provide the incident beam of timed neutrons, the uncertainty in timing being about 0.08μ sec/m. The output pulses from the NaI detector were fed to a 1024-channel time analyzer [3]). It is important to recognize that the neutron energy corresponding to the time of formation of a detector pulse is the incident energy rather than the capture energy. We have this direct relationship between time and incident energy only because, for the case studied, the time the neutron spends in the sample is small in comparison with the resolution width used in the measurement. The experimental measurement, therefore, gives the distribution of probability of capture only as a function of the incident energy, not as a function of the capture energy.

The principal purpose of our study of the γ-rays from resonant capture has been to measure the γ-ray spectra. These results need not be presented here since they have already been published elsewhere [4]). Therefore, we restrict ourselves to another kind of information, namely, the capture probability as a function of incident energy. Results of this kind are shown in fig. 2 for two samples of different thickness. For comparison the total cross section of Mn^{55} is also given [5]). The γ-ray data of fig. 2a are presented in the form of the

number of counts in a time channel of constant width as a function of the energy of the incident neutron. No correction has been made for background counts or for the shape of the spectrum of incident neutrons. The background was approximately the same for all channels and contributed roughly

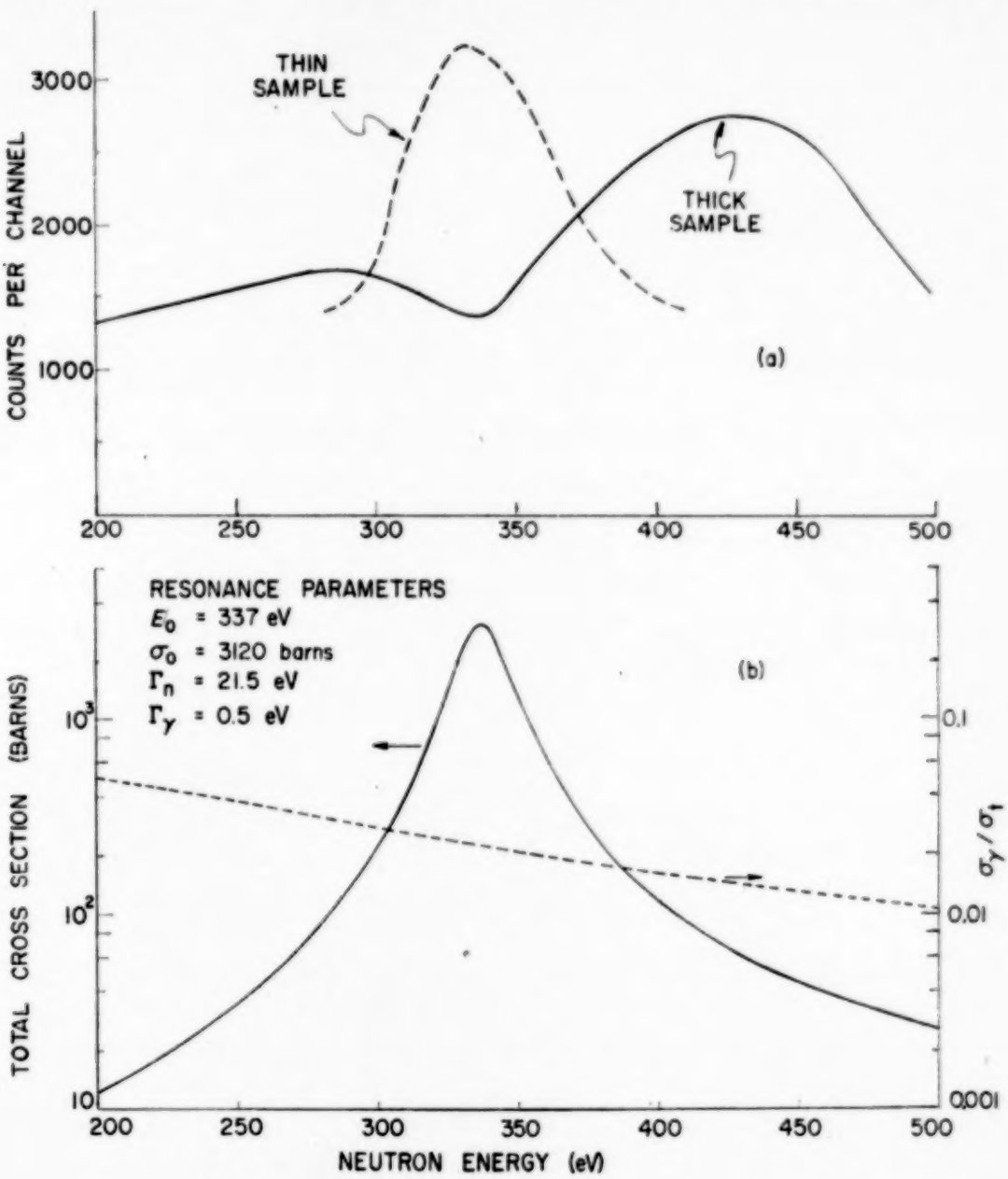

Fig. 2. Graph (a) shows the relation between γ-ray counting rate and incident neutron energy for a thick and thin sample of Mn. The thicknesses were $n = 0.057$ and $n \approx 0.001$ atom/barn respectively. Both curves represent experimental data for which no correction for background or spectrum shape has been made. Graph (b) shows the total cross section and the ratio σ_γ/σ_t for this energy region.

30 % of the counting rate at 337 eV. The intensity of incident neutrons varies approximately as $E^{\frac{1}{2}}$, except for a broad dip of about 15 % in the

neighborhood of 337 eV. The data given in fig. 2a were obtained by accepting all events having pulse heights greater than 1 MeV. Curves having essentially the same shape were also obtained with a bias level of about 6 MeV and when requiring coincidents counts in two NaI scintillators.

The most striking feature of the data of fig. 2 is the prominent peak in the capture probability for the thick sample at an incident energy of 430 eV, an energy at which no resonance is detectable in the total cross section. One reasonable interpretation of the unexpected peak in the γ-ray counting rate might be that it is caused by an exceptionally narrow resonance for which the peak cross section is small, say less than 100 barns. A small resonance of this kind could not be detected in the total cross section because of its proximity to the wide level at 337 eV. Also, a narrow resonance would necessarily have a neutron width Γ_n which is much less than the radiation width Γ_γ, so that the ratio σ_γ/σ_t of the capture to the total cross section would be exceptionally high. Since the probability of capture is crudely proportional to σ_γ/σ_t when the sample is thick enough that all incident neutrons must interact, we would expect to find a marked increase in the counting rate at our hypothetical narrow resonance. Moreover, we might also expect an increase in the rate on the low-energy side of the resonance at 337 eV, since there the value of σ_γ/σ_t also increases. For a thin sample, on the other hand, the probability of capture is proportional to σ_γ, a quantity which could be small enough to make the effect of a narrow resonance undetectable above the background counting rate.

The above discussion shows that the dependence of the capture probability on incident energy, as given in fig. 2, is qualitatively consistent with our expectations if we postulate the presence of a narrow resonance at 430 eV. As an experimental check on this possibility, measurements were made of the γ-ray spectra resulting from capture of neutrons whose incident energies were in the neighborhoods of 430 and 337 eV. These spectral data, which give the probabilities for individual γ-ray transitions from the initial state to the first few excited states of the compound nucleus, were obtained with the coincidence technique previously described by Kennett *et al.* [4]). It was found that the spectra at the two energies being considered were identical within the rather poor statistical accuracy of the measurements. If it is assumed that a resonance is present at 430 eV, this similarity of spectra is rather surprising in that the spectra for the resonances at 2360, 1090, and 337 eV, and for thermal neutrons were all found [4]) to be quite different.

A possible alternative explanation of the peak in the γ-ray counting rate at 430 eV is that, by virtue of the rapidly varying cross section in the neighborhood of the 337-eV resonance, it results from multiple scattering of the incident neutrons. The principal purpose of this paper is to show that the experimental data are in fact consistent with this latter interpretation.

3. Monte Carlo Calculation

The principle of the Monte Carlo type of calculation is by now well known and many applications of it have been described [6]). This method was applied to our problem † of the multiple scattering of neutrons under the following restrictions:

(1) Only s-wave scattering is considered, so the scattering is isotropic in the centre-of-mass system.

(2) It is assumed that the cross section at any energy can be represented by the superposition of two single-level Breit-Wigner formulae. The capture and scattering cross sections, σ_γ and σ_s, are then given by

$$\sigma_\gamma = \sum_{i=1}^{2} \sigma_{0i} \frac{\Gamma_{\gamma i}}{\Gamma_i} \left[\frac{E_{0i}}{E}\right]^{\frac{1}{2}} \frac{1}{1+x_i^2}$$

$$\sigma_s = 4\pi R^2 + \sum_{i=1}^{2} \sigma_{0i} \frac{\Gamma_{ni}}{\Gamma_i} \left[1 + \frac{2R\Gamma_i x_i}{\lambda_{0i}\Gamma_{ni}}\right] \frac{1}{1+x_i^2}$$

where

$$x_i = \frac{2}{\Gamma_i}(E - E_{0i}).$$

Here E is the kinetic energy of the neutron, E_0, $2\pi\lambda_0$ and σ_0 are the energy, wavelength and cross section at exact resonance, Γ, Γ_n and Γ_γ are the total, neutron and γ-ray widths of the resonance, and R is the nuclear radius. Note that interference between the resonance and the potential scattering has been included but no account has been taken of interference between resonances. Moreover, the effect of Doppler broadening of the resonances was ignored.

(3) The incident neutron energy can be monoenergetic or selected randomly over a given interval.

(4) The sample or target is a finite rectangular parallelepiped.

(5) The incident neutrons can impinge on the target at any prescribed angle.

(6) The incident neutrons can impinge on the target at a point or within a defined rectangle.

The important steps in the Monte Carlo calculation and their sequence are illustrated by the flow chart given in fig. 3. The heavily outlined boxes in the figure indicate the input data to the problem. The read-out for the problem is a rectangular matrix which gives the number of captured neutrons falling in discrete intervals of depth and energy. The sample thickness was usually divided into 14 intervals while from 50 to 100 energy intervals were used. The use of such a recording scheme permitted a correlation between the depth of penetration and the energy at capture.

† An application of the Monte Carlo method to a somewhat different problem of multiple scattering has been given in ref. [7]).

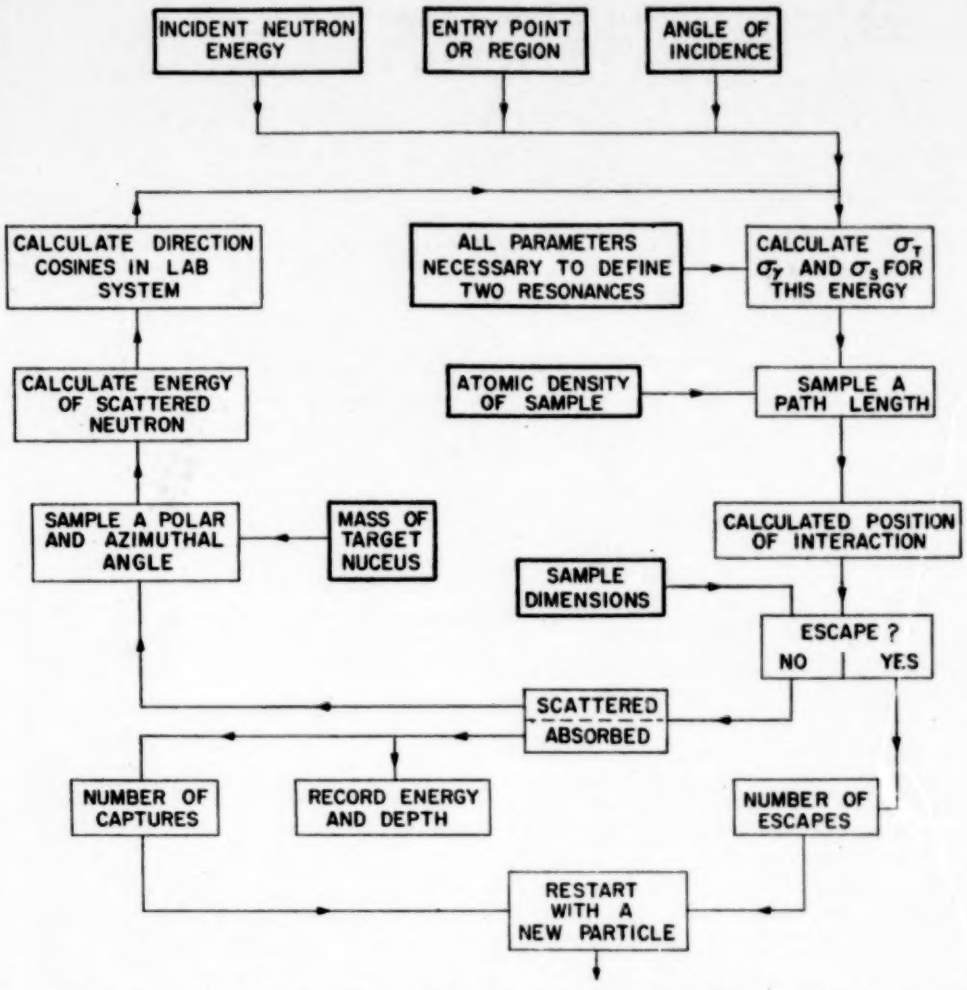

Fig. 3. Flow chart showing the important steps in the Monte Carlo calculation. The heavily outlined boxes indicate input data which are supplied at the beginning of the computation. Once a particle has been selected, the calculation proceeds around the loop and continues to do so until the particle either escapes from the sample or is captured. At this point a new particle is selected and the calculation restarted.

4. Results of the Monte Carlo Calculation

The Monte Carlo calculations † of the effect of multiple scattering of neutrons in manganese were carried out for the thicker of the two samples which were investigated experimentally. Since the thickness of this sample was 0.114 atoms/barn, as seen by the incident beam, multiple scattering was an important factor over a wide range of neutron energies about the 337-eV resonance, where the peak cross section is about 3100 barns. The partial cross sections were calculated from the parameters which describe the resonances at 337 and 1080 eV in Mn. The parameters used were; $E_{01} = 337$ eV, $\Gamma_{n1} = 21.5$ eV, $\Gamma_{\gamma 1} = 0.5$ eV, $\sigma_{01} = 3120$ barns, $E_{02} = 1080$ eV, $\Gamma_{n2} = 13.9$ eV, $\Gamma_{\gamma 2} = 0.6$ eV, $\sigma_{02} = 1350$ barns and $R = 5.5 \times 10^{-13}$ cm.

† The calculations were done on the Argonne digital computer GEORGE.

The calculated distributions of differential probabilities of capture as a function of the depth within the sample at which capture occurs are shown in fig. 4. The total area under each curve has been normalized to unity. A consideration of the significance of these data is deferred until a later paragraph.

The distributions of the energy at which capture occurs are shown in fig. 5 for neutrons of several different incident energies. For the sake of simplicity

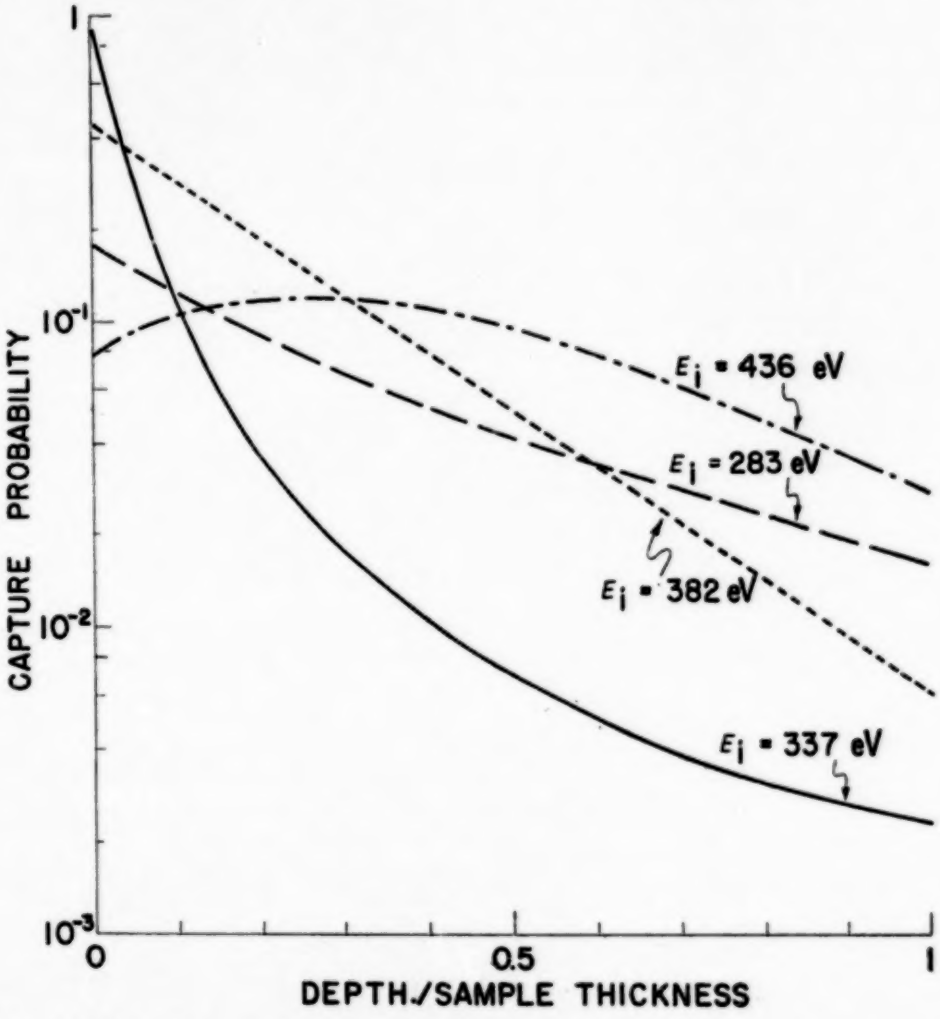

Fig. 4. Calculated curves showing the relation between capture probability and depth within the sample for various incident energies.

in presenting the data, the contribution which results from capture on the first interaction (a δ-function) has been subtracted. Moreover, the areas of the curves are normalized so as to be proportional to the fraction of interacting neutrons which are multiply scattered. Numerical values of some of these probabilities are given in table 1.

The data of table 1 are in a form which may be compared directly with the experimentally determined dependence of the γ-ray counting rate on the

incident neutron energy. The calculated results are presented in graphical form in fig. 6 as a curve of total capture probability vs. energy. Comparing this curve with the experimental results of fig. 2, we find the qualitative resemblance between the experimental and calculated data to be quite striking. On close examination, however, it is found that the two sets of data are not in complete quantitative agreement. These descrepancies are not

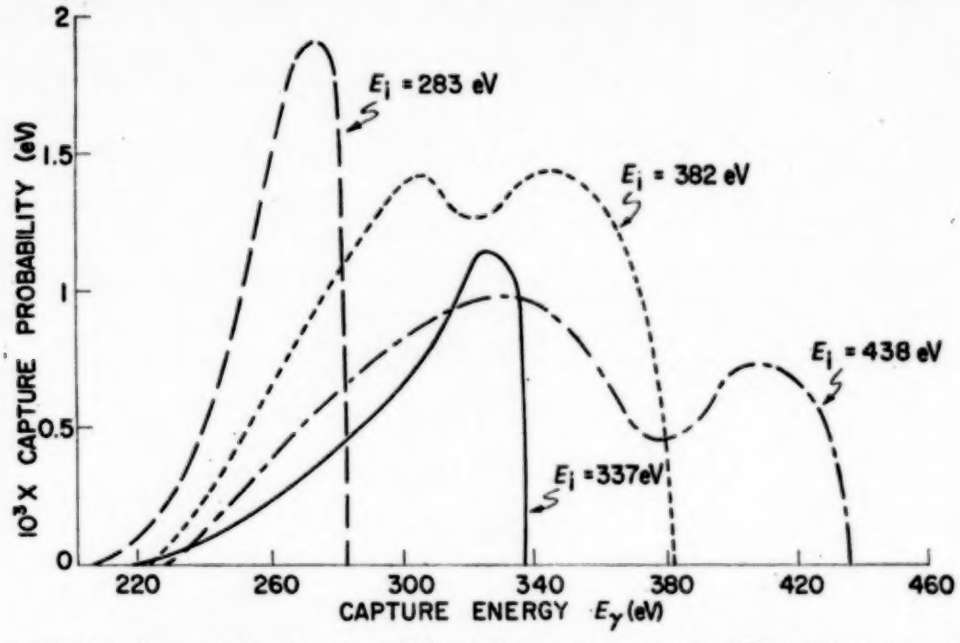

Fig. 5. Calculated curves showing the relation between capture probability and capture energy for various incident energies. The area under each curve gives the probability of capture for multiply scattered neutrons.

TABLE 1

Calculated capture probabilities

Incident energy (eV)	Transmission	No. Captured / No. Incident	F
202	0.469	0.0337	0.365
283	0.003	0.0969	0.683
310	0.000	0.1051	0.750
337	0.000	0.0907	0.750
355	0.000	0.1209	0.830
382	0.000	0.1611	0.890
400	0.001	0.1775	0.908
418	0.012	0.1748	0.914
436	0.046	0.1409	0.910
472	0.140	0.0675	0.820
500	0.225	0.0395	0.790

The standard deviation in the number captured is 5 % for all incident energies. The last column gives the fraction F of all the captured neutrons which are captured after having first been scattered. Specifically $F = [N_\gamma - (1-T)(\sigma_\gamma/\sigma_t)N_1]N_\gamma^{-1}$, where N_γ is the number of captured neutrons and N_1 the number of incident neutrons.

surprising in view of the known defects in both the experiment and the calculation. The most important approximations which need to be kept in mind are the following:

(a) No correction was made for the background counting rate in the experiment since this rate was quite uncertain.

(b) In the experimental data, no correction was made for the energy dependence of the spectrum of incident neutrons. The spectrum varied roughly as $E^{\frac{1}{2}}$ for a fixed time-of-flight interval.

(c) The single-level Breit-Wigner shape used in the calculation does not describe the cross section for the 337-eV resonance of Mn to an accuracy of better than about 10 %.

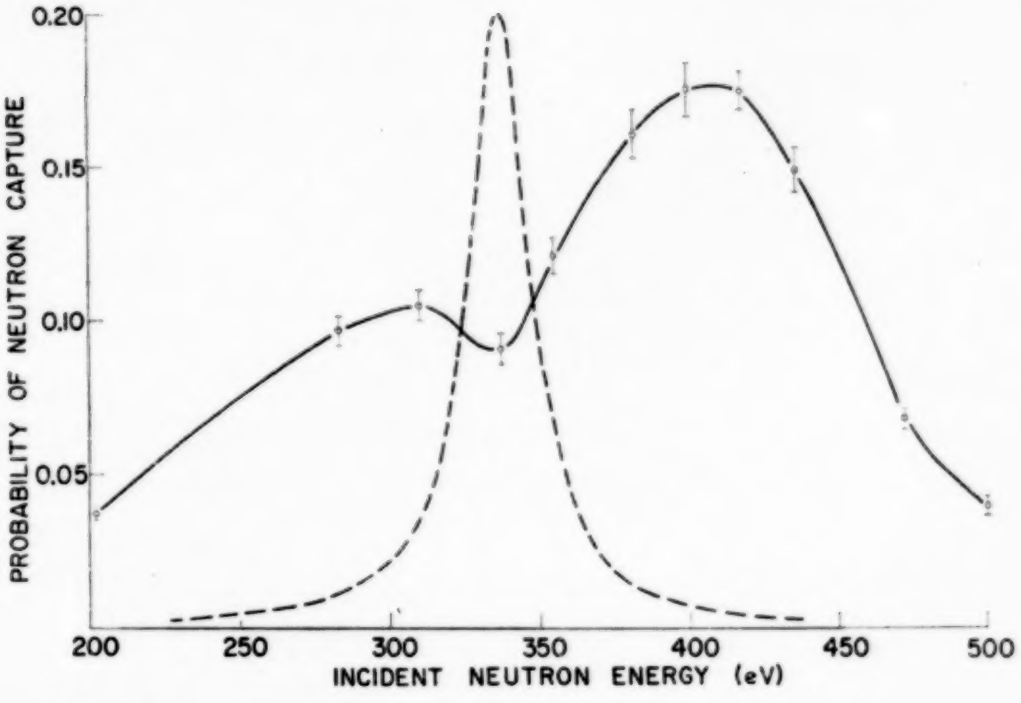

Fig. 6. Calculated curves showing the probability of capture as a function of incident neutron energy. The dashed curve is a plot of σ_γ, which corresponds to the shape obtained for an infinitely thin sample.

(d) The values of the level widths used in the calculation are probably not as accurate as are now available.

The presence of the above inaccuracies makes exact agreement between the experiment and calculation unlikely but they will not destroy the salient features of the results. The rather large amount of computational effort necessary to attempt to obtain a better fit was not considered to be justified, in view of the uncertainties in the experimental data †.

† The experimental data cannot be improved at the present time because the reactor used in the measurements is currently out of operation.

An inspection of the results already presented, especially those of fig. 5, is enough to indicate that the distribution of capture probability as a function of incident energy is only remotely related to the distribution as a function of capture energy. Although there is no known way in which this latter distribution can be measured, it is of some interest to inquire what it might look like. The result is easily obtained from the Monte Carlo calculation by requiring the incident neutrons to be uniformly distributed over some wide range of energy. The distribution of the capture energy obtained in this way is given in fig. 7 for incident neutrons in the range from 238 to 436 eV, a range which is broad enough to include most of the neutrons that are captured at energies near the 337-eV resonance. For comparison, the calcu-

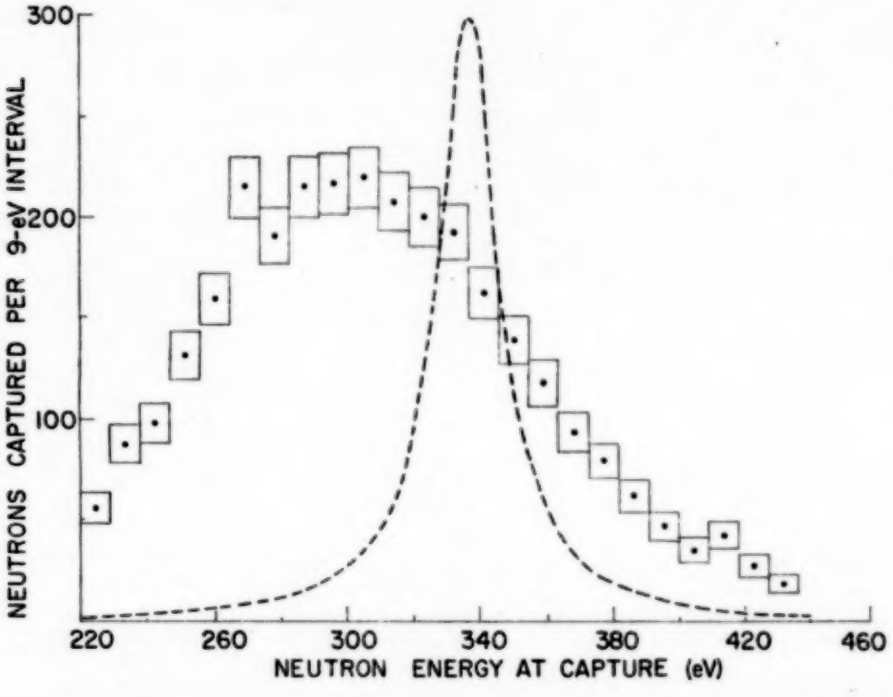

Fig. 7. The calculated distribution in capture energy for incident neutrons uniformly samples from 238 to 436 eV. The rectangles indicate the statistical uncertainty in the Monte Carlo calculation. The dashed curve is a plot of σ_γ and corresponds to the distribution for a thin sample.

lated capture cross section is also given in fig. 7, this cross section being identical with the distribution in capture energy for an infinitely thin sample, of course.

The general features of the distributions which were presented in figs. 4—7, can be quantitatively explained by a consideration of the behaviour of neutrons which are incident in the following energy regions:

(a) $E_1 < 200$ eV and $E_1 > 500$ eV. In these regions, $n\sigma_t$ is relatively small so the sample appears thin to the incident neutron. Multiple scattering

is then a rather unimportant factor and the time-of-flight spectrum will tend to be directly related to σ_γ.

(b) $E_1 = 436$ eV. Here the transmission is zero but the mean position of the first interaction is well within the sample. Following the first scattering, the mean free path becomes smaller since σ_t is increasing with decreasing energy. After a few collisions the sample appears to the neutron to be of almost infinite size. The capture probability then becomes quite large since escape is rather unlikely. This description is well substantiated by fig. 4, in which the 436-eV curve of capture probability vs. depth has a maximum that clearly shows a trapping action. In this figure the captures were counted without regard to the energies of the neutrons at the instant of capture.

(c) $E_1 = 337$ eV. The large value of $n\sigma_t$ implies that the first interaction is very near the surface of the sample. Following this interaction the mean free path is longer, thus enhancing the loss of back-scattered neutrons out through the incident face of the sample. The second interaction leads to a similar situation so that the fraction of neutrons captured for this incident neutron energy is expected to be small. Figure 4 shows the capture distribution for $E_1 = 337$ eV to be markedly different from that for $E_1 = 436$ eV.

(d) $E_1 = 283$ eV. The incident neutron penetrates more deeply than for the 337-eV case. However, the shape of the capture distribution should be similar for the two cases since σ_t decreases with decreasing energy for both. Because of this behaviour of the cross section no trapping action is possible. Figure 4 shows that the capture distributions for $E_1 = 283$ eV and 337 eV are similar, but that the 283-eV neutrons tend to penetrate more deeply into the sample. It seems probable that the 283-eV neutrons have a higher capture probability than those incident at 337 eV because of the increase in σ_γ/σ_t although the slower rate of change of σ_t with energy may also be a contributing factor.

The preceding discussion can also be presented on the basis of the distribution in capture energy for various incident energies. Here the degree of multiple scattering is indicated by the magnitude of the degradation in neutron energy before capture occurs. From this criterion, the results of fig. 5 show clearly that many more collisions occur when the incident energies are above the resonance than when they are at or below the resonance.

5. Discussion and Conclusion

It has been shown both by experiment and by calculation that time-of-flight measurements of neutron capture in thick samples can lead to complex results that are apt to be misleading. Multiple scattering of the incident neutrons makes the assumption that capture takes place at or near the incident energy a poor approximation to the process which actually occurs.

Thus both the distribution of the position at capture and the distribution of the energy at capture are markedly influenced. The case considered, capture in the neighborhood of the 337 eV resonance in Mn, is particularly favorable for the demonstration of these effects, because $\sigma_\gamma/\sigma_t \ll 1$ and because the average energy loss per collision is less than the width of the level. Similar effects of multiple scattering were also found experimentally at the 1080 and 2360 eV resonances in Mn, although for these levels the structure is less easily resolved.

The agreement between the calculated and the experimental results shows that the Monte Carlo calculation provides a good representation of the effects of multiple scattering. In view of this agreement and the simplicity of the processes involved, one would expect that the calculation could be made to reproduce the experimental results to any required degree of accuracy. Thus, we conclude that measurements of neutron capture in thick samples can be used to obtain quantitative information about cross sections by using a Monte Carlo calculation to take into account the effects of multiple scattering of neutrons.

The authors take pleasure in acknowledging the assistance of Dr. L. Wos and Mr C. Harrison who coded the Monte Carlo calculation.

References

1) For example, see E. R. Rae, E. R. Collins, B. B. Kinsey, J. E. Lynn and E. R. Wiblin, Nuclear Physics **5** (1958) 89
2) L. M. Bollinger, R. E. Coté and G. E. Thomas, Proceedings of the 1958 International Conference on the Peaceful Uses of Atomic Energy, P/686
3) R. W. Schumann, Rev. Sci. Instr. **28** (1957) 489
4) T. J. Kennett, L. M. Bollinger and R. T. Carpenter, Phys. Rev. Lett. **1** (1958) 77
5) L. M. Bollinger, D. A. Dahlberg, R. R. Palmer and G. E. Thomas, Phys. Rev. **100** (1955) 126
6) Symposium on Monte Carlo Methods edited by H. A. Mayer (John Wiley and Sons, New York, 1954)
7) K. W. Morton, Journal of Nuclear Energy **5** (1957) 320

3.A *Nuclear Physics* **12** (1959) 261—268; © *North-Holland Publishing Co., Amsterdam*
Not to be reproduced by photoprint or microfilm without written permission from the publisher

THERMAL NEUTRON CROSS-SECTIONS FOR PRODUCING SOME ISOMERS

M. L. SEHGAL, H. S. HANS and P. S. GILL
Department of Physics, Muslim University, Aligarh, India

Received 9 April 1959

Abstract: Thermal neutron cross-sections have been measured for producing some isomers; making irradiations with the 'Swimming Pool" reactor at Trombay, Bombay. The cross-sections for the following cases have been measured: $Pd^{108}(n, \gamma)Pd^{109m}$, $Pd^{110}(n, \gamma)Pd^{111m}$, $Sb^{121}(n, \gamma)Sb^{122m}$, $Nd^{150}(n, \gamma)Nd^{151}$, $Dy^{158}(n, \gamma)Dy^{159}$, $Hg^{196}(n, \gamma)Hg^{197m}$, $Hg^{196}(n, \gamma)Hg^{197}$, $Hg^{198}(n, \gamma)Hg^{199m}$. Scintillation technique was used in these measurements.

1. Introduction

The measurement of the thermal neutron cross-sections for the production of isomers has been undertaken to obtain isomeric ratios [1]), and also to complete the data of the thermal neutron cross-sections. Activation method was employed for these measurements. Previous workers [2]) have generally employed β-counters for such measurements and therefore they were able to study only those cases in which the relevant γ-rays have large conversion coefficients. Because in most of the isomers, energies of conversion electrons are low; more errors are liable to be introduced by using β-counters due to large value of absorption coefficient for β-rays. Detection of γ-rays by scintillation technique in these cases is more suitable. Also where the conversion coefficient is comparatively small, γ-ray detection is more advantageous. We have, therefore, used in nearly all the cases scintillation technique for γ-ray detection. We have also measured by this method a few cases involving electron capture.

2. Experimental Procedure

The thermal column as well as the core of the "Swimming Pool" reactor [3]) at Trombay (Bombay) were used for irradiation of the various samples. In those cases in which the thermal column was used; the sample, enclosed in a perspex container, was placed in a small hole in a graphite block, which could be inserted in the thermal column. This ensured the reproducibility of the position of irradiation. The thermal neutron flux at the place of irradiation in most of these cases was of the order of 10^7 neutrons/cm^2 · sec.

In some cases where the half-lives of the activities were small, the substances were irradiated near the core of the reactor. In these cases the irradiated samples could be taken out of the core in less than a minute, making it possible to study short life activities.

The substances studied in the present case were obtained from Johnson-Matthey & Co, Ltd, London, and had a purity better than 99.9 %. The substances which were in powder form were put in a thin walled perspex tube for irradiation. For isotopes which were β-emitters, an end window β-counter was employed with a window thickness of 1.94 mg/cm^2. In such cases, immediately after the irradiation a foil was made by sandwiching the powder uniformly between two thin cellotapes over a well defined area. To take into account the effect of the resonance neutrons, for those irradiations which were made near the core, the samples were also irradiated after covering the container with cadmium tubing of wall thickness 0.4 mm. The induced activity due to thermal neutrons was found by the well known cadmium ratio method. The various errors involved in measuring the activation cross-sections for thermal neutrons are discussed by Sehgal [4]).

A well type NaI(Tl) crystal of dimensions $1\frac{3}{4}''$ diameter, 2'' height and $1\frac{1}{2}''$ well, mounted on a 6292 DuMond photomultiplier tube was used as the detector. The pulses from the photomultiplier tube were fed through a cathode follower to a single channel γ-ray spectrometer. The crystal and the photomultiplier were shielded in a lead house of wall thickness 10 cm to reduce the background. The perspex tube containing the sample after

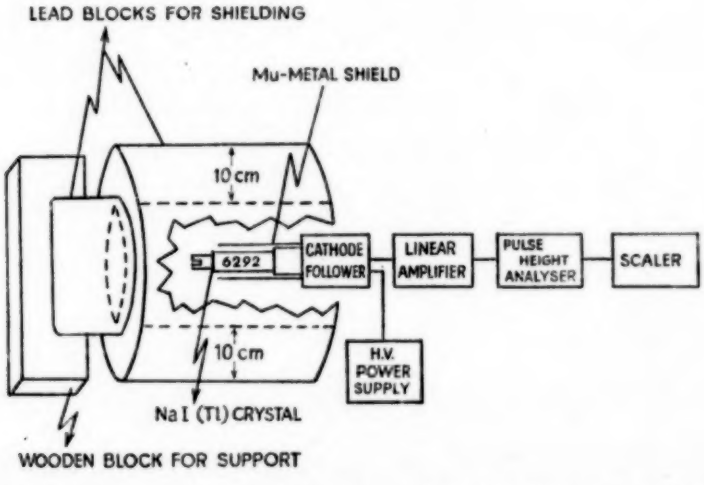

Fig. 1. Experimental arrangement used for measuring the γ-ray activities of the sample in the study of the thermal neutron cross-sections.

irradiation was placed in the centre of the well of the NaI(Tl) crystal and the spectrum was studied. The experimental arrangement for detection is shown in fig. 1.

The well known formula for the activation cross-section may be expressed as

$$IN\sigma = \frac{\left(\frac{dn}{dt}\right)_{t_2} e^{-\lambda t_2}}{1-e^{-\lambda t_1}}, \quad (1)$$

where I is the flux of the neutrons at the point of irradiation of the sample, N the total number of nuclei of the isotope in the irradiated sample; σ the relevant thermal neutron cross-section for the isotope; $(dn/dt)_{t_2}$ the disintegration rate of that isotope at time t_2 after the substance is removed from the pile; t_1 is the time of irradiation, and λ the decay constant of the radioactive isotope formed by the absorption of neutrons by the initial isotope.

As it is not convenient to measure I directly, Au^{197} was used as the standard substance whose thermal neutron cross-section is accurately known to be $\sigma = 98 \pm 1$ b [2]). By comparing the disintegration rate of the sample with that of Au^{198} under the same geometry it is possible to obtain the ratio of the two cross-sections. Au^{198}, whose decay scheme is well known [5]), gives predominantly a γ-ray of 0.411 MeV (≈ 99 %) and therefore one may get the disintegration rate of Au^{198} from its γ-ray spectrum quite accurately. The disintegration rate from a particular substance is given by

$$\frac{dn}{dt} = \frac{\text{Couting Rate}}{\text{Detection Efficiency}} \cdot \frac{1}{G}, \quad (2)$$

where G is the overall geometry factor. Because of the comparison of all the cross-sections with Au^{197} in the same geometry, G gets cancelled. The total number of counts due to a γ-ray from a particular isomer as detected by the scintillation crystal are first measured. This gives us the counting rate in eq. (2). Detection efficiency will be given by $(1-e^{-\mu d})$, where μ is the total linear absorption co-efficient of the particular γ-ray in the NaI(Tl) crystal and d is the effective path length of the γ-ray inside the crystal. The total number of γ-rays were detected by taking all the counts above a certain low bias, and the corrections were applied for the contribution below that bias. Most of the cases involved one γ-ray. In a few cases where more than one γ-ray were involved, and the decay scheme was known, the contribution to the total counts from a particular γ-ray could be calculated.

In those cases where more than one γ-ray is present and it is possible to measure the whole spectrum, it is better to use the area under the photo-peak for the particular γ-ray for the counting rate. In such cases, it is required to know the efficiency for the photo-peak. This was found by the well known method of taking the ratio of the areas under the photo-peak to the total area for γ-rays of various energies, and then multiplying this ratio with the total efficiency for that particular γ-ray. To find the ratio of the areas as a function of energy of the γ-rays, three standard sources, Cs^{137}(0.661 MeV), Au^{198}(0.411 MeV) and Hg^{203}(0.279 MeV), were used.

3. Measurements

3.1. $Pd^{108}(n, \gamma)Pd^{109m}$ and $Pd^{110}(n, \gamma)Pd^{111m}$

In these measurements, palladium metal foils (99.99 %) of thickness 0.001 inch were taken and irradiations were made in the thermal column. The cross-section for the reaction $Pd^{108}(n, \gamma)\ Pd^{109m}$ was measured by taking the number of counts under the photo-peak of the 190 keV γ-ray due to the decay of Pd^{109m} into Pd^{109} by isomeric transition. Fig. 2 shows the decay

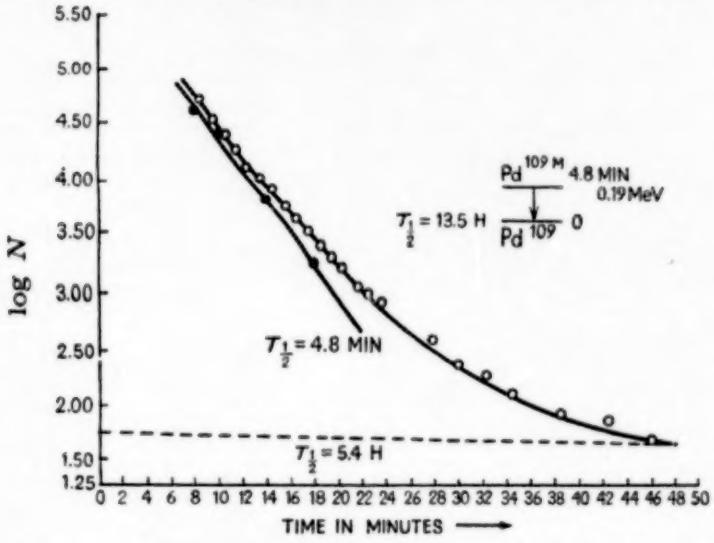

Fig. 2. Half-life curve of Pd^{109m}. $N = \frac{1}{128}$ (counting rate/minute). Decay scheme of Pd^{109m} taken from Z. Naturforsch. **12a** (1957) 939.

curve of Pd^{109m}. The cross-section for $Pd^{108}(n, \gamma)Pd^{109}$ reaction was also measured by a β-counter as well as the scintillation counter. Similarly the cross-section for 24 min activity from $Pd^{110}(n, \gamma)Pd^{111}$ was also measured. Palladium activity of 5.5 h from $Pd^{110}(n, \gamma)Pd^{111m}$ was hardly observable above the background counts. Only an upper limit for its cross-section could be obtained.

3.2. $Sb^{121}(n, \gamma)Sb^{122m}$

Antimony metal powder (99.995 %) was used for the above cross-section measurement. Fig. 3 shows the half-life curve of Sb^{122m} excluding the contribution of the KX-ray. The contribution to the counting rate comes from the unconverted part of 75.3 keV and 60.7 keV γ-rays, which were in cascade. Conversion coefficients of the two γ-rays were obtained from the known nature of the γ-rays. Total counts (excluding the KX-ray contribution) will be given by

$$N_T = G \frac{dn}{dt} \left(\frac{\epsilon_1}{\alpha_1} + \frac{\epsilon_2}{\alpha_2} \right),$$

where ϵ_1 and ϵ_2 are the efficiencies of detection of the 75.3 keV and 60.5 keV

γ-rays in the crystal α_1 and α_2 the ratios of the total disintegration to the number of unconverted γ-rays for these γ-rays, respectively, and dn/dt the

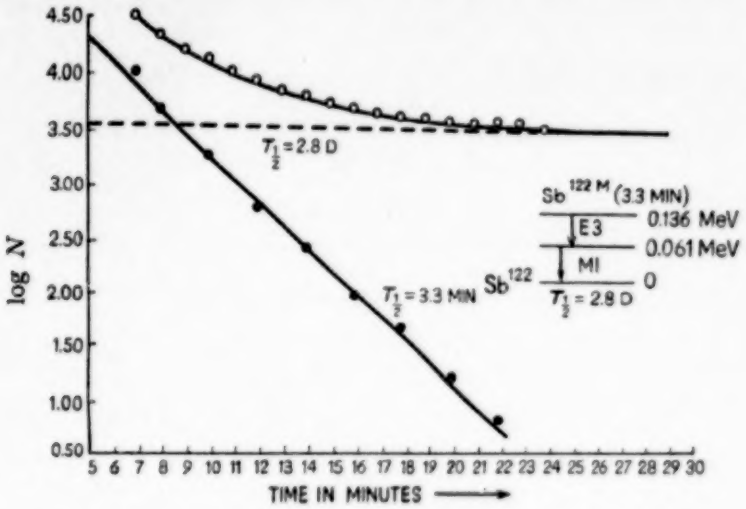

Fig. 3. Decay curve of antimony excluding contribution due to KX-rays.
$N = \frac{1}{128}$ (counting rate/minute).
Decay scheme of Sb^{122m} taken from Phys. Rev. **98** (1955) 39.

disintegration rate. From the above equation it was found that the contribution in the counting rate due to the 60.5 keV γ-ray is 95.9 %.

3.3. $Nd^{150}(n, \gamma)Nd^{151}$

Spectrographically standardised Nd_2O_3(99.9 %) was used for the above cross-section measurements and irradiations were made in the thermal column. Fig. 4 shows the decay of neodymium. The 1.8 h activity due to

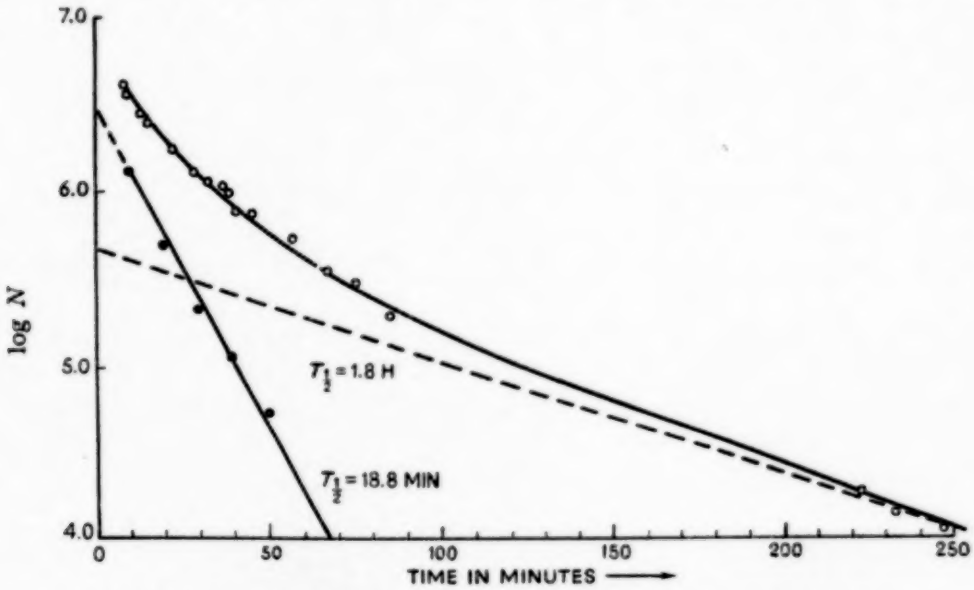

Fig. 4. Decay curve of neodymium. N = (counting rate/minute).

Nd^{149} was subtracted from the main curve and the residual activity was found to decay with a half-life of 18 minutes which was attributed to Nd^{151} [6]). The energy of the β-particle from Nd^{151} is taken to be 1.93 MeV [6]).

3.4. $Dy^{164}(n, \gamma)Dy^{165m}$ and $Dy^{158}(n, \gamma)Dy^{159}$

For the study of the cross-section of the $Dy^{164}(n, \gamma)Dy^{165m}$ reaction, Dy_2O_3(99.7 %) was irradiated near the core at a low power level. In this case the integrated counting rate was taken for all pulses above 3 volts, and corrections were applied for counts below that. The contribution due to the resonance neutrons at the place of irradiation was taken into account by the usual cadmium ratio method.

The cross-section for $Dy^{158}(n, \gamma)Dy^{159}$ was measured by irradiating Dy_2O_3 near the core of the reactor at high power level of the reactor for a long time. The short life-time activities due to other isotopes were allowed to decay for 12 days and then the spectrum was studied. The identification of the activity was made by measuring the γ-ray energy. The half-life of Dy^{159} for calculating the value of the cross-section was taken to be 140 days [7]).

3.5. $Hg^{196}(n, \gamma)Hg^{197m}$ and $Hg^{196}(n, \gamma)Hg^{197}$

The decay scheme of Hg^{197} is given in fig. 5. As is clear from this decay scheme, one is required to measure either the 133 keV or the 164 keV γ-ray

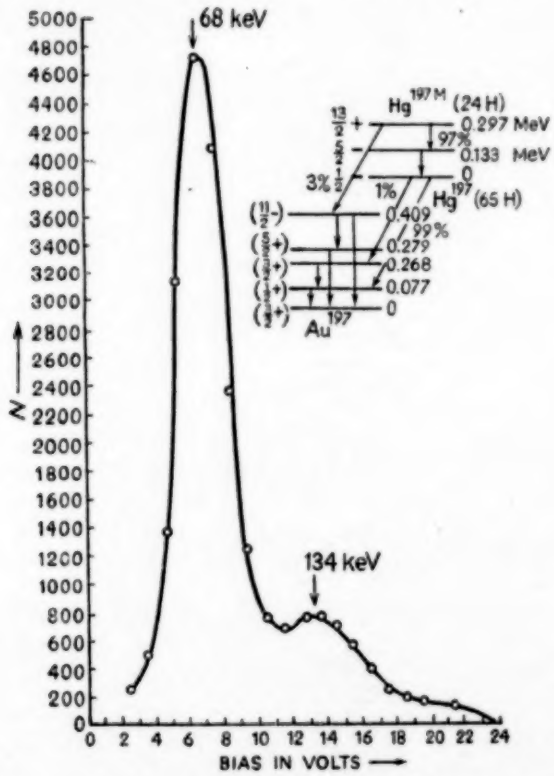

Fig. 5. Spectrum of mercury^{197m}. N = counting channel/minute.
Decay scheme of Hg^{197m} taken from Revs. Modern Phys. **30** (1958) 777.

for obtaining the cross-section for $Hg^{196}(n, \gamma)Hg^{197m}$ reaction. The cross-section for $Hg^{196}(n, \gamma)Hg^{197}$, on the other hand, may be obtained either by measuring the 77 keV γ-ray from Au^{197}, or from the X-ray arising from electron capture, taking the proper K/L ratio. As the 77 keV γ-ray and the X-ray are not resolved, one can only measure their sum. The contribution from either the X-ray or the 77 keV γ-ray alone may be calculated from the knowledge of the decay scheme of Hg^{197}. The cross-section measured for the $Hg^{196}(n, \gamma)Hg^{197}$ reaction in this manner will also include the cross-section for the formation of the 133 keV excited state of Hg^{197}.

Fig. 5 gives the spectrum of the γ-ray measured 5 hours after taking out the sample from the reactor. The peak at 68 keV is taken to be due to the sum of the X-rays and the 77 keV γ-ray. Similarly, the broad peak at higher energy is taken as the sum of the 133 keV and 164 keV γ-rays. From these two peaks the cross-section for the above reactions were calculated. The contribution due to the formation of the ground level of Hg^{197} due to the decay of Hg^{197m} during and after the irradiation time were of course taken into account.

3.6. $Hg^{198}(n, \gamma)Hg^{199m}$

Hg^{199m} decays by the emission of 368 keV and 158 keV γ-rays in cascade. As the 368 keV γ-ray is strongly internally converted, the cross-section was measured by taking the photo-area under the 158 keV γ-ray. Fig. 6 shows the

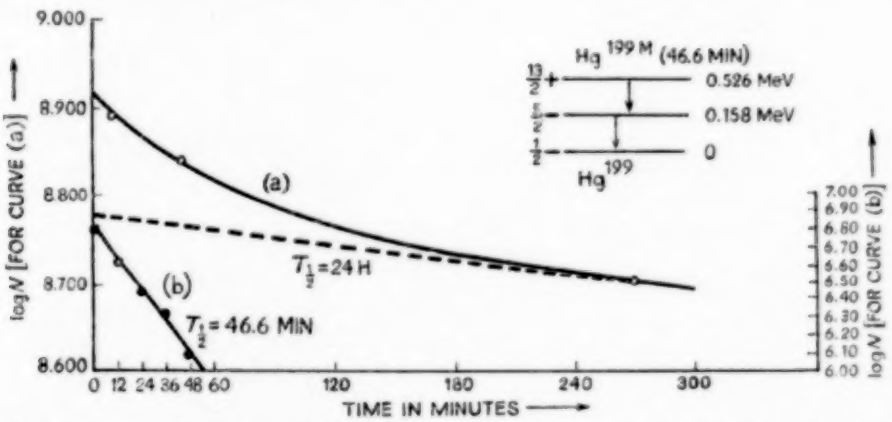

Fig. 6. Decay curve of mercury when the counting rate was taken under the photo-peak of the 159 keV γ-ray. N = counting rate/minute.
Decay scheme of Hg^{199m} taken from Revs. Modern Phys. **30** (1958) 779.

decay of Hg when the counts were taken under the photo-peak of the 158 keV γ-ray. As the spins and parities of the various levels involved are completely known, the value of the internal conversion coefficients may be calculated.

The results of the above measurements are given in table 1. The isomeric ratio rule of Mateosian and Goldhaber [8]) in slow neutron capture

TABLE 1

Reaction	Half-life Measured (min)	Cross-section (b)
$Pd^{108}(n, \gamma)Pd^{109m}$	4.8	0.26 ± 0.04
$Pd^{108}(n, \gamma)Pd^{109}$	13.5 ×60	14.0 ± 2.0
$Pd^{110}(n, \gamma)Pd^{111m}$		<0.05
$Pd^{110}(n, \gamma)Pd^{111}$	23.6	0.19 ± 0.03
$Sb^{121}(n, \gamma)Sb^{122m}$	3.3	0.19 ± 0.03
$Nd^{150}(n, \gamma)Nd^{151}$	18.8	1.5 ± 0.2
$Dy^{158}(n, \gamma)Dy^{159}$		96 ± 20
$Dy^{164}(n, \gamma)Dy^{165m}$	1.15	2490 ±300
$Dy^{164}(n, \gamma)Dy^{165}$	143	<840
$Hg^{196}(n, \gamma)Hg^{197m}$		420 ± 80
$Hg^{196}(n, \gamma)Hg^{197}$		880 ±175
$Hg^{198}(n, \gamma)Hg^{199m}$	46	0.018± 0.004

is verified for those cases in which the spins of the various levels involved are known.

The authors are thankful to the Department of Atomic Energy, Government of India, and specially to Dr. Ramanna, for providing the facilities at Trombay. One of the authors (M.L.S.) is thankful to the Tata Institute of Fundamental Research Bombay, for providing him facilities during the course of the present work.

References

1) E. Segrè and A. C. Helmholz, Revs. Mod. Phys. **21** (1949) 271
2) Neutron Cross-sections, compiled by D. J. Hughes and J. A. Harvey, Brookhaven National Laboratory Report BNL-325 (1955)
3) R. Ramanna, Journal of Scientific & Industrial Research **15A** (1956) 432
4) M. L. Shegal, Ind. J. Phys. **31** (1957) 630
5) D. Strominger *et al.*, Revs. Mod. Phys. **30** (1958) 774
6) W. C. Rutledge, J. M. Cork and S. B. Burson, Phys. Rev. **86** (1952) 775
7) B. H. Ketelle, Phys. Rev. **76** (1949) 1256
8) E. D. Mateosian and M. Goldhaber, Phys. Rev. **108** (1957) 766

1.D.4 *Nuclear Physics* **12** (1959) 269—273; © *North-Holland Publishing Co., Amsterdam*
Not to be reproduced by photoprint or microfilm without written permission form the publisher

QUADRUPOLE INTERACTION IN SU_2-COUPLING AND CRANKING MODEL

HARTMUT PILKUHN

Physikalisches Staatsinstitut, Hamburg

Received 23 March 1959

Abstract: For nuclei possessing stable deformations, the two-particle quadrupole interaction is expressed in terms of a deformed harmonic oscillator potential, and the moments of inertia in the corresponding coupling schemes (SU_2-coupling, and cranking model) are shown to be the same.

1. Introduction

In order to get a better understanding of rotational states of deformed nuclei, Elliott [1]) has introduced the SU_3-coupling scheme, in which the quadrupole interaction

$$V = -\varepsilon\hbar \sum_{i<j} r_i^2 r_j^2 P_2 (\cos \omega_{ij}) \tag{1}$$

is approximately diagonal. In this work we compare the coupling parameter ε and the moment of inertia to the potential deformation $\Delta\omega$ and moment of inertia of the cranking model of a deformed harmonic oscillator potential. Since the cranking model is essentially two-dimensional, we restrict our considerations to two dimensions, employing SU_2-states. The calculation of rotational properties in two dimensions may be justified for nuclei possessing cylindrical symmetry: we then know that the nucleus rotates about an axis perpendicular to the symmetry axis, and keeping this axis fixed in space would have about the same effect as replacing the eigenvalues $l(l+1)$ of $\mathbf{L}^2$ by l^2. (For two dimensions, $m = \pm l$.)

The group SU_2 is isomorphic to R_3; this enables us to employ spin formalism. Moreover, we consider spinless identical particles, as has been done in cranking model considerations [2,3]).

2. SU_2-Functions in Rectangular and Cyclic Coordinates

2.1. RECTANGULAR COORDINATES

Defining the creation and destruction operators

$$a^+ \equiv \begin{pmatrix} a_x^+ \\ a_y^+ \end{pmatrix} \equiv \frac{1}{\sqrt{2}} \begin{pmatrix} x - \dfrac{\partial}{\partial x} \\ y - \dfrac{\partial}{\partial y} \end{pmatrix}, \qquad a \equiv \begin{pmatrix} a_x \\ a_y \end{pmatrix} = \frac{1}{\sqrt{2}} \begin{pmatrix} x + \dfrac{\partial}{\partial x} \\ y + \dfrac{\partial}{\partial y} \end{pmatrix}, \tag{2}$$

with $[a_x, a_x^+] = 1$ etc., we put the harmonic oscillator hamiltonian into the form

$$H = a_x^+ a_x + a_y^+ a_y.$$

The normalized eigenstates are expressed by

$$|n_x n_y\rangle = \frac{1}{\sqrt{n_x!\, n_y!}} a_x^{+n_x} a_y^{+n_y} |00\rangle$$

in terms of the vacuum state

$$|00\rangle = \frac{1}{\sqrt{\pi}} \exp(-\tfrac{1}{2}(x^2+y^2)),$$

and

$$H|n_x n_y\rangle = (n_x+n_y)|n_x n_y\rangle \equiv n|n_x n_y\rangle.$$

Note that our x and y are dimensionless: they denote the position coordinates multiplied by $\sqrt{(m\omega/\hbar)}$.

Now consider the combinations

$$\begin{aligned} T_1 &= a^+\sigma_1 a = a_x^+ a_y + a_y^+ a_x = xy - \frac{\partial}{\partial x}\frac{\partial}{\partial y}, \\ T_2 &= a^+\sigma_2 a = \frac{1}{i}(a_x^+ a_y - a_y^+ a_x) = \frac{1}{i}\left(x\frac{\partial}{\partial y} - y\frac{\partial}{\partial x}\right), \\ T_3 &= a^+\sigma_3 a = (a_x^+ a_x - a_y^+ a_y) = \tfrac{1}{2}\left(x^2 - y^2 - \frac{\partial^2}{\partial x^2} - \frac{\partial^2}{\partial y^2}\right). \end{aligned} \tag{3}$$

They all commute with $H = a^+\sigma_0 a = a^+ a$. The commutation relations of the T_ν follow from those for Pauli's σ_ν:

$$[T_1, T_2] = 2iT_3; \quad [T_2, T_3] = 2iT_1; \quad [T_3, T_1] = 2iT_2. \tag{4}$$

The operator T_3 is diagonal:

$$T_3|n_x n_y\rangle = (n_x - n_y)|n_x n_y\rangle = t_3|n_x n_y\rangle. \tag{5}$$

For k particles,

$$H = \sum_{i=1}^{k} H(i); \qquad T_\nu = \sum_{i=1}^{k} T_\nu(i); \qquad t_3 = \sum_{i=1}^{k} (n_x(i) - n_y(i)).$$

$$|n_x(1) \ldots n_y(k)\rangle = A_k |n_x(i) n_y(i)\rangle;$$

A_k indicates the normalized antisymmetrization. For closed shells, $t_3 = 0$; therefore, we take k to be the number of particles in the open shell.

There are $\binom{n+1}{k}$ antisymmetrical eigenstates. Now, we can show from (4) and (5) that certain linear combinations of them will be eigenstates of $T^2 = T_1^2 + T_2^2 + T_3^2$. These are the SU_2-functions $\phi^t_{t_3}(a)$:

$$T^2 \phi^t_{t_3}(a) = t(t+2)\phi^t_{t_3}(a), \qquad T_3 \phi^t_{t_3}(a) = t_3 \phi^t_{t_3}(a). \tag{6}$$

In general, there will be many t-bands, there may even be several bands with the same t. There is only one band of maximal anisotropy:

$$t_{\max} = t_{3\max} = (\sum(n_x - n_y))_{\max} \equiv k(n-k+1). \tag{7}$$

This will turn out to be the ground state band.

2.2. CYCLIC COORDINATES

Now, we employ cyclic coordinates to construct eigenstates of the total angular momentum, which is just T_2:

$$M = \frac{1}{i}\sum_{i=1}^{k}\frac{\partial}{\partial\varphi}(i) = T_2.$$

So we have to go over from T_3-eigenstates to T_2-eigenstates. This is accomplished by means of the unitary transformation

$$b^+ \equiv \begin{pmatrix} b_+^+ \\ b_-^+ \end{pmatrix} \equiv \frac{1}{\sqrt{2}}\begin{pmatrix} -a_x^+ - ia_y^+ \\ -a_x^+ + ia_y^+ \end{pmatrix}, \qquad b \equiv \begin{pmatrix} b_+ \\ b_- \end{pmatrix} \equiv \frac{1}{\sqrt{2}}\begin{pmatrix} -a_x + ia_y \\ -a_x - ia_y \end{pmatrix}. \tag{8}$$

Then $[b_+, b_+^+] = 1$ etc., $H = b^+b$, $C_\nu(b) = b^+\sigma_\nu b$. We get all the formulas of section 2.1 with the substitutions $a \to b$, $T_\nu \to C_\nu$, $|n_x n_y\rangle \to |n_+ n_-\rangle$.

Evaluating T_ν by means of (8), we find

$$C_3 = T_2 = M, \qquad C_2 = T_1, \qquad C_1 = T_3. \tag{9}$$

These operators have been introduced by Lipkin [4]). Hence, the cyclic SU_2-functions are eigenstates of $T^2 = C^2$ and of M:

$$T^2\phi_m{}^t(b) = t(t+2)\phi_m{}^t(b), \qquad M\phi_m{}^t(b) = m\phi_m{}^t(b), \tag{10}$$

$$m = \begin{cases} \pm 1, \pm 3, \pm 5 \ldots \pm t & \text{for } k \text{ and } n \text{ odd} \\ 0, \pm 2, \pm 4 \ldots \pm t & \text{for } k \text{ and/or } n \text{ even.} \end{cases}$$

The coordinate transformation implies a linear transformation of the $t+1$ states within a band of given t:

$$\phi_m{}^t(b) = \sum_{t_3=-t}^{t} \alpha_{t_3}^t \phi_{t_3}^t(a). \tag{11}$$

3. Quadrupole Interaction

Now, we take the hamiltonian of the system to be $H+V$, with

$$V = -\tfrac{1}{2}\varepsilon\hbar\sum_{i\neq j} r_i^2 r_j^2 \cos 2(\varphi_i - \varphi_j) = -\tfrac{1}{2}\varepsilon\hbar\sum_{i\neq j}\left((x_i^2 - y_i^2)(x_j^2 - y_j^2) + 4x_i y_i x_j y_j\right) \tag{12}$$

In a harmonic oscillator representation, the diagonal elements of x^2 and xy are the same as those of $\frac{1}{2}[x^2 - (\partial^2/\partial x^2)]$, $\frac{1}{2}[(xy - (\partial/\partial x)(\partial/\partial y)]$, respectively. Thus, for the diagonal elements, we may take

$$V = -\tfrac{1}{2}\varepsilon\hbar(T_1^2+T_3^2) = -\tfrac{1}{2}\varepsilon\hbar(C_2^2+C_1^2) = -\tfrac{1}{2}\varepsilon\hbar(t(t+2)-m^2). \quad (13)$$

Here we have tacitly included some self-energy terms corresponding to $i = j$. For many particles, this should not be dangerous, and may partly be compensated by reducing ε.

For closed shells, the matrix elements of the operator V given by eq. (12) are zero. For an open shell, we omit the off-diagonal elements of (12); they could be taken into account in second order perturbation theory, to give the effects of the "core". Thus, we now take for V the form (13):

$$\begin{aligned} &V = E'+E_{\text{rot}}, \\ &E' = -\tfrac{1}{2}\varepsilon\hbar t(t+2), \qquad E_{\text{rot}} = \tfrac{1}{2}\varepsilon\hbar m^2; \end{aligned} \quad (14)$$

E_{rot} is interpreted as rotation energy because of its proportionality to the square of the total angular momentum, and we get the moment of inertia

$$\mathcal{J} = \hbar/\varepsilon; \quad (15)$$

E' is the deformation energy. In terms of a deformed harmonic oscillator potential, we have, for one particle,

$$E' = \hbar\Delta\omega(n_x-n_y), \qquad \Delta\omega \equiv \omega_0-\omega_x,$$

and summing over all particles,

$$E' = \tfrac{1}{2}\sum_i E'(i) = -\tfrac{1}{2}\hbar\Delta\omega \cdot t. \quad (16)$$

Now, if for large t, we approximate the expression (14) for E' by $-\frac{1}{2}\varepsilon\hbar t^2$, we get

$$\Delta\omega = \varepsilon t, \quad (17)$$

which means that the deformation of the collective potential is proportional to the anisotropy in the open shell. From (15) and (17), we get

$$\mathcal{J} = \frac{\hbar}{\Delta\omega}t. \quad (19)$$

These results hold for small deformations only: $\Delta\omega \ll \omega_0$. In the cranking model, one obtains for small deformations [3])

$$\mathcal{J} = \tfrac{1}{2}\hbar\frac{1}{\omega_x\omega_y}\frac{(\omega_x+\omega_y)^2}{\omega_y-\omega_x}t \approx \frac{\hbar}{\Delta\omega}t,$$

which agrees with (19). Thus, we see that the quadrupole interaction in SU_2-coupling gives about the same moment of inertia as the cranking model. A similar result has been shown to hold in the j_n-configuration in the limit of large j [5]).

4. Intrinsic State and Collective Angle

So far, we have obtained our results from linear combinations of single-particle states. Now, we use the method of redundant variables [6]) to approximate (11) by

$$\phi_m{}^t(b) = \phi_i{}^t(a')e^{im\theta}; \tag{20}$$

a' are rectangular coordinates relative to θ, and θ is chosen to make the intrinsic expectation value $\langle T'_1 \rangle$ zero:

$$\operatorname{tg} 2\theta = T_1/T_2. \tag{21}$$

We may even take

$$M = \frac{1}{i}\frac{\partial}{\partial\theta} = -2i\left(T_3\frac{\partial}{\partial T_1} - T_1\frac{\partial}{\partial T_3}\right), \tag{22}$$

which formally satisfies the commutation relations (4), with $M = T_2$. Since $\langle T'_1 \rangle = 0$, the intrinsic expectation value of the quadrupole energy is

$$\langle V' \rangle = -\tfrac{1}{2}\varepsilon\hbar\langle T'_3 \rangle^2 = -\tfrac{1}{2}\varepsilon\hbar t^2 = E', \tag{23}$$

according to eq. (14). Thus, by averaging V over the intrinsic state, we just lose the rotational energy.

This work has been suggested by Prof. G. Süssman. The author expresses his thanks for helpful discussions to Prof. G. Süssman, Dr. B. F. Bayman, and Dr. K. Helmers.

References

1) J. P. Elliott, Proc. Roy. Soc. A **245** (1958) 128, 562
2) D. R. Inglis, Phys. Rev. **96** (1954) 1059; **97** (1955) 701;
Nuclear Physics **8** (1958) 125
3) A. Bohr and B. Mottelson, Mat. Fys. Medd. Dan. Vid. Selsk. **30**, No. 1 (1955)
4) H. J. Lipkin, Nuclear Physics **8** (1958) 421
5) B. F. Bayman, Paris Conf. on Low Energy Nucl. Phys. (July 1958)
6) F. Villars, Ann. Rev. Nucl. Science **7** (1957)

2.F

Nuclear Physics **12** (1959) 274—290; © *North-Holland Publishing Co., Amsterdam*

Not to be reproduced by photoprint or microfilm without written permission from the publisher

MOMENTUM DISTRIBUTION OF NUCLEONS IN THE NUCLEAR SURFACE

I. E. McCARTHY †, E. V. JEZAK and A. J. KROMMINGA

University of Minnesota, Minneapolis, Minnesota

Received 6 April 1959

Abstract: The results of the 40 MeV (p, 2p) experiments of Griffiths and Eisberg are analysed on the basis of a model for the total momentum transfer. Assuming two-body collisions and the impulse approximation and representing the momentum distribution of bound protons by a Fermi distribution whose maximum momentum is p_f, it is almost certain that 0.5 MeV $< p_f^2/2m <$ 1.5 MeV. Assuming a semiclassical model for the reaction it is shown that the events observed in this experiment occur in the extreme nuclear surface. Thus the experiment is strong evidence in support of the Thomas-Fermi approximation for nucleons in a finite nucleus. Representing the main bulk of the nucleus by an absorbing sphere, it is shown that the observed ratio of (p, 2p) to (p, p′) events is consistent with the assumption that direct interactions all proceed from an initial two-body collision.

1. Introduction

Observations of (p, p′) energy spectra and angular distributions are consistent with two different models for the direct interaction. They may be called the collective model [1]) and the single collision model.

The single collision model assumes the impulse approximation. That is, it assumes that momentum is not transferred to the nucleus during the collision. The effect of the nucleus on the incident and product particles before and after the collision is described by an average potential such as the optical potential for continuum states and the shell model potential for bound states.

There are two approaches to this model, the conventional quantal approach and the semiclassical approach. In the conventional approach the matrix element for a direct interaction, assuming the impulse approximation, is written

$$M = \int \psi_1^* \psi_2^* v_{12} \psi_0 \phi \mathrm{d}\tau \qquad (1)$$

where ψ_0, ψ_1 and ψ_2 are the wave functions of the incident and each product particle respectively, v_{12} is the two-body interaction potential and ϕ is the wave function of the initially bound particle; ϕ is a single particle shell model wave function. It is found that experimental results up to the present can be interpreted with this model and that the angular momentum states of

† Present Address: Department of Physics, University of California, Los Angeles, California.

the bound particles are the main factors in the calculation in cases where one of the final particles remains bound. In other cases such as high energy (p, 2p) processes and (p, d) pickup processes the bound state can be described by a momentum distribution which is consistent with the shell model [3]), namely a gaussian of half width about 18 MeV.

The semiclassical approach assumes, essentially, that collisions take place at definite points in the nucleus. The main feature of this approach is that collisions from which a product particle can be observed are highly localized in the nuclear surface when the incident energy is of the order of 40 MeV. Elton and Gomes [4]) have shown that, at such energies, the products of a direct interaction occurring inside the optical potential will almost certainly be totally internally reflected at the boundary, and such a reaction would therefore not be observed. This model of collisions in the classically forbidden region with nucleons at rest was successful in fitting the (p, p′) results of Eisberg and Igo [5]). The dependence of the results on the angular momentum transfer in the semi-classical picture has been emphasized by Butler, Austern and Pearson [6]).

In this paper we will discuss an experiment performed by Griffiths and Eisberg [7]), in which the angular correlation between two protons in fast coincidence resulting from a reaction initiated by a 40 MeV proton was observed. This angular correlation should be highly sensitive to the momentum of the struck particle rather than to the angular momentum transfer as in the (p, p′) case.

If the collisions are really localized in the nuclear surface, the momentum distribution observed will be characteristic of the surface. This is the essential difference between this and previous experiments which measure the nuclear momentum distribution. The angular correlation function was observed to be peaked in accordance with what would be expected by analogy with free proton collisions.

The model that will be used to describe the results of this experiment involves the following assumptions:

(1) The primary process in direct interactions is a single collision between the incident particle and a bound particle.

(2) The effect of the residual nucleus may be represented by a potential which is capable of absorbing and refracting continuum particles.

(3) The momentum transferred to the residual nucleus at the collision instant is exactly the momentum of the struck particle at that instant (impulse approximation).

(4) The collision may be localized in space.

(5) The momentum distribution of the initially bound particle is given by that of a zero temperature Fermi gas.

(6) In regions where the gradient of the potential is not large, the classical

impact parameter of the incident particle is a good measure of the position of the collision.

It will be found possible to give quite a precise description of the momentum distribution of the initially bound proton on the basis of assumptions 1 to 3. With assumption 4, it will be shown that the collisions are localized in a manner consistent with the ideas of Elton and Gomes. Assumptions 5 and 6 are not necessary for the basic idea, but are used for calculational purposes. Assumptions 4 and 6 have been discussed by Eisberg, McCarthy and Spurrier [8]). They are quite realistic in this case.

One more question can be answered by the (p, 2p) experiment. It could be argued that the observed angular correlation shows that single collisions do occur, but that the fact that collectively excited states of the residual nucleus have been observed [10]) is evidence that the collective process is far more important. The ratio of (p, 2p) to (p, p′) events has been experimentally determined. It is at least 0.1. It will be shown that this is consistent with the idea that all events started with a single collision but that in many cases one particle was absorbed by the nucleus. It is perfectly possible that this absorption could result in the excitation of collective states, but it would be hard to understand the peak in the angular correlation function on the basis of the assumption that the primary interaction was of a collective nature [11]).

2. Classification of the Experimental Results

The experiment may be represented diagrammatically by fig. 1. The energies of both product particles are measured. The angle Θ is held fixed, and the angle θ is varied. Hence the momentum transfer $\mathbf{q}$ involved is

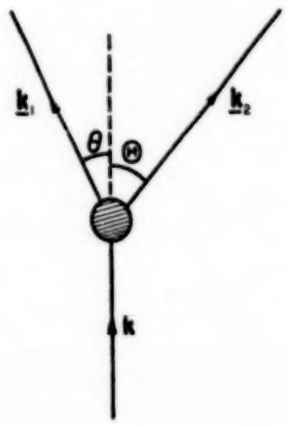

Fig. 1. Definition of the quantities used in the description of the (p, 2p) experiment.

completely determined for each event observed; $\mathbf{q}$ is the momentum transferred to the centre of mass of the residual nucleus in the reaction. The unit of momentum is the momentum of a proton whose energy is 1 MeV. One has

$$\mathbf{q} = \mathbf{k} - \mathbf{k}_1 - \mathbf{k}_2, \tag{2}$$

$$k^2 = E + k_1^2 + k_2^2; \tag{3}$$

E is the sum of the energy of the centre of mass of the residual nucleus and the excitation energy of the residual nucleus. Since the former will turn out to be very small in most cases, it will be neglected and E will be called the excitation energy. The mass difference of one unit between the initial and final nuclei will be neglected. It will be convenient to call the ratio of the final energies c:

$$c = k_1^2/k_2^2. \tag{4}$$

The square of the momentum transfer,

$$\begin{aligned} q^2 = 2k_1^2\{1 - mE/k_1^2 - [(1-2mE/k_1^2)/(1+c)]^{\frac{1}{2}}(\cos\Theta + c^{\frac{1}{2}}\cos\theta) \\ + c^{\frac{1}{2}}(1-2mE/k_1^2)\cos(\theta+\Theta)/(1+c)\}, \end{aligned} \tag{5}$$

is plotted against θ in fig. 2 for various values of c and E and for $\Theta = 45°$. In fig. 3 it is plotted for $\Theta = 25°$. It is assumed that the directions of the incident and both final particles are coplanar. This assumption is not correct, but it does not affect the value of q^2 seriously. The height of the counters was such that non-coplanar events would be counted. It is important to notice that the kinematics of the problem require a minimum momentum transfer for each set of values of E and Θ.

The way in which we want to look at the experimental data is as follows. There is a distribution of momentum transfers, of which the experiment measures a sample. We must assume that the sample, or in the following discussion several sub-samples defined for different ranges of values of E and Θ, are good estimates of the distribution. To obtain the sub-sample for particular ranges of E and Θ from the experimental results we must use sets of curves like those in figures 2 and 3 to look up the value of q^2 for events with different c and θ. In these figures, the number of events with a given θ is multiplied by q^2 $(\mathrm{d}\theta/\mathrm{d}q^2)$ and plotted against q^2. All possible values of c and θ have not been measured, and we must make an extrapolation. It will be seen that our conclusions are independent of reasonable extrapolations. We will only assume that the angular distribution of θ exhibits a peak in the region of minimum momentum transfer and of the width indicated experimentally.

We will make a model for the interaction from which we can deduce a q^2 distribution. We will compare this distribution with those obtained from the various sub-samples of the experimental distribution. If the sub-samples are all consistent with the model, this will serve as evidence that they are representative samples and that the model represents the interaction.

In the experiment of Eisberg and Griffiths, E and c were measured for $\Theta = 45°$ and $\theta = 25°$, $35°$, $65°$ and $55°$ in the cases of nickel and copper. (Lead did not yield enough results to draw conclusions.) In neither of these

cases was the distribution of θ peaked, but it appeared to indicate that a peak would occur at about 20°. Owing to the experimental geometry it was impossible to measure this, so Θ was changed to 25°. In this case a peak was

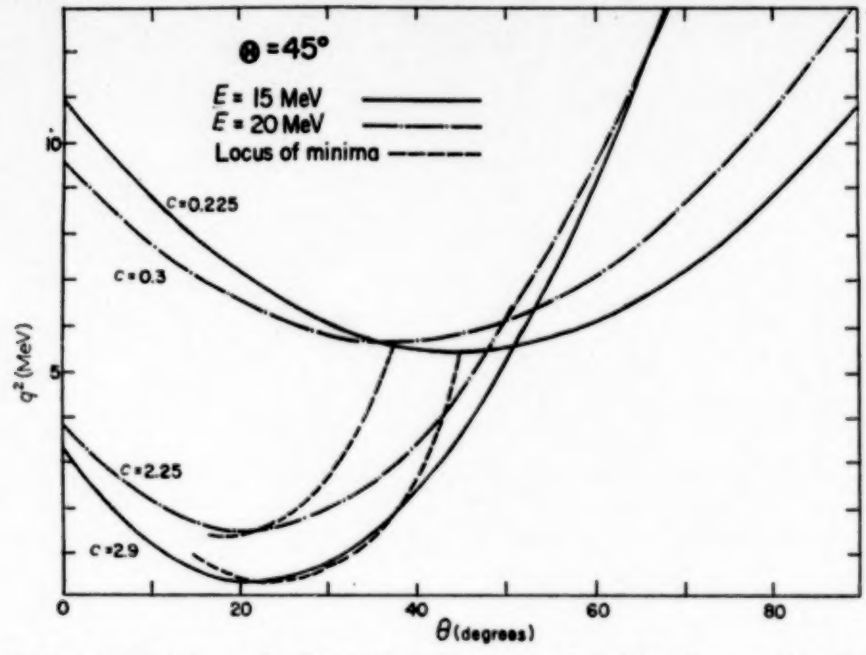

Fig. 2. Solutions of equation (5) which expresses the conservation of momentum for $\Theta = 45°$ and various excitation energies and c values.

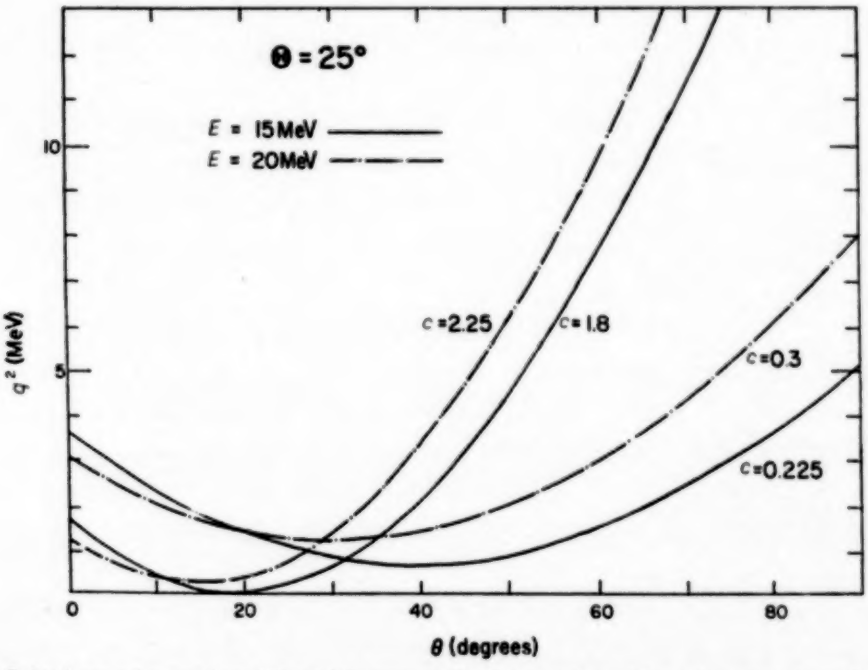

Fig. 3. Solutions of equation (5) which expresses the conservation of momentum for $\Theta = 25°$ and various excitation energies and c values.

observed in nickel for $\theta \approx 35°$. A peak could not be observed in copper, but the data were consistent with one at $\theta \approx 30°$.

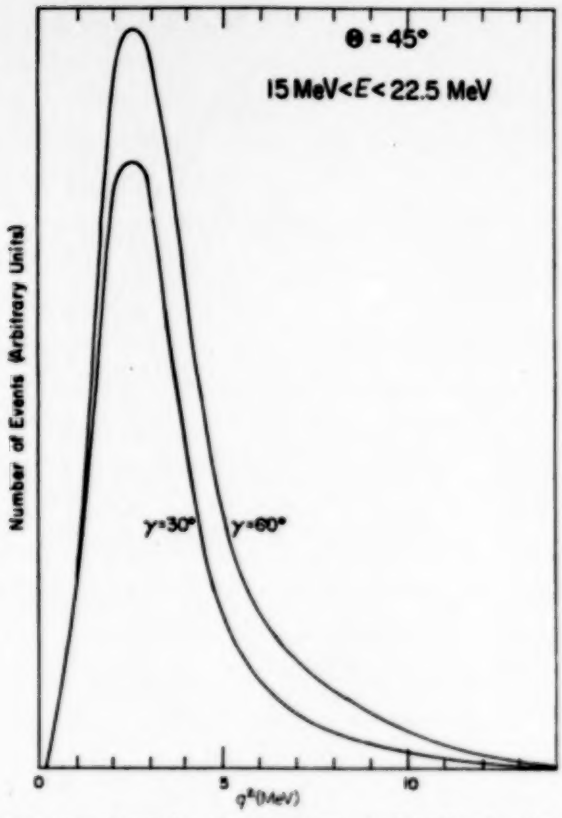

Fig. 4. Sub-sample momentum transfer distribution. A distribution is plotted for each of two extreme assumptions about the number of events far from the peak in the θ distribution.

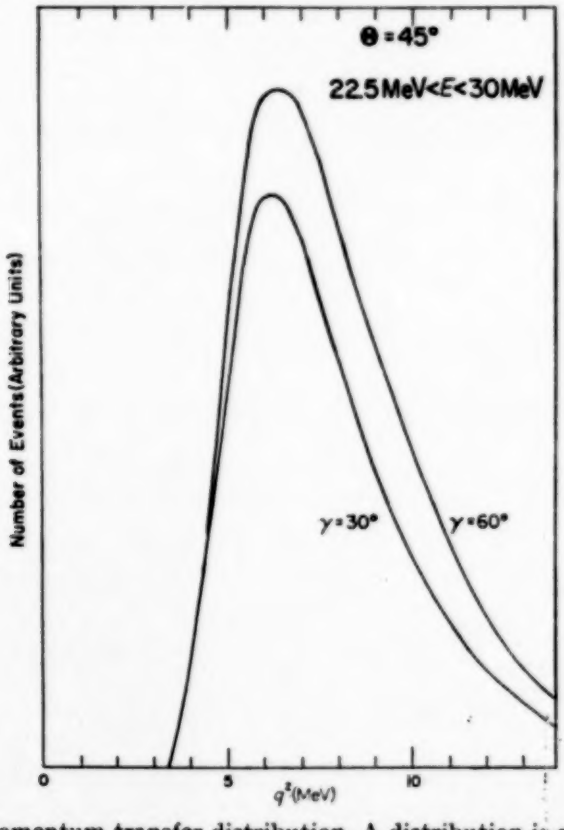

Fig. 5. Sub-sample momentum transfer distribution. A distribution is plotted for each of two extreme assumptions about the number of events far from the peak in the θ distribution.

The number of events for values of θ far from the peak was not observed. Its estimate requires an extrapolation which is the most serious in the theory. Assuming that there is only one peak, extreme shapes for the extrapolated angular distribution will be described in terms of the full width at half maximum, γ. Extreme values of γ are 30° and 60°. The results for $\Theta = 45°$ were consistent with the assumption that all values of c within the energetically allowed range were equally probable, but there was some evidence that extreme values of c were favoured. At $\Theta = 25°$, E and c were not measured explicitly, and the angular distribution must therefore be considered to be the integrated distribution over those two variables.

In making the sub-sample distributions we assumed that the data for $\Theta = 45°$ would exhibit a peak at $\theta = 20°$ of width γ between 30° and 60° for all values of E and c, that is, the same width as the peak for $\Theta = 25°$. The sub-sample distributions for $\Theta = 45°$ and $\gamma = 30°$ and 60° are illustrated in figs. 4 and 5 for 15 MeV $< E <$ 22.5 MeV and 22.5 MeV $< E <$ 30 MeV. In the necessary extrapolations, it was assumed that all values of c are equally probable. This assumption is not critical.

The striking feature of these distributions is that the peak is sharply defined at low values of the momentum transfer and its position is essentially independent of extrapolations provided we assume that the angular distribution is peaked in essentially the same way as in the one case (nickel for $\Theta = 25°$) where the peak is actually observed. All data are consistent with this assumption, and with the assumption, that, in the other cases, only one side of the peak is observed.

We must also assume at this stage that departures from coplanarity are not important. This assumption is consistent with the model which will be suggested. If most non-coplanar events are observed, the maximum possible effect of non-coplanarity would be to increase the position of the peak by about 2 MeV.

The experimental results are thus interpreted as follows. Each sub-sample of the momentum distribution determines two numbers, namely the low momentum cut-off (which is fixed when E and Θ for the subsample are defined) and the peak in the momentum distribution which is determined to within 1 MeV. Hence it will be possible to make a two-parameter model with which to compare the data. The shape of the distribution on the high-momentum side is also qualitatively determined and this could be used to improve on the two-parameter model.

One other experimental fact is important. This is that the excitation energy E shows a monotonic spectrum, with larger numbers of events at high values of E.

3. Impulse Approximation Model

We will first attempt to make a model for the interaction using only assumptions 1, 2, 3, and 5 of section 1. Assumption 3 says that the momentum transfer **q** may be thought of as the sum of two momentum transfers **p** and $\mathbf{p}_e$:

$$\mathbf{q} = \mathbf{p} + \mathbf{p}_e; \tag{6}$$

p is the momentum transferred to the nucleus at the collision instant. Essentially, this idea involves redefining the nucleus at the collision instant. If it had A particles initially, it has $A-1$ after the collision. The centre of mass of the $(A-1)$-nucleus has momentum **p** if the struck particle initially had momentum $-\mathbf{p}$. The momentum transfer $\mathbf{p}_e$ is due to all processes except the collision. According to assumption 2, $\mathbf{p}_e$ is made up of the momenta transferred elastically to the nucleus by the interaction of the incident and product particles with the optical potential of the nucleus. No assumptions are yet made about the form of the optical potential; we are interested only in its effect on the motion of the centre of mass of the nucleus.

We must now assume distribution functions for **p** and $\mathbf{p}_e$. For **p** we will assume a Fermi distribution, that is **p** is isotropic and all values of p^2 are equally probable up to a maximum p_f^2. Whether this assumption is realistic will be discussed in the light of the results. At present it is sufficient to say that a one-parameter distribution is the simplest assumption.

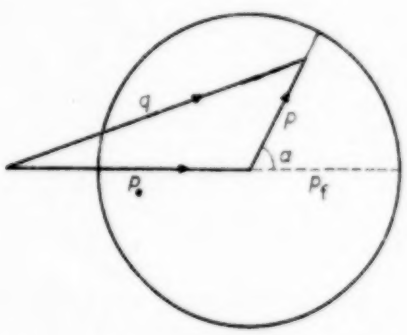

Fig. 6. Definition of the quantities used in the impulse approximation model.

As a first approximation, seeing that we only hope to determine two parameters with any precision, we will assume that $\mathbf{p}_e$ is constant. This assumption is reasonable in the light of the ideas of Elton and Gomes [4]). Only a small range of impact parameters is likely to contribute to the reaction and the momentum transferred elastically is not very sensitive to the impact parameter if the reaction occurs in the region where the Coulomb potential s the dominant one.

We will now calculate the distribution function $F(q^2)$ where **q** is defined by eq. (6), $\mathbf{p}_e$ is constant, and the distribution function for p is given by

$$f(p) = \begin{cases} \dfrac{3}{4\pi p_t^3}, & p \leqq p_t \\ 0 \quad , & p > p_t. \end{cases} \tag{7}$$

The definition of **q** is illustrated in fig. 6.

Since $\mathbf{p}_e$ is constant and **p** is isotropic, **q** is defined by either of the pairs of numbers p and α or q and α. Hence,

$$dN(q, \alpha) = dN(p, \alpha), \tag{8}$$

where the notation is such that dN followed by a set of coordinates is the differential number of events for variation of all those coordinates. From (8),

$$dN(q, \alpha)dq d\alpha = f(p)p^2 \frac{dp}{dq} dq \sin \alpha d\alpha, \tag{9}$$

$$p = p_e \cos \alpha \pm \sqrt{p_e^2 \cos^2 \alpha - p_e^2 + q^2}. \tag{10}$$

Hence, integrating (9) with respect to α,

$$dN(q)dq = dq \int \sin \alpha d\alpha f(p) \frac{dp}{dq} p^2 \tag{11}$$

$$= q dq \int_{-1}^{1} dx f(p)p^2/(p - p_e x) \tag{12}$$

where

$$x = \cos \alpha. \tag{13}$$

The integral over x can be evaluated and the result is as follows. Putting

$$F(q^2) \equiv 2q dN(q), \tag{14}$$

one finds, for $p_t < p_e$,

$$F(q^2) = \begin{cases} 0 \quad \text{for} \quad q < p_e - p_t \\ 3\dfrac{q^2}{p_t^3}\left[\dfrac{p_t^2 + p_e^2 - q^2}{2p_t p_e}\left\{\dfrac{(p_t^2 + p_e^2 - q^2)^2}{4p_t^2} - p_e^2 + q^2\right\}^{\frac{1}{2}} + q\right] \\ \qquad\qquad \text{for} \quad p_e - p_t \leqq q \leqq p_e + p_t \\ 0 \quad \text{for} \quad q > p_e + p_t. \end{cases} \tag{15}$$

For $p_t \geqq p_e$, $F(q^2)$ is proportional to q^3 up to $q = p_t - p_e$ and has the same form as (15) beyond that. This case, however, is not interesting in the present problem because the kinematics of the problem requires a low-momentum cut-off. $F(q^2)$ is illustrated in fig. 7 for various values of p_e^2 and p_t^2.

It must now be determined what values of p_e and p_t fit the subsample distributions from the experiment. In fitting the data, sufficient accuracy is obtained by saying that the low momentum cut-off is at $(p_e - p_t)^2$, the peak is at $p_e^2 + p_t^2$, and the high momentum cut-off is at $(p_e + p_t)^2$. In equating the low momentum cut-off in the model to that in the sub-sample we are constraining the model to satisfy the kinematical conditions of the sub-sample. The positions of the peak are then equated.

Reasonable values for p_e^2 and p_f^2 which fit fig. 4 are

$$p_f^2 = 0.5 \text{ MeV}, \quad p_e^2 = 1.6 \text{ MeV}.$$

Fig. 5 is fitted by

$$p_f^2 = 0.6 \text{ MeV}, \quad p_e^2 = 5.2 \text{ MeV}.$$

Consider fig. 4. The high momentum cut-off in the model is at about 4 MeV.

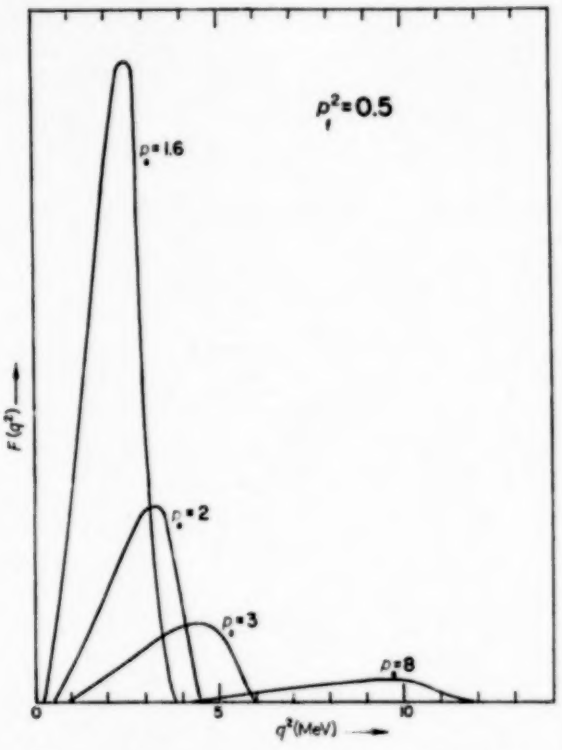

Fig. 7. The distribution of eq. (14) plotted so as to illustrate how the experimental data of fig. 4 may be fitted by including different values of p_e^2 with different weights.

Clearly this does not fit the sub-sample. There are small numbers of events whose momentum transfer is much higher, up to about 16 MeV. Keeping the most general assumptions about the impulse approximation, this inadequacy of the model must be due to our assumptions for the distributions of $\mathbf{p}_e$ and $\mathbf{p}$. There must be a high-momentum cut-off in the $\mathbf{p}$ distribution. We are not trying to determine more details of this distribution than one parameter, so we must assume that a Fermi distribution is an adequate description, although we could not distinguish between this and a cut-off Gaussian †. Any higher momenta would reduce the low-momentum cut-off in the model, and in order to fit the data, a third momentum would be necessary in eq. (6), in violation of the impulse approximation.

The assumption of a constant $\mathbf{p}_e$ is clearly not very realistic. A distribution

† If the actual momentum distribution has components greater than p_f, this would mean that the struck proton is sometimes correlated with another. These events would appear in a sample of higher E.

for p_e^2 like those of figs. 8 and 9 would allow the model to fit the respective sub-samples.

The numbers for p_e^2 and p_f^2 which fit the respective sub-samples are not unique, but this method gives a very strong indication of the order of magnitude of p_f^2. For example it would be difficult to fit either sub-sample

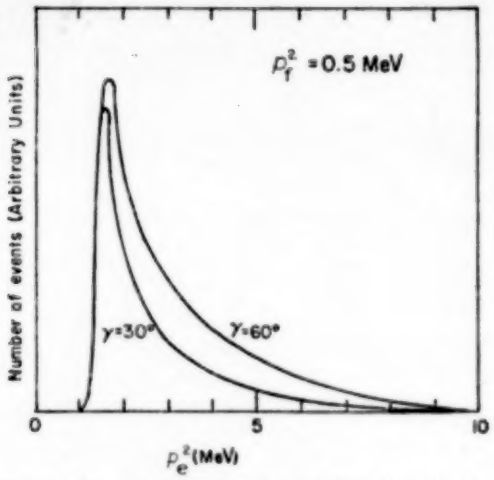

Fig. 8. Rough illustration of the distribution of p_e^2 which would be necessary to fit the sub-sample of fig. 4.

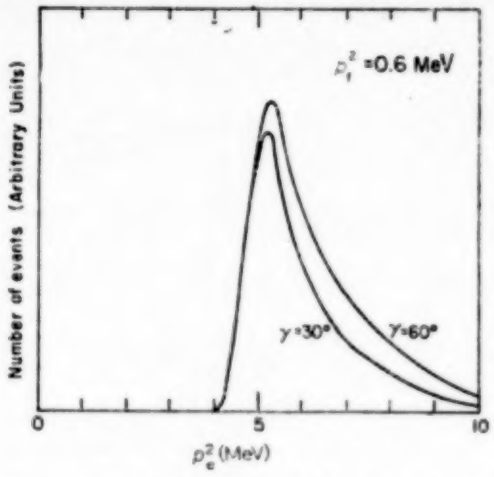

Fig. 9. Rough illustration of the distribution of p_e^2 which would be necessary to fit the sub-sample of fig. 5.

with a value of p_f^2 as high as 1.5 MeV. In the next section it will be shown that this model fits in with considerations about the momentum transfer in the optical model potential.

4. Localization of Collisions

We now have a model which fits the sub-samples of the momentum transfer distribution. Let us consider the distributions which it is necessary to assume for p_e^2, such as those in figs. 8 and 9, in the light of the semi-classical model for direct interactions. Fig. 10 shows the real part of a reasonable optical potential [12]) for nickel for particles whose energy is near 10 MeV.

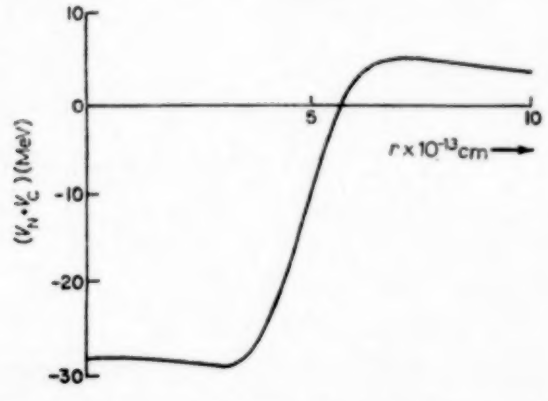

Fig. 10. The real part of a reasonable optical model potential for protons scattered by nickel.

The idea of Elton and Gomes, namely that reflection in the potential gradient prevents direct interaction products from escaping if the collision occurs inside the potential, suggests that the most likely collision distances are outside of 7×10^{-13} cm. At this distance, the density of nuclear matter is falling off rapidly so that collisions further out are very improbable. Collisions closer in are more probable because the potential gradient is small until 6×10^{-13} cm or less and the nucleon density increases rapidly. It must be realised that the nuclear radius is uncertain to within about 10^{-13} cm.

It is possible to make a crude estimate of the momentum transferred elastically in this collision by using the elastic scattering of particles in the Coulomb field. It has been shown by Eisberg, McCarthy and Spurrier [8]) that the classical flux of particles in the region where the potential gradient is not large is very similar to the quantal flux, so we expect classical arguments to give a good idea of the localization of the collision. The momentum transferred to the nickel nucleus by a 40 MeV proton with an impact parameter of 8×10^{-13} cm is equivalent to about 0.6 MeV. Assume that half this momentum is transferred before the collision and that the momentum transferred by each product particle is inversely proportional to its speed in the potential. With this crude model, we find p_e^2 is about 2 MeV for 8×10^{-13} cm, 4 MeV for 7×10^{-13} cm.

The crude model for p_e^2 enables us to establish a qualitative correspondence between the distributions for p_e^2 of figs. 8 and 9 and distributions of impact parameters. The sharp drop in the p_e^2 distributions on the low momentum transfer side reflects the small number of possible collisions outside 7×10^{-13} cm. The fact that the inhibition of direct interactions due to the potential gradient is not strong until about 6×10^{-13} cm and also the fact that the impact parameter model tends to underestimate the momentum transfer explains the increased possibility of higher momentum transfers.

The difference between the sub-samples centered about $E\approx19$ MeV and $E\approx26$ MeV is that the second one comes from events which occur at smaller impact parameters, since p_e^2 is larger. It is also possible that p_t^2 is higher for these events. The higher density of nucleons in this region would account for the significant increase in the number of events with larger E. Each subsample contains a large energy range, so all these effects are expected to be blurred.

This semiclassical model also enables us to estimate the additional momentum transfer due to non-coplanarity. It could lead to values of p_t^2 slightly higher than 1 MeV, but not as large as 1.5 MeV, so to the order of accuracy of these calculations it is a minor effect.

5. Ratio of (p, 2p) to (p, p′) Events

Let us assume that the first process in a direct interaction is always a two-body collision. In some cases both product particles will be absorbed, in

some cases neither will be absorbed and in some cases one will be absorbed. Let us represent the nucleus by a totally absorbing sphere of radius R, and assume that the collision occurs in a spherical shell of outer radius R' with probability independent of its radial coordinate but dependent on its angular position in the same way as the divergence of the flux of the incoming particles in the optical model [13]). Let us represent the paths of all particles by straight lines and calculate the ratio ρ of (p, 2p) events to (p, p') events for different values of R, R' and the angular dependence of the collision probability.

Table 1 gives values of this ratio, for $\Theta = 45°$. The angular dependence of the collision probability is crudely represented by the volumes x, y and z of fig. 11 in which the collision probability is assumed to be constant and equal respectively to A, 1 and 0. Experimental values are about 0.1 for both nickel and copper.

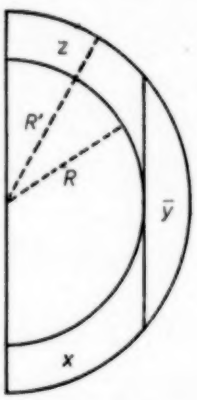

Fig. 11. Definition of the model for the shadow effect.

For this calculation we assume a gaussian angular correlation function centered at $\theta = \theta_0$ and of width σ. The ratio ρ is not sensitive to the values assumed for these parameters. The ratio $\rho(\theta)$ of (p, 2p) to (p, p') events for a particular value of θ is assumed to be the ratio of the length of the path of the incoming particle inside the collision shell from which both product particles would not enter the absorbing centre to that from which one of them would.

Fig. 12 shows $\rho(\theta)$ plotted against θ for various values of R and R'. It is independent of A because the probability of seeing a (p, 2p) event originating in the region x is assumed to be zero. The curves give an indication of why it is difficult to observe a peak in the angular distribution if it occurs near small values of θ. Events at small angles are much less inhibited by the shadow effect and the small angle side of the peak would be difficult to observe.

The numbers displayed in table 1 are meant to indicate the sensitivity of the calculation to the values of the parameters used rather than to indicate any accuracy in the calculation. The experimental numbers are also subject to large errors. However it is safe to conclude that this effect is capable of

explaining all the events on the assumption of the single collision model with reasonable values of the necessary parameters. At worst it indicates that the single collision model represents an important fraction of all direct interactions.

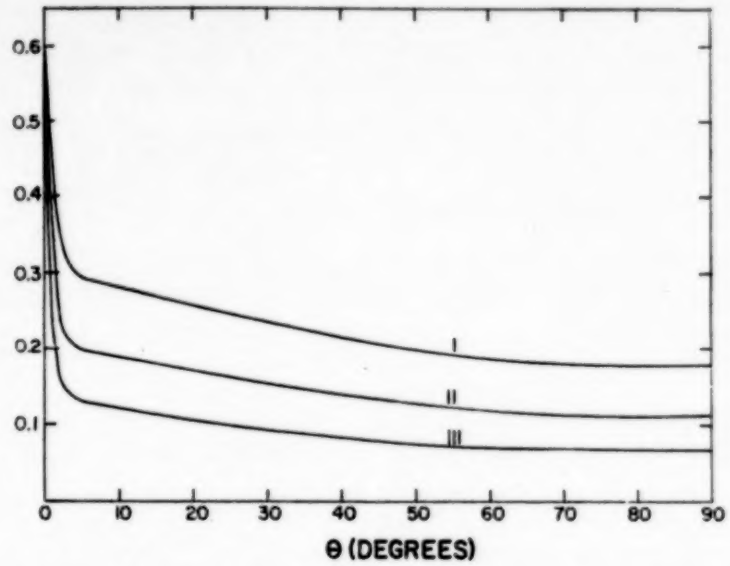

Fig. 12. The probability of seeing a (p, 2p) event for different θ and for $\Theta = 45°$, assuming the event takes place with equal probability for all θ and allowing for the shadow effect. Curves I, II, and III are for $R' = 8$ and $R = 6.8$, 7 and 7.2×10^{-13} cm, respectively.

TABLE 1

The ratio ρ of (p, 2p) events to (p, p′) events for different values of the parameters R, R', A, θ_0, σ

$R'(10^{-13}$ cm)	$R(10^{-13}$ cm)	A	θ_0(degrees)	σ(degrees)	ρ
8	7	4	40	15	0.062
8	7	3	40	15	0.086
8	7	2	40	15	0.141
8	7.2	2	40	15	0.086
8	6.8	2	40	15	0.219
8	7	3	25	15	0.107
8	7	3	25	20	0.123

6. Conclusion

It is possible to measure directly the momentum transferred to the nucleus in each (p, 2p) event observed. A distribution of momentum transfers can be inferred from these measurements. The momenta in this distribution are very much lower than those inferred for the struck particle from high energy (p, 2p) and (p, d) experiments. Making the impulse approximation it is possible to calculate a momentum distribution for the struck particle. The shape of this distribution is not determined, but if it is represented by a Fermi distribution, the maximum energy p_f^2 is between 0.5 MeV

and 1.5 MeV. It is also possible to calculate a distribution of momenta transferred elastically to the nucleus by the incident and final particles before and after the collision. Making a classical approximation in an optical model potential, these momenta would arise from events occurring in the extreme nuclear surface. Assuming that single collisions do occur in the extreme surface and that a proton which would pass through any part of the nucleus where the potential is strong would be absorbed, it is possible to calculate a ratio of (p, 2p) to (p, p′) events which is consistent with the experimental value. This suggests that single collisions are a very important mechanism in inelastic proton scattering.

The conclusions are based on certain approximations and extrapolations and it is necessary to examine the results in the light of the assumptions to see if the theory is internally consistent or if the experiments are capable of another interpretation.

For given values of E and Θ, momentum transfer distributions are inferred from the sample of momentum transfers observed. This involves the assumption that the angular distribution over θ is peaked and that the peak occurs in the position indicated by the one case in which it is observed. The geometry of the experiment would prevent peaks being observed in the other cases. In the case of the two sub-samples discussed, namely those illustrated in figs. 4 and 5 for $\Theta = 45°$ it is clear that the theory determines similar distributions for the struck particle. In the case of $\Theta = 25°$, assuming that the distributions of E and c are similar to the $\Theta = 45°$ case, it is possible to estimate a q^2 distribution. For $20° < \theta < 30°$ some momentum transfers much less than the minimum predicted in the theory could be observed. As c has not been measured in this case, it is not clear whether they are really seen. However, the tendency for extreme values of c to predominate would reduce the number of very small momentum transfers in this range of θ. Also the angular correlation function is peaked sharply at $\theta = 35°$ in the case of nickel, and therefore, in any case, the anomalously small momentum transfers would be a small fraction of the whole distribution. Since events with such a small momentum transfer would violate the impulse approximation if the value of p_f^2 is the same for this sub-sample, these results tend to confirm the validity of the impulse approximation, as well as to indicate further that the predicted value of p_f^2 for a given E is independent of the sub-sample. Measurements of k_1^2 and k_2^2 for $\Theta = 25°$ should be critical in determining the validity of the theory.

It has also been assumed that all non-coplanar events are counted. If there are non-coplanar events which have not been counted they would increase the position of the peak in the momentum transfer distribution considerably. However, they should not affect our conclusions about p_f^2 because the collision itself is coplanar. Particles are bent out of the plane by

the potential; therefore, additional momentum transfers due to non-coplanarity should contribute to p_e^2, not p_f^2. The results obtained for p_e^2 are consistent with the assumption that non-coplanar events are all counted, considering the angular width of the counters. It would be informative to have experimental results on non-coplanar events.

Since the results of this experiment seem violently to contradict the results of all other experiments [3]) which measure a nucleon momentum distribution, it is worthwhile to consider the certainty of the conclusions drawn here. If the large momentum components observed in the previous experiments were observed in this one, the angular correlation function either would not be peaked, or would be peaked far from the angles for minimum momentum transfer. Regardless of details, the certainty for small momenta is determined by the degree of certainty that there is a peak and that it is in the region of minimum momentum transfer.

The evidence for the prevalence of high momenta (e.g. a gaussian momentum distribution of width 18 MeV) is based on photoproduction of nucleons, (p, p') reactions, and deuteron pickup reactions, all initiated by particles of about 300 MeV. The analysis of these experiments is based on the Born approximation, i.e. the momentum transfer to the residual nucleus is assumed to be entirely due to the motion of the struck particle. Analysis of these experiments by the methods of this paper confirms that the elastic processes are in fact negligible. Thus, in view of the fact that we believe that the wave functions of all bound nucleons extend throughout the nucleus as they do in the simple shell model, and that the momentum distribution is a property only of the nucleon wave function, there does appear to be a serious contradiction.

In terms of the semiclassical idea of localization of the reactions, the essential difference between the two methods of observation is that the high energy experiments observe reactions taking place throughout the nucleus, whereas the low energy experiment observes only reactions at the surface. The latter conclusion is reached directly from the experiment without external inferences. To see that the high energy experiments observe the whole nucleus we must use external ideas, mainly the idea that the mechanism which prevents observation of reactions in the centre is reflection of the longer wave-length product particles in the potential boundary. At the high energies used, this effect should not be nearly as important as at 40 MeV. It is true that the absorption in the optical model reduces the probability of reactions occurring in the centre, but it has been shown by McCarthy [13]) that this effect is not very important. The probability of a reaction occurring in the centre is reduced by only a factor of about 4 in the case of strongly absorbed α-particles in argon.

The essential difference between the two momentum distributions is that

the one measured by the high energy experiments is associated with particles throughout the nucleus, the one measured by the low energy experiments is associated with particles in the extreme surface. It is possible to represent a nucleon in a very general potential by a wave function which is a function only of the coordinates of the one nucleon [14]). According to present shell model ideas this wave function is spread out through the whole nucleus for all nucleons. The concept of a momentum distribution characteristic of the surface layer, which is a volume much smaller than the volume occupied by the wave function, is necessary in order to explain the two different momentum distributions.

Since the momentum distributions arise from an ensemble of nuclei it may be possible to interpret the experiments by means of Wigner's phase space distribution function [15]),

$$f(p, q) = \int \psi^*(q+\tfrac{1}{2}\xi)e^{ipx/\hbar}\psi(q-\tfrac{1}{2}\xi)d\xi, \qquad (16)$$

where p and q are the phase space coordinates of a nucleon relative to a given nucleus, and the ψ are shell model wave functions. This will be discussed in a future publication.

In conclusion, it is interesting to note that the result described here is in accord with the Thomas-Fermi approximation, which predicts a Fermi energy of roughly 1 MeV in the region of the nucleus observed by the experiment. Theories of the finite nucleus based on this approximation predict also that, in the region considered, correlation effects in the nuclear wave function are insignificant in comparison with single particle effects [9]), and the assumption of a zero temperature Fermi distribution is therefore justified by the result.

The authors would like to thank Drs. F. Coester, R. M. Eisberg, C. E. Porter and H. Weidenmüller for many discussions.

References

1) S. Hayakawa and S. Yoshida, Prog. Theor. Phys. **14** (1955) 1
2) C. A. Levinson and M. K. Banerjee, Annals of Physics **1** (1957) 499
3) K. A. Brueckner, R. J. Eden and N.C. Francis, Phys. Rev. **98** (1955) 1445
4) L. R. B. Elton and L. C. Gomes, Phys. Rev. **105** (1957) 1027
5) R. M. Eisberg and G. Igo, Phys. Rev. **93** (1954) 1039
6) S. T. Butler, N. Austern and C. Pearson, Phys. Rev. (to be published)
7) R. J. Griffiths and R. M. Eisberg, Nuclear Physics **12** (1959) 225
8) R. M. Eisberg, I. E. McCarthy and R. A. Spurrier, Nuclear Physics **10** (1959) 571
9) K. A. Brueckner, private communication
10) B. L. Cohen, Proceedings of the Paris Conference on Nuclear Physics (1958)
11) R. M. Eisberg, Proceedings of the Paris Conference on Nuclear Physics (1958)
12) A. E. Glassgold and P. J. Kellogg, Phys. Rev. **107** (1957) 1372
13) I. E. McCarthy, Nuclear Physics **10** (1959) 583
14) H. A. Bethe, Phys. Rev. **103** (1956) 1353
15) G. A. Baker, Phys. Rev. **109** (1958) 2198

2.A.1 *Nuclear Physics* **12** (1959) 291—297; © *North-Holland Publishing Co., Amsterdam*

Not to be reproduced by photoprint or microfilm without written permission from the publisher

TOTAL NEUTRON CROSS SECTIONS OF THE HYDROGEN AND HELIUM ISOTOPES

LOS ALAMOS PHYSICS AND CRYOGENICS GROUPS †

Los Alamos Scientific Laboratory, University of California, Los Alamos, New Mexico ††

Received 20 March 1959

Abstract: The following experimental total neutron cross section data are reported: for H^3 and He^3 in the energy region from about 0.2 to 20 MeV; for He^4 from 1 to 15 MeV; rather precise measurements for H^1 and H^3 at 14.10 MeV. Interesting comparisons are made with the theoretical calculations reported by Bransden, Robertson and Swan for H^3 and He^3.

Since 1952 several experimental studies of fast neutron total cross sections of the hydrogen and helium isotopes have been carried out at Los Alamos. Much of the work has been reported only locally [1–4]), although the measurements on H^2 and some of the measurements on H^1 and He^4 have been published [5–7]). The present report presents the unpublished data consisting of the following total neutron cross sections: for H^3 and He^3 in the energy region from about 0.2 to 20 MeV; for He^4 from 1 to 15 MeV; for H^1 at 14.1 MeV, this latter value having fairly high precision.

Monoenergetic neutrons were employed in conventional good geometry transmission experiments essentially like those described in refs.[5, 6, 7]). Gaseous samples at pressures up to 2500 psi were contained in a cylindrical steel cell 100 cm long. Gas transfer and measurement were carried out by the cryogenic methods described in ref. [5]). The cell was filled to suitable pressure by condensing the gas in a high pressure vessel cooled to low temperature. The vessel was then sealed with valves and warmed to a temperature where the vaporized gases exerted pressure suitable for charging the cell. Monoenergetic neutrons were produced over a wide range of energies by the H^3(p, n)He^3, H^2(d, n)He^3, and H^3(d, n)He^4 reactions with an electrostatic generator or a Cockcroft-Walton accelerator. Scintillation counters employing organic phosphors, or ionization chambers containing hydrogen or deuterium-argon mixtures at pressures up to 1200 psi were used as neutron detectors.

† Participants: M. E. Battat, R. O. Bondelid, J. H. Coon, L. Cranberg, R. B. Day, F. Edeskuty, A. H. Frentrop, R. L. Henkel, R. L. Mills, R. A. Nobles, J. E. Perry, D. D. Phillips, T. R. Roberts and S. G. Sydoriak. Inquiries regarding this work should be addressed to J. H. Coon, Los Alamos Scientific Laboratory.

†† Work performed under the auspices of the U.S. Atomic Energy Commission.

All samples were of high purity except the H^3 sample which contained 5 % H^1 and smaller amounts of H^2 and He^3. The atomic composition was accurately determined for all samples by mass spectroscopic methods and corrections made for the effect of impurities. Rather high precision was attempted in the case of H^1 and H^3 at 14.10 MeV where the statistical errors in the cross section were 0.4 % and all other errors combined were estimated to be about 0.5 %.

The measured cross sections for H^3, He^3 and He^4 are presented in tables 1, 2 and 3 where for the sake of completeness the published He^4 data of Day and

TABLE 1

Total neutron cross sections of H^3

Neutron energy (MeV)	Total neutron energy spread (MeV)	Cross section (barns)
0.29	±0.03	1.32 ±0.07
0.54	±0.03	1.52 ±0.05
0.71	±0.08	1.58 ±0.05
0.99	±0.08	1.69 ±0.05
1.11	±0.02	1.67 ±0.05
1.50	±0.06	1.89 ±0.04
2.03	±0.05	2.09 ±0.04
2.49	±0.05	2.28 ±0.05
2.99	±0.04	2.40 ±0.05
3.4	±0.63	2.43 ±0.05
3.73	±0.11	2.48 ±0.05
4.1	±0.41	2.40 ±0.05
4.77	±0.08	2.25 ±0.05
4.80	±0.24	2.28 ±0.05
5.34	±0.17	2.16 ±0.04
5.52	±0.10	2.16 ±0.04
6.07	±0.08	2.05 ±0.04
6.58	±0.08	1.90 ±0.04
6.97	±0.10	1.81 ±0.04
14.10	±0.05	0.978±0.007
18.0	±0.17	0.75 ±0.04
19.1	±0.11	0.75 ±0.04
20.0	±0.07	0.66 ±0.04

Henkel [7]) at 17.97, 19.00, and 20.07 MeV are included. The data for H^3 and for He^3 originate from the same experiments as those which form the basis of the values presented in the Brookhaven compilation [4]). Some of the values given in table 1 for H^3 differ slightly from those in the Brookhaven compilation because the values in table 1 have been corrected for the presence of a small He^3 contamination in the tritium sample. This correction made use of the He^3 cross sections given in table 2. Of the He^3 cross sections presented in the Brookhaven report, values are misplotted at 0.85, 8.2 and 9.1 MeV.

TABLE 2

Total neutron cross sections of He^3

Neutron energy (MeV)	Total neutron energy spread (MeV)	Cross section (barns)
0.14	±0.05	3.44
0.28	±0.04	3.12
0.39	±0.05	2.92
0.505	±0.05	2.82
0.736	±0.04	2.75
0.955	±0.04	2.85
1.17	±0.04	2.95
1.39	±0.03	3.09
1.60	±0.03	3.20
1.77	±0.03	3.20
2.02	±0.03	3.23
2.22	±0.02	3.28
2.42	±0.02	3.08
2.63	±0.02	3.06
2.83	±0.02	2.97
3.04	±0.02	2.95
3.23	±0.02	2.85
3.44	±0.02	2.86
3.64	±0.02	2.74
3.84	±0.02	2.66
4.05	±0.02	2.57
4.25	±0.02	2.58
4.85	±0.10	2.40
5.44	±0.08	2.28
5.97	±0.06	2.19
6.50	±0.06	2.04
7.00	±0.05	2.01
7.52	±0.05	1.90
8.03	±0.04	1.86
14.8	±0.25	1.14
16.0	±0.40	1.04
16.9	±0.20	1.02
17.6	±0.12	0.96
18.2	±0.09	0.88
18.8	±0.08	0.93
19.3	±0.06	0.88
19.9	±0.06	0.87
20.4	±0.05	0.87
20.9	±0.05	0.88
21.4	±0.04	0.81

Estimated error for the cross section values is ±0.06 barn.

The H^1 cross section at 14.10±0.03 MeV was determined to be 0.687±0.007 barn [8]), in good agreement with previously measured values [9]) the most accurate of which is the value 0.689±0.005 barn at 14.10±0.05 MeV

TABLE 3
Total neutron cross sections of He^4

Neutron energy (MeV)	Total neutron energy spread (MeV)	Cross section (barns)
0.94	±0.08	6.31 ±0.13
1.50	±0.06	5.62 ±0.11
1.98	±0.05	3.98 ±0.08
2.49	±0.05	3.16 ±0.06
2.99	±0.04	2.79 ±0.06
4.95	±0.25	2.183±0.02
5.52	±0.20	2.052±0.02
6.06	±0.17	1.961±0.02
6.59	±0.15	1.858±0.02
7.10	±0.14	1.780±0.02
12.35	±0.05	1.177±0.02
12.65	±0.05	1.157±0.02
13.13	±0.05	1.079±0.02
14.10	±0.05	1.03 ±0.02
14.14	±0.05	1.005±0.02
15.18	±0.05	0.967±0.02
17.62	±0.22	0.895±0.03
17.97	±0.22	0.848±0.03
19.00	±0.16	0.816±0.03
20.07	±0.13	0.770±0.03

reported by Poss, Salant, Snow and Yuan [10]). Error in the neutron energy quoted for the present experiment is principally due to the uncertainty in the H^3(d, n)He^4 reaction energy [11]). The slope of the $\sigma(E_n)$ curve at 14.1 MeV as deduced from the curve given in ref. [4]), is about 0.0015 barn per 0.03 MeV.

The He^4 cross sections presented in table 3 agree reasonably well with the Wisconsin data [12]) in the energy region 0.9 to 5 MeV where the experiments overlap. As was pointed out by the Wisconsin workers, some of their experimental data suffer from the presence of an unknown contribution of the low energy group of neutrons from the Li^7(p, n)Be^7 reaction. Their estimated uncertainties due to this cause are about 10 % in the region a few hundred keV above and below the peak of the resonance near 1 MeV. The present experiment employed the reaction H^3(p, n)He^3 to obtain neutrons in this energy region, and was therefore not subject to spurious neutrons. However, since in the present experiments only one point was measured in this energy region, as is seen in table 3, considerable experimental uncertainty remains in the n—He^4 cross section in the critical region of this resonance. The analysis by Dodder and Gammel [13]) of n—He^4 scattering probably gives the best values near 1 MeV.

The experimental H^3 cross section values reported by Katsaurov *et al.* [14]) at 2.5 and 14 MeV are 2.5±0.5 and 0.63±0.17 barns, respectively. The first

CROSS SECTION (BARNS)

of these is in agreement with the present report while the second disagrees significantly with the value 0.978 ± 0.007 barn at 14.10 ± 0.03 MeV reported here. Although the cause of the discrepancy is not known, it may be pointed out that the tritium sample used by Katsaurov *et al.* was water containing only 9.2 % T_2O, the remainder being H_2O. Accurate measurements would be much more difficult with this type of tritium sample than with the nearly pure gaseous samples employed in the present experiments.

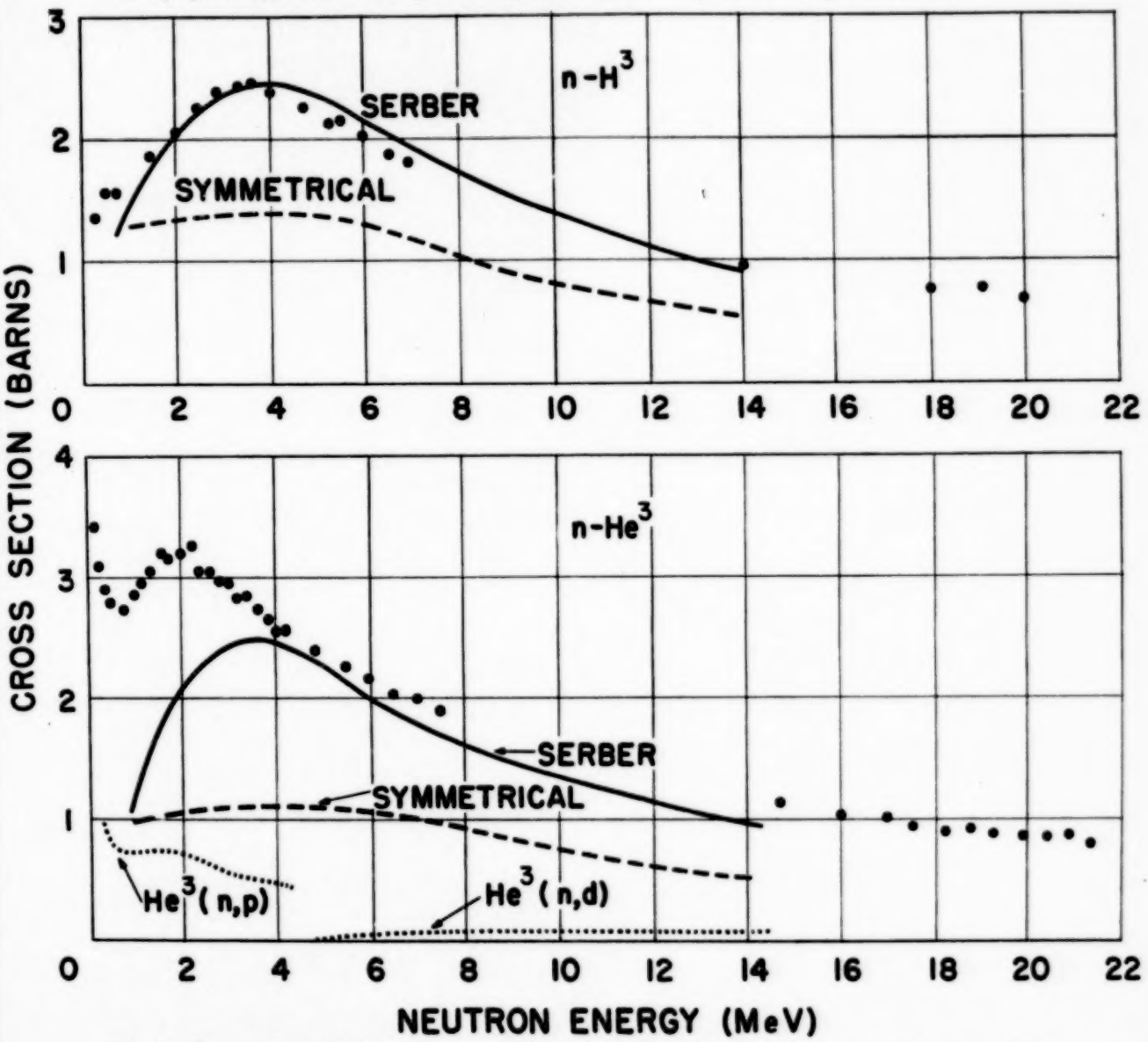

Fig. 1. Comparison of theoretical and experimental cross sections for n—H^3 and n—He^3 interactions. Experimental total cross sections from the present report are indicated by data points, while experimental He^3(n, p)H^3 and He^3(n, d)H^2 cross sections are taken from refs.[4]) and [16]), respectively, and are shown by dotted curves. Detailed balancing calculations by J. D. Seagrave (private communication) of He^3(n, p)H^3 cross sections based on unpublished H^3(n, p)He^3 measurements of J. E. Perry *et al.* strongly suggest that the He^3(n, p)H^3 cross section curve shown above is 15 to 20 % too low. The solid and dashed curves are the theoretical total cross sections [15]) based on Serber and symmetrical forces respectively.

Theoretical calculations of the elastic scattering of neutrons by H^3 and He^3 have been made by Bransden *et al.* [15]) for two types of exchange forces, symmetrical and Serber. A comparison between these calculations and the present experimental total cross sections is shown in fig. 1. This comparison is somewhat ambiguous, particularly for He^3, because in the calculations only elastic scattering was considered whereas other possible interactions might contribute significantly to the total cross section. Table 4 presents

TABLE 4

Reaction energies Q for the nuclear reactions possible in the bombardment of H^3 and He^3 by neutrons

H^3+n		He^3+n	
Reaction	Q(MeV)	Reaction	Q(MeV)
$H^3(n, 2n)H^2$	−6.26	$He^3(n, p)H^3$	+0.76
$H^3(n, 3n)H^1$	−8.48	$He^3(n, d)H^2$	−3.27
		$He^3(n; p, n)H^2$	−5.49
		$He^3(n; p, 2n)H^1$	−7.72

reaction energies for the various possible reactions. Only two of these reactions, namely $He^3(n, p)H^3$ and $He^3(n, d)H^2$, have been investigated experimentally [4, 16, 17]) either directly or indirectly through detailed balance calculations based on experimental measurements of the inverse reaction. In the case of the n—H^3 interactions, only elastic scattering can take place below a laboratory neutron energy of 8.4 MeV, and the comparison should therefore be valid up to this energy. It is seen in fig. 1 that for the n—H^3 interaction the agreement between experiment and the Serber force calculation is quite good, even up to 14 MeV. The greatest discrepancy is at energies below 1 MeV. For the n—He^3 case there is again fair agreement with the Serber force calculation if the experimental $He^3(n, p)H^3$ and $He^3(n, d)H^2$ cross sections (see refs. [4]) and [16]), respectively) are simply subtracted from the total cross section, although there is no *a priori* reason to suppose this procedure is valid. The situation appears sufficiently promising to justify further effort to obtain more complete experimental data and to carry out calculations which account for the various reaction channels.

The n—H^3 and n—He^3 elastic scattering angular distribution experiments recently reported by Los Alamos workers [18]) should furnish more sensitive evidence regarding the validity of different types of forces.

References

1) J. H. Coon, R. O. Bondelid and D. D. Phillips, Los Alamos Report La-1483 (1952) (unpublished)
2) R. L. Mills, F. Edeskuty and A. Sesonski, Los Alamos Report LAMS-1411 (1952) (unpublished)

3) L. Cranberg, R. L. Mills and T. R. Roberts, Los Alamos Report LA-1853 (1954) (unpublished)
4) D. J. Hughes and R. B. Schwartz, Brookhaven National Laboratory Report BNL-325, second edition (1958)
5) J. D. Seagrave and R. L. Henkel, Phys. Rev. **98** (1955) 666
6) R. B. Day, R. L. Mills, J. E. Perry and F. Scherb, Phys. Rev. **98** (1955) 279A; a complete report has been submitted for publication in The Physical Review
7) R. B. Day and R. L. Henkel, Phys. Rev. **92** (1953) 358
8) This value has been previously quoted by J. H. Coon, H. H. Barschall and E. R. Graves, Phys. Rev. **88** (1952) 562
9) J. L. Fowler and J. E. Brolley, Revs. Mod. Phys. **28** (1956) 103
10) H. L. Poss, E. O. Salant, G. A. Snow and Luke C. L. Yuan, Phys. Rev. **87** (1952) 11
11) C. W. Li, Ward Whaling, W. A. Fowler and C. C. Lauritsen, Phys. Rev. **83** (1951) 512; R. M. Williamson, C. P. Browne, D. S. Craig and D. J. Donahue, Phys. Rev. **84** (1951) 731; R. W. King, Revs. Mod. Phys. **26** (1954) 327
12) S. Bashkin, F. P. Mooring and B. Petree, Phys. Rev. **82** (1951) 378
13) D. C. Dodder and J. L. Gammel, Phys. Rev. **88** (1952) 520
14) L. H. Katsaurov, P. M. Musaelian and B. N. Popov, Soviet Journal of Atomic Energy, Supplement No. 5 (1957) 71
15) B. H. Bransden, H. H. Robertson and P. Swan, Proc. Phys. Soc. A **69** (1956) 877; B. H. Bransden and H. H. Robertson, Proc. Phys. Soc. A **72** (1958) 770
16) J. N. Bradbury and L. Stewart, Bull. Am. Phys. Soc. **3** (1958) 417
17) A. Sayers, K. W. Jones and C. S. Wu, Bull. Am. Phys. Soc. **3** (1958) 365
18) J. D. Seagrave, J. E. Simmons and L. Cranberg, Bull. Am. Phys. Soc. **3** (1958) 338 [abstracts R9 and R10]

2.B *Nuclear Physics* **12** (1959) 298—304; © *North-Holland Publishing Co., Amsterdam*
Not to be reproduced by photoprint or microfilm without written permission from the publisher

(α, d) REACTIONS ON N^{14} AND Li^6

B. ZEIDMAN and J. L. YNTEMA
Argonne National Laboratory, Lemont, Illinois †

Received 20 March 1959

Abstract: Angular distributions of the emergent deuterons from the reactions $Li^6(\alpha, d)Be^8$ and $N^{14}(\alpha, d)O^{16}$, have been obtained for an incident alpha-particle energy of 43 MeV. The experiment was performed in the 60-in. scattering chamber, the deuterons being selected by a system employing a double NaI(Tl) crystal detector. The distributions, which cover the angular range between approximately 15° and 90° in the centre-of-mass system, exhibit oscillatory behaviour and forward peaking. Attempts to fit the data have been made. In the case of N^{14} a satisfactory fit can be obtained using spherical Bessel functions. Inclusion of some heavy-particle stripping improves the fit to the data. In the case of Li^6 it was not possible to obtain a satisfactory fit.

1. Introduction

It has been observed that the angular distributions of protons and inelastically scattered alpha particles from reactions initiated by alpha particles at approximately 30 to 40 MeV are frequently forward peaked and may exhibit an oscillatory behaviour [1]). In a number of cases the angular distributions are in fair agreement with the shape predicted by direct interaction theories [2]). The theories would indicate that the primary factors affecting the shape of the angular distributions are the momentum transfer ††, the change of angular momentum, and the interaction radius. In the present state of the theories, detailed consideration of the internal structures of the various nuclei involved is of lesser importance.

Since the deuteron is a loosely bound particle, it is of interest to see whether (α, d) reactions can be considered in the same light as (α, p) and (α, α') reactions. The targets chosen were those which a priori seemed to be most favourable both for the occurrence of the reactions and for determining whether more than one mechanism is involved in such a reaction.

2. Experimental Details

The experiments were performed with the 60-in. scattering chamber and the 43-MeV external beam of the Argonne 60-in. cyclotron. The deuterons

† Work performed under the auspices of the U.S. Atomic Energy Commission.

†† A discussion of the ways in which the momentum transfer may be considered for the various processes is contained in ref. [3]).

were detected by a previously described system [4]) which uses a double NaI(Tl) crystal. Aluminium foil was inserted between the target and the detector in order to stop elastically scattered alpha particles. Background at all angles was negligible.

The targets, located at the centre of the scattering chamber, were placed at an angle of 45° to the incident beam. The Li^6 target was an unsupported foil approximately 0.0015 in. thick which was rolled from 99.3 % enriched Li^6 metal supplied by Oak Ridge National Laboratory †. The target was admitted into the scattering chamber through a vacuum lock. The N^{14} target was prepared from Parez 613 resin in the form of an unsupported foil of non-uniform thickness.

3. Results

The data at each angle were recorded on a 100-channel analyzer which was gated to count only deuterons. Spectra from the two targets studied are shown in figs. 1 and 3. Spectra were obtained at approximately 3° intervals between 10° and 75° in the laboratory system. At each angle, the

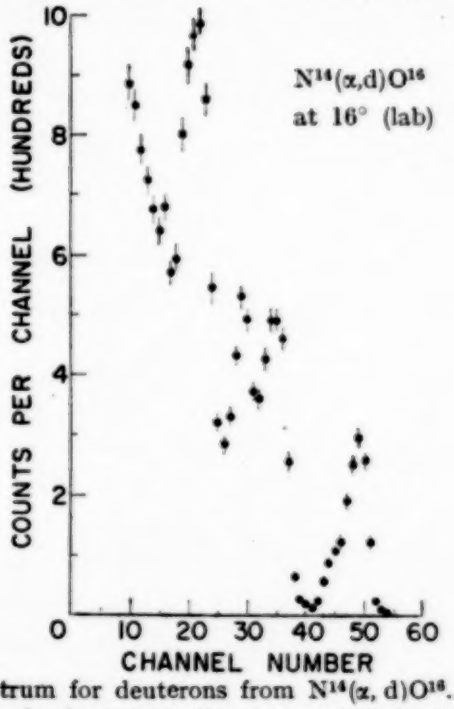

Fig. 1. Pulse-height spectrum for deuterons from $N^{14}(\alpha, d)O^{16}$. The deuteron energy is a reasonably linear function of pulse height above channel 20. In this region, one channel corresponds to approximately 400 keV.

numbers of counts in the states of interest were determined. After conversion from the laboratory system to the centre-of-mass system, the data were plotted as a function of the centre-of-mass angle to obtain the angular distributions shown in figs. 2 and 4.

† The Li^6 was rolled by Mr. F. Karasek of the Metallurgy Division of Argonne National Laboratory.

3.1. $N^{14}(\alpha, d)O^{16}$

The deuteron spectrum shown in fig. 1 shows a well isolated peak at approximately channel 50 and several other peaks in lower channels. Because of the non-uniformity in target thickness, a peak from an isolated level is very wide and it is difficult to resolve groups corresponding to the formation of excited states of O^{16}. The first excited state of O^{16} lies 6.06 MeV above the ground state [5]; therefore, the width of the ground-state group is still smaller than the separation between levels. The strong group in the vicinity of channel 23 is due to the $C^{12}(\alpha, d)N^{14}$ raection.

The angular distribution of deuterons leading to the ground state of O^{16} is shown in fig. 2. The distribution has a strong forward maximum and the two secondary maxima of approximately equal intensity at 40° and 60°.

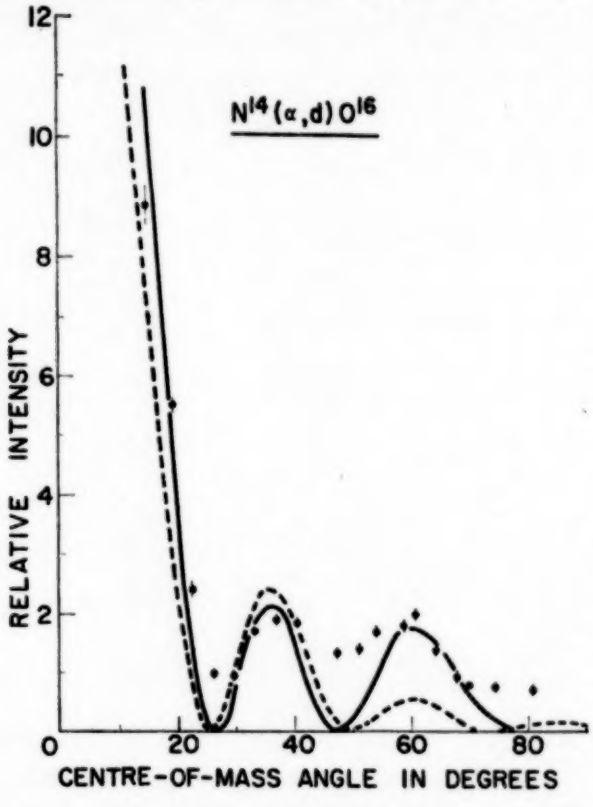

Fig. 2. Angular distribution of deuterons from the $N^{14}(\alpha, d)O^{16}$ reaction. The dashed curve is calculated on the basis of a knock-out process while the solid curve includes heavy-particle stripping.

A fit to the angular distribution was made under the assumption of a knock-out process, using for the shape of the differential cross section an expression of the form

$$\frac{d\sigma}{d\Omega} \propto |F(\theta) j_l(QR)|^2, \tag{1}$$

where $F(\theta)$ is a form factor, Q is the appropriate momentum transfer vector

defined below, R is the interaction radius, and l is the change of angular momentum. The form factor used was $(Q^2+\beta^2)^{-1}$, where β is a constant determined by the binding energies. The dashed line in fig. 2 is the curve for $l = 0$ and $R = 5.6\times 10^{-13}$ cm. The agreement with the data is satisfactory for the positions of the peaks but not for their heights. Better agreement in peak heights may be obtained if another process, namely heavy-particle stripping [6]), is considered as contributing to the reaction.

The differential cross section for heavy-particle stripping is of the same form as eq. (1) but $\mathbf{Q} = [\mathbf{K}_\alpha+(M_\alpha/M_f)\mathbf{K}_d]$ in contrast to $\mathbf{Q} = [(M_1-M_d)/M_1][\mathbf{K}_\alpha-(M_1/M_f)\mathbf{K}_d]$ for the knock-out process. The $\mathbf{K}_\alpha$ and $\mathbf{K}_d$ are the wave numbers for the alpha particle and deuteron in the centre-of-mass system, and M_1, M_f, M_α, and M_d are the masses of the initial nucleus, final nucleus, alpha particle and deuteron, respectively. The other parameters in the differential cross section are those characteristic of heavy-particle stripping and are not necessarily the same as those for the knock-out process [3, 6]). The two processes are coherent so that interference between the mechanisms occurs.

In order to observe the qualitative effect of considering both mechanisms, it is sufficient to use a differential cross section whose shape is given by

$$\frac{d\sigma}{d\Omega} \propto |F_1(\theta) j_{l1}(Q_1 R_1)+A F_2(\theta) j_{l2}(Q_2 R_2)|^2, \qquad (2)$$

where the subscripts 1 and 2 refer to knock-out and heavy-particle stripping, respectively, and A is an adjustable coefficient. If the same parameters as before are used for the knock-out process, eq. (2) gives, for $l_2 = 0$ and $R_2 = 4.6\times 10^{-13}$ cm, the solid curve in fig. 2 as the shape of the differential cross section. It is seen that the curve is in satisfactory agreement with the data over the entire range of angles studied for reasonable radii and l values. Since the minimum value of Q_2 is relatively large, it is not possible to make a unique determination of l_2. With only slight variation in R_2, the data can also be fitted with other values for the change in angular momentum in heavy-particle stripping. A more general form of eq. (1) involves summation over all possible values for the change of angular momentum. Inclusion of l values greater than zero, however, does not result in improved agreement with the data. If it is assumed that the reaction proceeds via a stripping of the incident alpha particle, the shape of the angular distribution would remain essentially the same. It is encouraging that agreement with the data can be obtained by the use of only two Bessel functions, for which there is theoretical basis, and a qualitative relation between them.

3.2. $Li^6(\alpha, d)Be^8$

The deuteron spectrum shown in fig. 3 exhibits only two prominent peaks — the ground-state peak and the broad 2.9-MeV first excited state.

The level diagram for Be^8 shows only these two states below approximately 11-MeV excitation [7]). The sharpness of these peaks, particularly that of the ground-state peak, indicates that the lifetime of Be^8 is long compared to

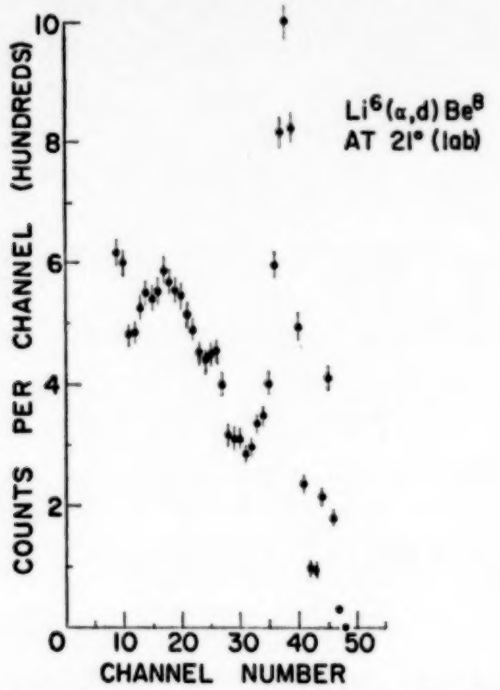

Fig. 3. Pulse-height spectrum for deuterons from $Li^6(\alpha, d)Be^8$. The deuteron energy is a reasonably linear function of pulse height above channel 20. In this region, one channel corresponds to approximately 400 keV. The peak of the broad 11-MeV level is in channel 17.

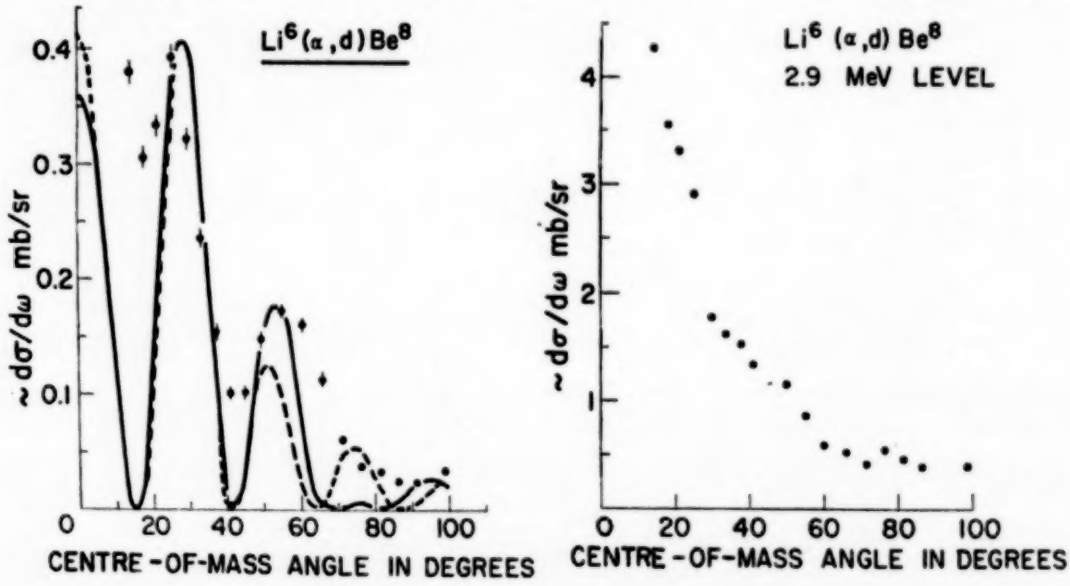

Fig. 4. Angular distributions from $Li^6(\alpha, d)Be^8$. (a) Reaction leading to ground state. The dashed curve is calculated on the basis of a stripping process while the solid curve includes heavy-particle stripping. (b) Reaction leading to 2.9-MeV level.

the reaction time, i.e., the residual Be^8 nucleus does not dissociate until the deuteron can no longer be affected by the breakup. The sharpness of the

peaks also indicates that the deuterons result from the formation of Be^8 and not simply from a knock-out of the deuteron leaving two independent alpha particles. The deuterons observed between the 2.9-MeV level and the very broad 11-MeV level may be due to a three-body breakup, the presence of weakly excited states of Be^8, or (α, d) reactions on small amounts of contaminants such as Li^7 and C.

The angular distributions for the reactions leading to the ground state and first excited state are shown in figs. 4(a) and (b) respectively. The scales indicating the absolute differential cross sections are known only to within ±30 % since the target thickness is not well known. Both angular distributions show forward peaking, but only the ground-state group exhibits a pronounced oscillatory behaviour. Attempts to fit this distribution with a function of the type given by eq. (1) do not produce agreement with the data for any reasonable choice of parameters if a knock-out process is assumed to be the dominant reaction mechanism.

In most reactions it is extremely difficult to distinguish between a knock-out process and a stripping process. In this reaction, however, the low mass of the target nucleus and the effects of the binding energies result in considerably different parameters for the two mechanisms. In particular, the momentum transfer vector is 50 % larger for stripping than for knock-out. The dashed curve in fig. 4(a) was obtained when $R = 8\times10^{-13}$ cm, $l = 0$, and the parameters associated with stripping were substituted in eq. (1). Better agreement can be obtained if a heavy-particle stripping component is included in a qualitative fashion. If the shape of the angular distribution is given by eq. (2), then for $R_1 = 8\times10^{-13}$ cm, $l_1 = 0$, $R_2 = 5.4\times10^{-13}$ cm and $l_2 = 0$, one obtains the solid curve in fig. 4(a). Use of the Butler formalism [2]) results in similar curves for the same l values, but for different radii. The "best fit radii" are 7.2×10^{-13} cm for stripping and 10×10^{-13} cm for knock-out. Combinations of l values or reaction mechanisms do not produce any better agreement with the data. In all cases, however, the use of a heavy-particle stripping component improves the fit to the data.

4. Summary

It should be emphasized that the preceding discussion of heavy-particle stripping and other direct interaction mechanisms is qualitative and that much further work, both experimental and theoretical, is required before quantitative results can be obtained. For example, only even values of l have been used since the parities of the initial and final states are the same. In the case of the B^{11}(d, n)C^{12} reaction, which has been studied over a range of incident energies, the l value for heavy-particle stripping is zero [6, 8]) even though the parities of the initial and final states differ. This has been ex-

plained by assuming that the core configuration for the reaction is not the same as that of B^{10}. In the present experiment, it is not possible to distinguish between various l values for heavy-particle stripping and there are no bases for assumptions concerning the core configurations.

For $N^{14}(\alpha, d)O^{16}$, the data indicate that basically this reaction may be treated in the same way as, for example, an (α, p) reaction and the internal structure of the deuteron is not of major importance. The $Li^6(\alpha, d)Be^8$ reaction, however, is one reaction which the current theoretical approach does not appear to explain satisfactorily.

We wish to acknowledge the cooperation of W. Ramler and the cyclotron group and the help of W. J. O'Neill in obtaining data. We also wish to thank Dr. J. Monahan for several stimulating discussions.

References

1) C. E. Hunting and N. S. Wall, Phys. Rev. **108** (1957) 901;
H. J. Watters, Phys. Rev. **103** (1956) 1763;
P. C. Gugelot and M. Rickey, Phys. Rev. **101** (1956) 1613
R. Sherr and M. Rickey, Bull. Am. Phys. Soc. **2** (1957) 29;
B. Zeidman and J. L. Yntema, Bull. Am. Phys. Soc. **4** (1959) 9
2) Austern, Bulter and McManus, Phys. Rev. **92** (1953) 350;
S. T. Butler, Phys. Rev. **106** (1957) 272
3) G. F. Pieper and N. P. Heydenburg, Phys. Rev. **111** (1958) 264
4) J. L. Yntema, Phys. Rev. **113** (1959) 261;
Argonne National Laboratory Report ANL 5890 (unpublished)
5) F. Ajzenberg and T. Lauritsen, Revs. Mod. Phys. **27** (1955) 777
6) G. E. Owen and L. Madansky, Phys. Rev. **105** (1957) 1766
7) F. Ajzenberg and T. Lauritsen, Nuclear Physics **11** (1959) 1
8) B. Zeidman and J. M. Fowler, Phys. Rev. **112** (1958) 2020

NORTH-HOLLAND BOOKS

ANALYTICAL and CANONICAL FORMALISM in PHYSICS

by ANDRÉ MERCIER

Head of the Department of Theoretical Physics University of Berne

6×9″ VIII + 222 pp. Guilders 20.00 (40s.)

CONTENTS

i. LAGRANGIAN FORMALISM
ii. LAGRANGIAN DENSITY
iii. CANONICAL FORMALISM
iv. CANONICAL FORM OF ELECTRODYNAMICS
v. HAMILTONIAN DENSITIES
vi. TRANSFORMATIONS
vii. CANONICAL FORMALISM WITH VANISHING JACOBIAN DETERMINANT

Those who are not highly specialized in these matters but do want to get a fairly broad knowledge of the subject are not aware of the fact that the greater parts of this formalism, including many specific conclusions of physical concern, do not involve in the least quantum theory, i.e. "quantization" of the fields. To show this and to provide the reader with a fairly complete presentation of the *classical* (i.e. not yet quantized) theory of fields is one of the main aims of the book.

This formalism is presented with great generality. Some special topics have also been included when they are found to be of importance in connection with the problems raised; however, they are not elaborated with the same generality, but just formulated as far as is found necessary for the understanding of these connections; for instance we can name: tensorial formalism and spinorial formalism.

A special chapter has been devoted to transformations of several kinds including canonical transformations, reversibility and the like as well as their interrelations, so that the ground is prepared for an understanding of the CPT-Theorems.

A short chapter on Dirac's dynamics with vanishing Jacobian closes the book.

The work builds upon the well-known *Principles of Analytical Dynamics* by the same author (in French), where particular weight is laid upon the homogeneous formalism, but it can easily be read with profit without knowledge of the latter by any advanced students in physics, astronomy or mathematics as well as by research workers who want to get a thorough practice in the use of these methods.

Many examples and as many as 124 problems illustrate the formalism exposed.

Sole Agency for U.S.A.: Interscience Publishers Inc.-New York

NORTH-HOLLAND PUBLISHING COMPANY - AMSTERDAM

NORTH-HOLLAND BOOKS

TURNING POINTS IN PHYSICS

A series of lectures given at

OXFORD UNIVERSITY in TRINITY TERM 1958

5 × 8″ viii + 192 pages Guilders 10.50 (20s.)

THE CONTENTS

INTRODUCTION
by A. C. Crombie,
All Souls College, Oxford

i. THE END OF MECHANISTIC PHILOSOPHY AND THE RISE OF FIELD PHYSICS
by R. J. Blin-Stoyle,
Clarendon Laboratory, Oxford

ii. THE QUANTUM NATURE OF MATTER AND RADIATION
by D. ter Haar,
Clarendon Laboratory, Oxford

iii. PROBABILITY ENTERS PHYSICS
by K. Mendelssohn,
Clarendon Laboratory, Oxford

iv. FROM THE RELATIVE TO THE ABSOLUTE
by G. Temple,
Mathematical Institute, Oxford

v. THE DECLINE AND FALL OF CAUSALITY
by F. Waismann,
New College, Oxford

vi. TOWARDS NEW CONCEPTS: ELEMENTARY PARTICLES
by D. H. Wilkinson,
Clarendon Laboratory, Oxford

THIS VOLUME CONTAINS the text of a series of six lectures organised by the Reader in the Philosophy of Science and the Lecturer in the History of Science in the University of Oxford and given by senior members of the University to an audience composed mainly of philosophers and scientists, who were not physicists. As a consequence these lectures are non-technical and can be understood by laymen who are interested to read about the development of physics in the last hundred years.

The first lecture describes how the concept of fields was introduced by Faraday and Maxwell, the next two lectures and the fifth lecture describe the changes in outlook brought about by the advent of quantum mechanics. These changes incorporate a change in the concepts of probability, causality and determinism, as well as the introduction of the idea of quantisation. The fourth lecture deals with relativity and the last lecture describes the galaxy of so-called elementary particles which nowadays dominate such a large part of physics.

Sole Agency for U.S.A.: Interscience Publishers Inc. - New York

NORTH-HOLLAND PUBLISHING COMPANY - AMSTERDAM